Numerical methods for multiphase flows

International Journal of Multiphase Flow 191 (2025) 105285

Contents lists available at ScienceDirect

International Journal of Multiphase Flow

journal homepage: www.elsevier.com/locate/ijmulflow

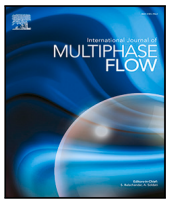

Research Paper

Numerical methods for multiphase flows

Manuel Garcia-Villalba [a,*], Tim Colonius [b], Olivier Desjardins [c], Dirk Lucas [d], Ali Mani [e], Daniele Marchisio [f], Omar K. Matar [g], Francesco Picano [h], Stéphane Zaleski [i]

[a] Institute of Fluid Mechanics and Heat Transfer, TU Wien, Getreidemarkt 9, Vienna, 1060, Austria
[b] Division of Engineering and Applied Science, California Institute of Technology, Pasadena, CA 91125, USA
[c] Sibley School of Mechanical and Aerospace Engineering, Cornell University, Ithaca, NY 14853, USA
[d] Institute of Fluid Dynamics, Helmholtz-Zentrum Dresden-Rossendorf, Bautzner Landstraße 400, Dresden, 01328, Germany
[e] Department of Mechanical Engineering, Stanford University, Stanford, CA 94305, USA
[f] Department of Applied Science and Technology, Institute of Chemical Engineering, Politecnico di Torino, Torino, 10129, Italy
[g] Department of Chemical Engineering, Imperial College London, London, SW7 2AZ, United Kingdom
[h] Department of Industrial Engineering, Università degli Studi di Padova, via Venezia 1, Padova, 35131, Italy
[i] Sorbonne Universite and CNRS, Institut Jean Le Rond d'Alembert UMR7190, Paris, F-75005, France

ARTICLE INFO

Keywords:
Numerical methods

ABSTRACT

Multiphase flows are ubiquitous in both nature and engineering. Over the past two to three decades, substantial progress has been made in developing numerical methods for simulating these complex flows. Yet, significant challenges persist in accurately capturing intricate interfacial dynamics and the multi-scale interactions inherent to multiphase systems. This review focuses on several key numerical approaches that have proven particularly relevant from both practical and theoretical perspectives. In particular, we discuss Volume-Of-Fluid techniques, level set methods, diffuse interface models, and front tracking methods, along with immersed boundary strategies designed for particle-laden flows. We also examine multi-fluid Eulerian frameworks, population balance models for reactive processes, and sub-grid scale techniques for handling unresolved dynamics. Furthermore, emerging hybrid strategies that integrate conventional numerical methods with data-driven machine learning techniques are highlighted as promising directions. In conclusion, while current methodologies offer valuable insights into multiphase flow behavior, continued interdisciplinary efforts are essential to enhance predictive accuracy, computational efficiency, and the overall applicability of these simulations to real-world challenges.

1. Introduction

Multiphase flows are ubiquitous, manifesting in both natural phenomena and a wide range of technical applications. In nature, they play an important role in processes such as cloud formation, ocean wave dynamics, and volcanic eruptions. In engineering, multiphase flows are central to the design and operation of systems like chemical reactors, pipelines transporting oil and gas, and cooling systems in power plants, among others. Accurate predictions of these complex flows are essential for optimizing performance, ensuring safety, and mitigating environmental impacts. Over the past 20–30 years, significant advances have been made in developing numerical methods to simulate multiphase flows. Indeed, by some measures the grid resolution of simulations has doubled every 2.5 years (Kulkarni et al., 2025). However, numerous challenges remain, particularly in modeling intricate interfacial dynamics and multi-scale interactions that are inherent to these systems.

Given the vastness of the field, this review cannot offer an exhaustive survey of all numerical methods for multiphase flows. Instead, we focus on several areas that we find particularly relevant, both from a practical and theoretical standpoint, and which are rich with challenges and open issues for future research. For readers seeking a broader background, we recommend well established books (Prosperetti and Tryggvason, 2009; Tryggvason et al., 2011; Gross and Reusken, 2011; Yeoh and Tu, 2019; Subramaniam and Balachandar, 2023) and other excellent review articles (Fuster et al., 2009; Subramaniam, 2013; Sommerfeld, 2017; Mirjalili et al., 2017; Elghobashi, 2019; Soligo et al., 2021; Roccon et al., 2023), which provide comprehensive insights into multiphase flow phenomena and modeling techniques.

This review is organized following a logical progression of numerical approaches and the underlying challenges they address. We begin with Volume-Of-Fluid (VOF) methods (covering *geometric* techniques

* Corresponding author.
E-mail address: manuel.garcia-villalba@tuwien.ac.at (M. Garcia-Villalba).

https://doi.org/10.1016/j.ijmultiphaseflow.2025.105285
Received 12 February 2025; Received in revised form 5 May 2025; Accepted 9 May 2025
Available online 28 May 2025

and touching on *algebraic* approaches) and level set methods which lay the groundwork for accurately capturing interfaces in multiphase systems. Then, we discuss diffuse interface methods, encompassing both interface-capturing techniques and phase-field methods. These approaches are particularly effective in handling complex interface topologies and transitions. Next, we explore front tracking techniques, which offer alternative strategies for sharp interface reconstruction. In many applications, especially those involving particulate matter, the interaction between fluid and discrete solid phases is critical; hence, we dedicate a section to Immersed Boundary Methods (IBM) tailored for particle-laden flows. Following this, we introduce multi-fluid models that employ an Eulerian framework to represent all phases, offering a robust alternative for simulating large-scale multiphase interactions.

Recognizing the importance of reactive processes in multiphase systems, we also examine population balance models, which are vital for understanding the evolution of particle size distributions due to phenomena like coalescence and breakage. Addressing the limitations of resolution in large-scale simulations, our discussion extends to sub-grid scale modeling techniques that tackle issues such as topology changes and manifold death. Furthermore, we delve into coupled multi-physics simulations, including fluid–solid interactions with hydraulic fracturing and damage mechanics, and also surfactant-laden interfaces, thereby capturing the interplay between different physical processes. We also highlight the emerging role of data-driven models by briefly reviewing articles that have been published on machine learning in multiphase flows. The integration of traditional numerical methods with machine learning techniques will be the focus of much work in the near future. This integration deserves a dedicated review of its own, as it is a topic of intense research. It is omitted from the present review due to space constraints and the authors' areas of expertise. The article concludes with a brief discussion of other important topics that will need further work in the near future, followed by some closing remarks.

2. Geometric methods

2.1. Volume-Of-Fluid method

The Volume-Of-Fluid (VOF) method, which enables the precise Eulerian capturing of phase interfaces required for accurately simulating multiphase flows, is almost as old as the International Journal of Multiphase Flow. First introduced by Hirt and Nichols (Nichols et al., 1980; Hirt and Nichols, 1981), VOF methods were later improved by using the Simple Line Interface Calculation (SLIC) of Noh and Woodward (1976) and then the Piecewise Line Interface Calculation (PLIC) of Youngs (1982), providing an intuitive geometric description of the phase interface. In their simplest interpretation, VOF methods solve a material transport equation for a phasic volume fraction α, i.e.,

$$\frac{\partial \alpha}{\partial t} + \mathbf{u} \cdot \nabla \alpha = 0, \tag{1}$$

where $\mathbf{u}$ is the fluid velocity. Without loss of generality, consider α to be the liquid volume fraction in a liquid–gas flow, then $\alpha = 1$ for fully liquid cells, $\alpha = 0$ for fully gas cells, while $0 < \alpha < 1$ represents the ratio of liquid volume to cell volume in mixture cells. Alternatively, it can be more powerful to consider the VOF methodology in the context of *moment methods*, wherein α is the normalized zeroth order spatial moment of the point-wise phase indicator function χ over a grid cell, defined for example as

$$\chi(\mathbf{x}, t) = \begin{cases} 1, & \text{if } \mathbf{x} \text{ is in the liquid} \\ 0, & \text{if } \mathbf{x} \text{ is in the gas.} \end{cases} \tag{2}$$

In the absence of phase change, χ is materially transported at the fluid velocity, i.e.,

$$\frac{\partial \chi}{\partial t} + \mathbf{u} \cdot \nabla \chi = 0. \tag{3}$$

Assuming an incompressible velocity field, integrating over a volume of interest Ω bounded by $\partial\Omega$ with outward normal vector $\mathbf{n}$, and applying Gauss' theorem leads to

$$\int_{\Omega} \frac{\partial \chi}{\partial t} \, \mathrm{d}\mathbf{x} + \int_{\partial\Omega} \chi \, \mathbf{u} \cdot \mathbf{n} \, \mathrm{d}\mathbf{x} = 0. \tag{4}$$

By invoking the Reynolds transport theorem to recast the left-hand-side of the previous equation as a Lagrangian derivative, we obtain

$$\frac{\mathrm{d}}{\mathrm{d}t} \int_{\Omega(t)} \chi \, \mathrm{d}\mathbf{x} = 0, \tag{5}$$

where the Lagrangian volume $\Omega(t)$ is materially advected at the fluid velocity $\mathbf{u}$. By time-integrating over a time step, we finally obtain

$$\int_{\Omega(t^{n+1})} \chi\left(\mathbf{x}, t^{n+1}\right) \, \mathrm{d}\mathbf{x} = \int_{\Omega(t^n)} \chi\left(\mathbf{x}, t^n\right) \, \mathrm{d}\mathbf{x}. \tag{6}$$

Following a semi-Lagrangian approach, the $\Omega\left(t^{n+1}\right)$ volume is taken at each new time step to coincide with a grid cell with volume V. Dividing the previous equation by V gives

$$\alpha^{n+1} = \frac{1}{V} \int_{\Omega(t^n)} \chi\left(\mathbf{x}, t^n\right) \, \mathrm{d}\mathbf{x}, \tag{7}$$

which can be readily evaluated to update the volume fraction field once a discrete approximation for $\Omega(t^n)$ has been provided. For example, it is customary to transport a polyhedral representation of $\Omega\left(t^{n+1}\right)$ backwards in time, as illustrated in Fig. 1. Finally, once α^{n+1} has been updated over the entire grid, the interface (i.e., the distribution function χ) can be reconstructed, e.g., using a PLIC closure model. Such a solution procedure is referred to as an *unsplit geometric VOF scheme*, and after several years of development went from non-conservative (e.g., Rider and Kothe (1998)), to conservative but 2D only (López et al., 2004) to fully 3D and exactly bounded and conservative (Owkes and Desjardins, 2014) as well as applicable to unstructured meshes (Chiodi and Desjardins, 2022). Another advantage of such methods is that they can be expressed in flux form, with fluxes obtained from geometric considerations at each cell face (Owkes and Desjardins, 2014), thereby enabling discretely consistent coupling with other transport processes. The main downside of these methods is their inherently high cost due to the complex geometric operations required for transport. On structured meshes, *split geometric VOF schemes* such as the scheme of Weymouth and Yue (2010) can achieve comparable accuracy at a lower cost.

Once the VOF field has been transported, the surface tension force $\mathbf{F}_\sigma$ can be readily computed using the Continuum Surface Force model first introduced by Brackbill et al. (1992),

$$\mathbf{F}_\sigma = \sigma \kappa \nabla \alpha, \tag{8}$$

where σ is the surface tension coefficient and κ is the interface curvature. If the gradient operator in this equation is discretized in the same way as the pressure gradient in the Navier–Stokes equation, then such a model is well-balanced, meaning that for a discretely constant curvature surface, there exists a numerical pressure that balanced surface tension exactly, therefore generating no parasitic current. In realistic flows, curvature needs to be approximated, which can be achieved by a wide range of methods such as height function (Nichols et al., 1980; Hirt and Nichols, 1981; Torrey et al., 1985) and parabolic fitting of the PLIC surface (Jibben et al., 2019). If the VOF field is transported with second order accuracy, then the curvature cannot be expected to converge. However, a recent comparative study suggests that parabolic fitting of the surface is quasi second-order for a fairly wide range of conditions (Han et al., 2024b).

Current research in geometric VOF methods focuses on improving accuracy. Beyond curvature calculation, numerical errors in unsplit geometric VOF schemes come from three distinct sources: the numerical integration of the trajectory followed by the grid cell as it is materially transported backwards in time, the polyhedral approximation of the

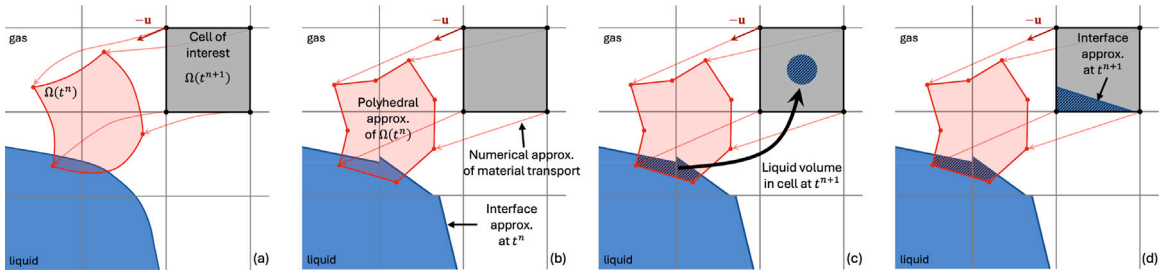

Fig. 1. Schematic representation of the semi-Lagrangian geometric transport of volume fraction showing (a) the exact liquid–gas interface and volume $\Omega(t^n)$ obtained by material transport of a grid cell at velocity $-\mathbf{u}$, (b) the numerical approximations typically performed, including a piecewise planar representation of the interface and a polyhedral representation of $\Omega(t^n)$, (c) the geometric calculation of the liquid volume in $\Omega(t^n)$ as described by Eq. (7), (d) and the final step of interface reconstruction.

$\Omega(t^n)$ volume, and the piecewise planar approximation of the liquid–gas interface itself (Remmerswaal and Veldman, 2022). While the first error can be readily controlled by selecting an appropriate trajectory integration method (including spatial interpolator and time integrator), the other two are more challenging to tackle. Going beyond a polyhedral approximation for $\Omega(t^n)$ has been explored for example by Zhang (2013), which considers a spline representation, and by Comminal et al. (2015) who retains straight edges but exploits sub-stepping to improve the geometric representation of the deformed cell. Reducing the error associated with the interface reconstruction involves going beyond piecewise planar models, and was achieved for example by Han et al. (2024a) with reconstruction with 2 Planes (R2P) (discussed in more details in Section 8.1), by Shashkov and Kikinzon (2023) with elliptic reconstructions in 2D (MOF2), and by Evrard et al. (2023) with piecewise parabolic reconstructions (PPIC).

In contrast to the geometric VOF approach, *algebraic* VOF methods differ in the numerical modeling of the phase indicator function, χ (Maric et al., 2020). These methods avoid explicit reconstruction of the interface in favor of approximating χ in a computational cell using algebraic functions; these functions could involve polynomial approximations or hyperbolic tangent profiles. The computation of the face fluxes needed to advect χ involves a finite-volume discretization that obviates the need for interface reconstruction and geometric volume integration. High-resolution schemes are used to counter the natural numerical smearing that accompanies the use of such approaches. These involve the use of compressive high-resolution schemes, or the addition of anti-diffusive terms to Eq. (3).

Use of high-resolution schemes in conjunction with the algebraic VOF method, however, could give rise to spurious features (Maric et al., 2020), which has motivated the use of blended high-resolution schemes within algebraic VOF methods that switch between compressive downwind and diffusive upwind schemes depending on interfacial alignment as set by the normal vector to the interface. These methods include high-resolution interface capturing (HRIC) (Muzaferija and Peric, 1997), compressive interface capturing for arbitrary meshes (CICSAM) (Ubbink and Issa, 1999), switching techniques for advection and capturing of surfaces (STACS) (Darwish and Moukalled, 2006), flux blending interface capturing (FBIC) (Tsui et al., 2009), and cubic upwind interpolation-based blending (CUIBS) (Patel and Natarajan, 2015), amongst others. Despite the use of these techniques, however, numerical smearing can still be observed wherever the local value of the Courant number is insufficiently low. It is, therefore, possible to say that although they may be simpler to implement than their geometric counterparts, algebraic VOF method are, in general, not as accurate.

The tangent of hyperbolic interface capturing (THINC) approach (Xiao et al., 2005) is a hybrid geometric/algebraic method based on a geometric formulation that uses a hyperbolic tangent function for interface reconstruction. It combines the simplicity of algebraic VOF methods with an accuracy comparable to that of geometric VOF techniques (Xiao et al., 2005; Yokoi, 2007; Xiao et al., 2011; Ii et al., 2012). Unstructured multi-dimensional THINC (UMTHINC) methods extend the THINC approach to triangular and quadrilateral meshes in 2D (Ii et al., 2014) and tetrahedral and hexahedral meshes in 3D (Xie and Xiao, 2014). Furthermore, use of quadratic surface representation and Gaussian quadrature (in so-called THINC/QQ methods) allow THINC to be used for unstructured meshes (Xie and Xiao, 2017; Chen and Xie, 2022). More recently, in an effort to reduce numerical dissipation in algebraic VOF methods without using artificial sharpening techniques, Kim et al. (2021) developed a scheme that transitions smoothly between central differences and high-resolution schemes depending on the interfacial orientation at each cell face where fluxes are to be computed. Flux limiters were also used to ensure volume fraction boundedness in arbitrary unstructured meshes. Kim et al. (2021) demonstrated that their algebraic VOF approach has similar accuracy to geometric VOF methods.

2.2. Level set method

Level set methods have existed as an alternative to VOF methods since the seminal work of Osher and co-workers (Sussman et al., 1994) for the simulation of two- and multiphase flows. Its popularity stemmed from its ease of implementation and the fact that it facilitated accurate calculation of the normal to the interface as well as interfacial curvature (Nagarth et al., 2005; Nourgaliev and Theofanous, 2007; Kees et al., 2011; Hysing, 2012). In a two-phase flow which occurs in a volume V, wherein phases 1 and 2 occupy volumes, V_1 and V_2, respectively, and $V_1 \cup V_2 = V$, the zero-contour of a level set function, $\psi(\mathbf{x}, t)$, captures the interface, ∂V, separating the two immiscible fluids. This function is positive in one phase and negative in the other, as shown in Fig. 2.

The interface can be advected using the following equation:

$$\frac{\partial \psi}{\partial t} + \mathbf{u} \cdot \nabla \psi = 0, \tag{9}$$

where $\mathbf{u}$ is the local velocity, which can be obtained from the solution of a single-fluid formulation which comprises the mass conservation and Navier–Stokes equations wherein the density and viscosity are calculated as a function of ψ as follows:

$$\rho(\psi) = \rho_1 H(\psi) + \rho_2 (1 - H(\psi)), \tag{10}$$

$$\mu(\psi) = \mu_1 H(\psi) + \mu_2 (1 - H(\psi)), \tag{11}$$

where ρ_1 and ρ_2, and μ_1 and μ_2, denote the density and viscosity of phases 1 and 2, respectively, and $H(\psi)$ is a Heaviside function smoothed over a number of grid cells. The Navier–Stokes equations include a term that represents the continuous force along the interface, which corresponds to the product of the surface tension, interfacial curvature $\kappa = -\nabla \cdot (\nabla\psi/|\nabla\psi|)$, and a smoothed Dirac delta function, $\nabla H(\psi)$. Following an advection step, the signed distance property of ψ is lost (a proof of this is provided by Khedkar et al., 2025) and a reinitialization step is necessary, which involves advancing the following equation to steady-state:

$$\frac{\partial \psi}{\partial \tau} + \mathrm{sgn}(\hat{\psi})\,(|\nabla\psi| - 1) = 0, \tag{12}$$

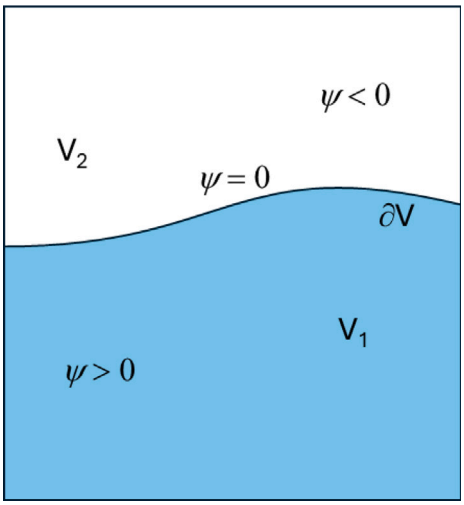

Fig. 2. Schematic representation of the level set function ψ, whereby $\psi = 0$ demarcates the interface ∂V separating the immiscible phases 1 and 2, which occupy volumes V_1 and V_2, wherein (by convention) $\psi > 0$ and $\psi < 0$, respectively.

where τ is a pseudo-time, and $\hat{\psi}$ denotes the level set function prior to reinitialization.

This reinitialization step, which leads to an artificial shift in the zero-contour of ψ, has been thought to be the culprit for a serious shortcoming of the level set method associated with inability to conserve mass (see, for instance, Solomenko et al. (2017) and references therein for some of the fixes that have been introduced in the literature). Some researchers have sought to address this issue by combining the level set method with schemes such as VOF that conserve mass (Enright et al., 2002; Sussman and Puckett, 2000; Dyadechko and M. Shashkov, 2007; Ahn and Shashkov, 2009; Wen et al., 2023) though these hybrid approaches are considerably more complicated than the original method.

More recently, Khedkar et al. (2025) have shown that the origin of the mass gain/loss associated with level set methods is not the reinitialization step but the smoothed Heaviside and Dirac delta functions used in the formulation, as highlighted above. By proposing an approach based on variational analysis, which makes use of a Lagrange multiplier to enforce mass conservation *and* preserve the signed distance property of ψ, Khedkar et al. (2025) appear to prevent mass gain/loss. Agreement with mass-conserving level set methods available in the literature was demonstrated and extensions to three-phase flows and fluid–structure interactions were also carried out.

2.3. Future work

1. Future work will focus on achieving better than second-order accuracy for geometric VOF transport, which remains a difficult problem and an active area of research.
2. Building on recent advances in preventing mass gain/loss constitutes a potentially fruitful avenue for future research in level set methods with possible extensions to flows featuring the presence of surfactants, complex geometries and flow–structure interactions, three-phase flows with phase change and moving contact lines.

3. Diffuse interface methods

Diffuse interface methods are Eulerian methods in which the interface separating two fluid phases is regularized to take place over a spatial region with a finite length scale. While true interfaces represented at the continuum level have a finite thickness on the order of molecular mean free path, diffuse interface methods artificially exaggerate the interface thickness to the level resolvable by the numerical mesh. The key advantage is that all physical fields, e.g., volume fraction or density, become differentiable and traditional numerical approximations can be utilized without special numerical treatments across the interface. As a result, diffuse interface methods are easy to program and are scalable, including on heterogeneous computing architectures (Radhakrishnan et al., 2023).

There are two broad classes of diffuse interface methods (Saurel and Pantano, 2018): methods in which a numerical scheme diffuses an interface, and methods in which modifications to the PDE models allow a diffuse representation of the interface. While, the latter techniques have been commonly termed phase-field methods in the literature, there may be some ambiguities in the nomenclature of the former. In the literature the former techniques are often referred to as interface capturing techniques (Johnsen and Colonius, 2006). However, the same terminology is sometimes used for broader category of Eulerian methods for interfaces, including sharp interface methods (Ubbink and Issa, 1999). In this section we use the term interface capturing to refer to the former subset of schemes within the diffuse interface methods.

3.1. Interface-capturing methods

Interface-capturing (IC) methods are designed analogous to shock-capturing methods for compressible flows. These methods rely on use of spatial discretizations with an upwind bias that provide sufficient numerical diffusion to artificially thicken sharp interfaces to a level resolvable by the numerical mesh. Shock- and interface-capturing methods, however, have the following key difference: in the former numerical diffusion is balanced by physical shock self-sharpening, leading to bounded numerical shock thicknesses, while in the latter an interface thickness can grow due to lack of any self-sharpening mechanism. Thus IC methods must either be used with care such that interfaces do not grow too diffuse, or they must be supplanted with numerical interface sharpening techniques or additional models that account for the unresolved physics.

Apart from phase-field methods, discussed in more detail below, a number of efforts have been made to try to prevent excessive numerical diffusion of interfaces over time. These include the use of limiters (Chiapolino et al., 2017), and nonlinear reconstruction of volume fraction with hyperbolic-tangent interpolants (Shyue and Xiao, 2014). The efficacy of such treatments depend on the discretization method, and there can be trade-offs between maintaining a sharp interface and introducing spurious anisotropies (Schmidmayer et al., 2020). The phase-field methods discussed next are an alternative that seek to solve this problem at the PDE level.

3.2. Phase-field methods

The second class of methods, which are commonly referred to as phase-field (PF) models, maintain finite interface thicknesses by explicitly adding interface regularization terms to the governing equations at the PDE level. These methods at core are inspired by the phase-field models that capture phase separation, namely the Cahn–Hilliard model (Cahn and Hilliard, 1958; Hohenberg and Halperin, 1977) and the Allen–Cahn model (Allen and Cahn, 1979). The Cahn–Hilliard model conserves the volume integral of the phase-field variable. Therefore it can be used readily for cases with no phase change. Based on this method, the advection equation (1) for the phasic volume fraction, $0 \leq \alpha \leq 1$, is written with a nonzero right hand side (Lowengrub and Truskinovsky, 1998; Abels et al., 2012; Ten Eikelder et al., 2023):

$$\frac{\partial \alpha}{\partial t} + \mathbf{u} \cdot \nabla \alpha = m \nabla^2 \left[\frac{1}{\epsilon} \alpha (1-\alpha)(1-2\alpha) - \epsilon \nabla^2 \alpha \right], \tag{13}$$

where parameter ϵ is a length scale, and parameter m, is referred to as the mobility parameter. The first term on the right hand side acts to sharpen the interface, while the second term acts to thicken the

interface. The balance between these two terms results in a quasi-steady and quasi-one dimensional interface with thickness $\mathcal{O}(\epsilon)$ with a tangent hyperbolic profile. To achieve this *equilibrium* solution in practice, ϵ is chosen to be on the order of the mesh size, hence making the interface small but resolvable, and m is chosen large enough to make the right hand side more stiff compared to the time scale of deformations by the advective term. This approach when coupled to a momentum solver is often referred to as Cahn–Hilliard Navier–Stokes (CHNS).

The original Allen–Cahn model (Allen and Cahn, 1979) requires some modification before use for simulation of two-phase flows when the expectation is that mass of each phase must be conserved. One such modification, also referred to as Conservative Allen–Cahn (CAC), is introduced by Stafford et al. (2001) and Brassel and Bretin (2011) in which mass conservation is enforced as a constraint by including a Lagrange multiplier (Brassel and Bretin, 2011; Chen et al., 2011; Kim et al., 2014; Huang et al., 2020). An alternative that achieves local conservation, also often referred to as conservative diffuse interface method (CDI), is based on the method of Chiu and Lin (2011) transformed from Sun and Beckermann (2007) in which a conservative PDE is written in the form[1]

$$\frac{\partial \alpha}{\partial t} + \mathbf{u} \cdot \nabla \alpha = \nabla \gamma \left[-\alpha (1-\alpha) \mathbf{n} + \epsilon \nabla \alpha \right], \tag{14}$$

where again the first and second term result in a dynamic similar to that achieved by the first and second term in (13). Likewise, ϵ is the interfacial length scale and γ is the stiffness parameter. It should be noted that some level set methods (Olsson and Kreiss, 2005; Olsson et al., 2007; Desjardins et al., 2008) use a regularization PDE with the same right hand side as in (14), however, these methods are inherently sharp interface methods aiming to track a discontinuous interface.

While comparative studies (Rossi et al., 2024) are needed to better understand the cost–accuracy trade offs of different methods, we here briefly describe the common use of various techniques mentioned above.

As mentioned, a key advantage of diffuse interface methods is in their ease of implementation and thereby parallel scalability since they allow a unified numerical scheme without the need for additional costly computations near the interfaces. However, within diffuse interfaces, one key difference between IC methods and PF methods is in regularization of the interface. Common IC methods allow the interface to numerically thicken indefinitely, while PF methods use sharpening terms to maintain a finite interface thickness, as shown in an example in Fig. 3. One can also see in the figure that PF's interface sharpening has the side effect of interface breakup which would be unexpected in the absence of physical surface tension.

Given these tradeoffs, IC methods are often used when interfaces have short residence time and when surface tension effects are not dominant, otherwise PF methods are more appropriate. In this context, some thermodynamically-inspired PF methods are formulated such that the interface sharpening ability is directly correlated to the surface tension (Jofre and Urzay, 2021; Zhao et al., 2023).

Based on recent literature, for compressible flows, which are also typically at higher Reynolds number, often IC (Johnsen and Colonius, 2006) and CDI-type methods (Shukla et al., 2010; Jain et al., 2020) are used, while for incompressible flows CHNS (Khanwale et al., 2020), CAC (Huang et al., 2020) and CDI (Mirjalili and Mani, 2021) are used more often than IC methods. However, very recent work includes compressible formulation for CHNS and CAC (Huang and Johnsen, 2024).

[1] In some studies, this method is also referred to as conservative Allen–Cahn (CAC), but we use CDI here to differentiate this work from studies in which conservation is achieved via use of Lagrange multipliers.

3.3. Coupling with momentum and energy equations

For compressible fluids the diffuse-interface formulations are most often based on the Baer and Nunziato (1986) equations for a mixture of materials with, in their most general form, no assumed chemical, thermal, or mechanical equilibrium between the components, together with appropriate closures for unresolved interactions between the components (fluxes of mass, momentum, and energy). These are sometimes referred to as the seven-equation model (Saurel and Abgrall, 1999; Tiwari et al., 2013), as, for a binary mixture, they comprise equations for volume fraction, and two each for conservation of mass, momentum, and energy. Reduction implied by imposing a common velocity, pressure, and/or Gibbs free energy between the components, results in several different models. The most commonly employed of these are the 6-equation model of Saurel et al. (2009), which assumes velocity equilibrium (and can be used with or without chemical equilibrium), and the 5-equation model (Kapila et al., 2000) that additionally assumes pressure equilibrium. We caution that the nomenclature of referring to these models by the number of equations leads to ambiguities as some of them have been applied to mixtures of more than two materials (increasing the number of equations).

In most target applications the interface is physically sharp on the order of nanometer scale, with very fast equilibrium time scale. Therefore, ideally a 4-equation model that assumes thermal, mechanical, and momentum equilibrium across the interface is most relevant to the physics. However, to ease numerical robustness often tight equilibrium is relaxed and 5- or higher equation models are used. Some implementations even include additional equations that would be redundant in the continuous limit but are useful in controlling their discretized behavior.

In incompressible formulations a single momentum equation is solved to obtain the velocity field subject to the incompressibility condition for the pressure. This equation is coupled to the phase-field evolution since fluid density and viscosity are explicit functions of the phase field variable, which are often assumed to take linear forms. Additionally, the surface tension representation is also diffuse and coupled to the phase field variable (Jacqmin, 1996, 1998, 2000).

In coupling interface evolution equation to the momentum (and energy equation in the case of compressible flows), one should carefully consider the implied mass–momentum inconsistency. The diffuse dynamics of the interface, e.g. due to numerical dissipation or right hand side terms in (13) and (14), implies a mass flux in addition to that implied by the explicit velocity field. For robust formulations, the momentum and energy transport due to this mass flux should be consistently accounted in the coupled equations (Shen and Yang, 2015; Mirjalili and Mani, 2021; Khanwale et al., 2022). Along this line of thinking, a key requirement is that the model obeys the second law of thermodynamics (Shen and Yang, 2015; Chen and Shen, 2016; Guo et al., 2017; Zhao and Han, 2021; Khanwale et al., 2022). Additionally, for compressible flows the model is expected to be hyperbolic (Toro, 2013) and such that shock-capturing methods and associated Riemann solvers can be devised for its solution.

Regarding discretization, see Maltsev et al. (2022) for a thorough review of the finite-volume, finite-difference, discontinuous Galerkin, and lattice Boltzmann methods that have been applied to these systems. In general, IC methods often use WENO-type spatial schemes to capture the interface (Jiang and Shu, 1996; Johnsen and Colonius, 2006; Coralic and Colonius, 2014). While earlier PF methods also relied on WENO-type schemes to achieve boundedness (Chiu and Lin, 2011; Mirjalili et al., 2020) showed that discretely bounded schemes are possible with centered schemes by identifying the stable zones in the map of input parameters.

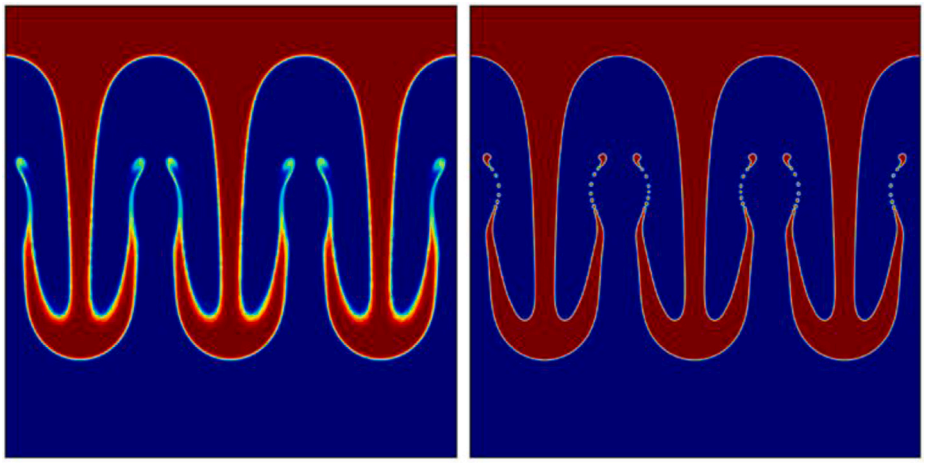

Fig. 3. Numerically simulated Rayleigh–Taylor instability. Shown is the unstable instantaneous interface between a heavy fluid on top (red) and a light fluid in the bottom (blue). Results are obtained under identical resolution and physical setting using IC (a) and CDI (b). (For interpretation of the references to color in this figure legend, the reader is referred to the web version of this article.)
Source: Figure reproduced from the data of Collis et al. (2025).

3.4. Future work

We close this section with our perspective on future research directions. While great progress has been made in diffuse-interface methods, there are several areas requiring more attention:

1. **Interfacial instabilities**. A variety of instabilities occur at fluid interfaces, including Kelvin–Helmholtz, Richtmyer Meshkov, and Rayleigh–Taylor instabilities. Results in the literature for model problems like triple-point shear layers and shock/helium–bubble interactions show varying amplitudes of instability waves at the interface of a shocked bubble that depend on the specific method (including both sharp- and diffuse-interface methods), the order of the scheme, and the resolution (Coralic and Colonius, 2014; Pan et al., 2018; Paula et al., 2023; Zhang et al., 2025; Jain et al., 2023). Fundamental work is required to establish benchmark problems with converged, validated solutions.
2. **Phase change**. While IC approaches based on the 5- 6-equation models discussed above can be used for phase change problems such as cavitation (Pelanti, 2022), the assumption of thermodynamic equilibrium, which is appropriate in the thin interfacial region, is problematic when, as is typical in applications, phase change is nucleated by (typically $O(\mu\text{m})$) imperfections or gas bubbles that cannot be expected to be resolved. Sub-grid-scale models to account for nucleation need to be developed.
3. **Diffusive effects.** Many models have neglected mass diffusion, heat condition, and/or viscosity, and to our knowledge no diffuse interface model consistently treats all diffusive effects. For example, Beig and Johnsen (2015) show that special treatment involving advecting material properties in the equations of state is required to avoid temperature oscillations near interfaces that would prevent an accurate assessment of heat conduction. To our knowledge, accurate IC treatment of mass diffusion, which would be important for systems involving both immiscible and miscible materials (for example evaporation of a fuel droplet) is missing.
4. **Comparative studies.** With the burgeoning literature on an array of schemes, it can be difficult to establish best practices for any given model problem. Drawing meaningful comparisons of differing methods on differing computing architectures is challenging, but the community should strive to carefully document performance on benchmark problems, including careful comparison against experiments (Khanwale et al., 2023).

4. Front-tracking techniques

We discuss here the use of interface-tracking techniques for accurate simulations of multiphase flows following the pioneering work of Unverdi and Tryggvason (1992). In some interpretations of these techniques (Tryggvason et al., 2001; Shin et al., 2005; Shin and Juric, 2007, 2009; Shin et al., 2017), the interface is approximated by a piecewise linear, or triangular, Lagrangian grids in two and three dimensions, respectively; the flow is resolved on a fixed grid. The interface corresponds to interconnected marker points that move in response to the motion of the fluid relying on accurate interpolation of flow variables from the Eulerian grid to the interface and smooth distribution of interfacial information on the grid via, e.g., an immersed boundary method (IBM) (Peskin and McQueen, 1995).

The Level Contour Reconstruction Method (LCRM), which is a hybrid front-tracking/level-set technique, was introduced by Shin and Juric (2002) and has been modified by Shin et al. (2005) and Shin and Juric (2007) to suppress parasitic currents. Shin and Juric (2009) made use of an indicator function, $\mathcal{H}$, calculated from the interface using a level-set function (Shin and Juric, 2002):

$$\nabla^2\mathcal{H} = \nabla\cdot\mathbf{G}, \tag{15}$$

where $\mathbf{G}$ is expressed by $\mathbf{G} = \int_{A_e} \mathbf{n}\delta(\mathbf{x}-\mathbf{x}_f)\,dA$ (Unverdi and Tryggvason, 1992; Shin and Juric, 2007) in which $\mathbf{n}$ is the outward-pointing unit normal to the interface, located at $\mathbf{x} = \mathbf{x}_f$, A_e is the interfacial area, and $\delta(\mathbf{x}-\mathbf{x}_f)$ is the Dirac delta function. Note that Eq. (15) is a modified version of the original relation between the divergence of the gradient field $\mathbf{G}$ and the Laplacian of the indicator function, first proposed by Unverdi and Tryggvason (1992).

In more recent versions of LCRM (Shin and Juric, 2007), isocontours of the indicator function $\mathcal{H}$ are drawn across each Eulerian grid cell at each time-step to represent the interface, similar to level-sets, from the tracked locations of the Lagrangian marker points, as shown in Fig. 4, discarded subsequently. New markers are then obtained from the isocontours using high-order splines and this interpolation connects neighboring points. This obviates the need for time-consuming bookkeeping and lends itself naturally to parallelization and the ability to handle topological transitions, while conserving mass (Shin et al., 2017). The Lagrangian interfacial elements are advected by integrating $\mathrm{d}\mathbf{x}_f/\mathrm{d}t = \mathbf{V}_f$, where $\mathbf{V}_f$ denotes the interface velocity, interpolated from the velocity field in the Eulerian grid.

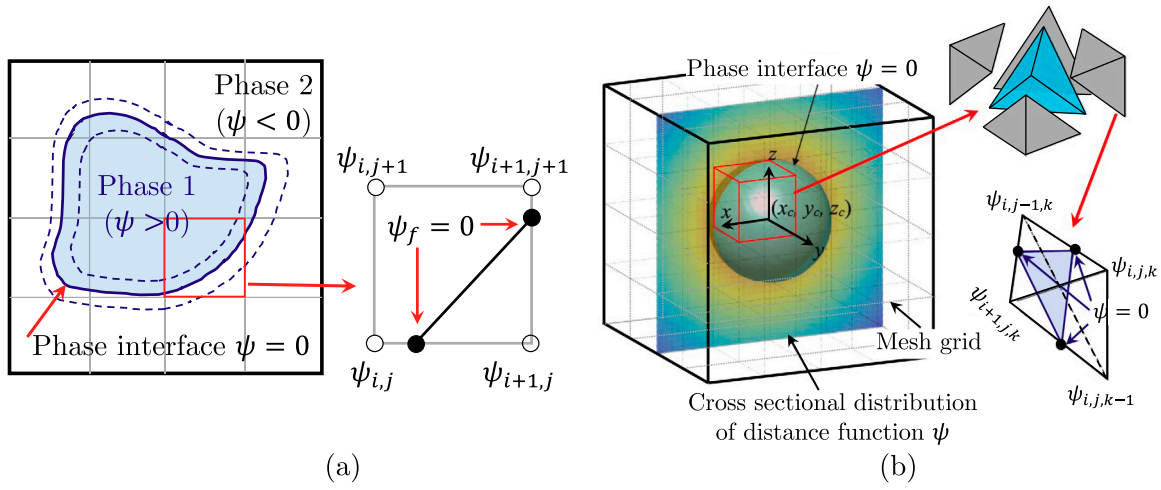

Fig. 4. Schematic representation of the LCRM showing (a) the definition of new marker points (black dots) from the reconstructed isocontours of the distance function field ψ in 2D; (b) shows how the Eulerian cells are sub-divided into five tetrahedra in 3D and an intersection between them and the isocontour is located.
Source: Image adapted from Shin et al. (2018, 2017).

Using IBM, a flow variable ϕ_f^l at the interface, located at $\mathbf{x}_f = (x_f^l, y_f^l, z_f^l)$, can be represented by the following summation (Tryggvason et al., 2001; Shin and Juric, 2002; Tryggvason et al., 2011):

$$\phi_f^l = \sum_{ijk} w_{i,j,k}^l \phi_{i,j,k}, \tag{16}$$

where $w_{i,j,k}^l$ is the weight of each Eulerian grid point with respect to $\mathbf{x}_f$, and $\phi_{i,j,k}$ correspond to the flow variable at $\mathbf{x} = (i, j, k)$, which consists of uniform cells of size $\Delta\mathbf{x} = (\Delta x, \Delta y, \Delta z)$. These weights are defined to ensure that the interpolated quantity remains bounded by the corresponding grid values and matches the grid value if the marker location coincides with the grid point; the sum of all weights with respect to a marker point must equal unity. Computing interfacial forces requires information transfer from the interface to the fixed Eulerian grid by constructing an approximation of the δ function $\phi_{i,j,k} = \sum_l \phi_f^l w_{i,j,k}^l \frac{\Delta A}{\Delta x \Delta y \Delta z}$, where ΔA denotes the area of the interface element located at $\mathbf{x} = \mathbf{x}_f$. Conservation of the interfacial quantity involved in the transfer process is connected to the choice of weighting functions, typically defined as a product of one-dimensional distribution functions: $w_{i,j,k}^l = d(r_x)d(r_y)d(r_z)$, where r_x, r_y, and r_z are the scaled distances between the front and the grid line in the x, y, and z directions, respectively; the distribution functions, $d(r)$, are due to Peskin and McQueen (1995).

Computing the surface tension force $\mathbf{F}_\sigma$ given by

$$\mathbf{F}_\sigma = \int_{A_e} \sigma\kappa\mathbf{n}\delta(\mathbf{x} - \mathbf{x}_f)\, \mathrm{d}A = \sigma\kappa_H \nabla\mathcal{H}, \tag{17}$$

utilizes a discrete curvature calculated on the Eulerian grid, κ_H, but incorporates information from the Lagrangian grid (Shin et al., 2018):

$$\sigma\kappa_H = \frac{\mathbf{F_L} \cdot \mathbf{G}}{\mathbf{G} \cdot \mathbf{G}}; \tag{18}$$

here, $\mathbf{F_L} = \int_{A_e} \sigma\kappa_f \mathbf{n}_f \delta(\mathbf{x} - \mathbf{x}_f)\, \mathrm{d}A$, and κ_f and $\mathbf{n}_f$ represent twice the mean curvature and the normal vector obtained from the Lagrangian structure, respectively.

The Edge-Based-Interface-Tracking (EBIT) is closely related to LCRM. Originally suggested in 2D by Serguei Semushin (1988) in an unpublished preprint, it has been revived by Chirco and Zaleski (2022) who discussed a simple *kinematic* version, with only front propagation without any dynamics. In this method, as in the LCRM, the front is tracked by markers on the edges, but unlike the LCRM the cubic element is not subdivided into tetrahedra, so there are no additional markers in the interior of the interface cutting the elements (Fig. 5a). Unlike also the LCRM, the method has not been coupled to the Level-Set method but to the Volume-Of-Fluid (VOF) method by Pan et al. (2024). The volume fraction in the cut cell is determined by the "Front2VOF" algorithm described in Kottilingal (2023). The Navier–Stokes equations are then solved using a standard Volume-OF-Fluid method with curvature computed by the Height-Function method (Popinet, 2009). As for the LCRM, the tethering of the markers to the grid allows for parallelization (Fig. 5b). In the implementation of Pan et al. (2024) the Basilisk C language is used which allows to re-employ the octree grid refinement. The method was tested on several simple flows, including the oscillating droplet (Fig. 5d), and the rising bubble test case of Shin and Juric (2002) with Eo $= \rho_l g d^2/\sigma = 100$, Mo $= g\mu_l^4/(\sigma^3\rho_l) = 1$, $\rho_l/\rho_g = 40$ $\mu_l/\mu_g = 50$. The simulation is performed in boxes containing $32 \times 32 \times 64$ and $64 \times 64 \times 128$ grid points. In the current version (or future version) the interface is not able to cross a grid refinement boundary.

4.1. Future work

1. While the LCRM and EBIT methods offer a significant improvement over the Front-Tracking method in terms of parallelization, they do not yet allow to have two fronts crossing a cell. This could be made kinematically possible in the EBIT method by allowing two markers per cell edge. However, the coupling with the VOF or Level-Set methods should also be modified in that case.
2. A more distant perspective is to develop multiscale and subgrid methods, such as those developed by Tryggvason for the classical Front-Tracking method (Thomas et al., 2010; Aboulhasanzadeh et al., 2012; Radl et al., 2008). Such extensions are under active investigation.
3. For subgrid heat and mass transfer modeling, the fact that markers are not advected in a Lagrangian manner by the flow in EBIT and LCRM impedes the use of the boundary layer integration method used in classical front tracking, which is a loss if such multiscale methods are needed.
4. Other types of multiscale computations involve the treatment of flow "singularities", such as small droplets, bubbles, ligaments, and thin sheets, as distinct objects that are specifically and simultaneously tracked. Although this goal remains a challenge for the future, computationally efficient Front-Tracking methods, such as EBIT and LCRM, are promising candidates for achieving it.

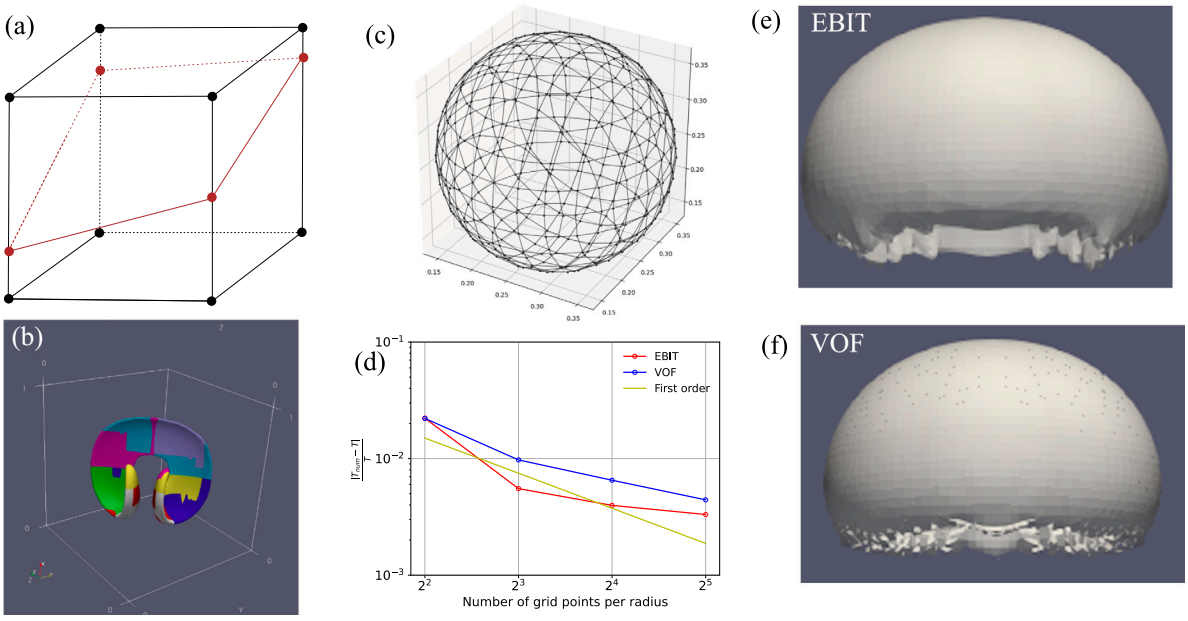

Fig. 5. (a) The principle of the EBIT method: at most one marker is placed on each edge of the grid. (b) The parallelization of the vortex-in-box kinematic test case in 3D. Each color corresponds to a different MPI process. (c) The gridding of a sphere by EBIT (d) Convergence test for the droplet oscillations in the pure VOF and the EBIT–VOF coupled case. (e) A rising bubble computed by the pure VOF method (f) A rising bubble computed by the EBIT method.

5. The main challenge of such multiscale methods is code development, since a general tracking code for ligaments and thin sheets is still missing, even if EBIT and LCRM are steps in the adaptation of Front Tracking towards more efficient and flexible massively parallel and multiscale modeling.

5. Immersed boundary methods for particle-laden flows

Particle-laden flows occur frequently in engineering applications and natural processes. These flows involve two phases: a continuous fluid phase and a dispersed particulate phase distributed within the fluid. The phases exchange mass, momentum, and energy across their interfaces. We distinguish between the flow features near the particles, i.e. the microscale, and the flow features at the scale of the considered problem (the river or the fluidized bed, for example) that we denote the macroscale. In general, flow features at intermediate scales are also relevant, and we denote them the mesoscale. In this section, we focus on numerical methods to solve for the microscale, the so-called particle-resolved direct numerical simulations (PR-DNS) (Uhlmann et al., 2023). For the reader interested in methods to solve for the mesoscale/macroscale, we refer to recent reviews (Maxey, 2017; Subramaniam and Balachandar, 2023). Other techniques for studying particle-laden flows, such as Lagrangian point particle methods (Brandt and Coletti, 2022) and Stokesian dynamics (Torre and de Graaf, 2025), are not discussed in this review due to space limitations.

There are two main strategies for simulating the flow around moving particles: boundary-conforming and non-conforming methods. In boundary-conforming methods, the grid needs to be adapted in time to accommodate for the varying position of the particles. This leads to costly remeshing operations and the corresponding mapping of flow velocities and pressure to the new grid. A review of such methods can be found in Wachs (2019). In non-conforming methods, the interface condition is imposed by using additional source terms in the governing equations or introducing Lagrange multipliers, among other alternatives. There are several successful methods being in use in the particle-laden flow community. However, for reasons of space we concentrate in this article in one of them: the immersed boundary method (IBM) (Mittal and Iaccarino, 2005; Verzicco, 2023). The reader interested in other alternatives is referred to the recent review of Uhlmann et al. (2023), where Boltzmann-equation-based methods and Lagrange multiplier methods are also discussed. The IBM was first developed by Peskin (1972, 2002) in the context of heart flow simulations and since then multiple variations have been published and are in use today for a variety of problems (Sotiropoulos and Yang, 2014; Kim and Choi, 2019; Griffith and Patankar, 2020; Mittal and Bhardwaj, 2022; Arranz et al., 2022).

One method that has found widespread use in the context of particle-laden flows is the direct-forcing IBM developed by Uhlmann (2005). It was developed for spherical particles and later extended to particles of arbitrary shape by Moriche et al. (2021). In this method, the Navier–Stokes equations of the incompressible flow are solved in an Eulerian grid, which is typically Cartesian; to track the motion of the particles a Lagrangian grid for each particle is employed. The equations read

$$\nabla \cdot \boldsymbol{u}_f = 0, \tag{19}$$

$$\frac{\partial \boldsymbol{u}_f}{\partial t} + \left(\boldsymbol{u}_f \cdot \nabla\right)\boldsymbol{u}_f = -\frac{1}{\rho_f}\nabla p + \nu\nabla^2\boldsymbol{u}_f + \boldsymbol{f}_{ibm}, \tag{20}$$

where $\boldsymbol{u}_f$ is the fluid velocity, p is the pressure, ρ_f the fluid density, ν the kinematic viscosity and $\boldsymbol{f}_{ibm}$ is a volume force, to enforce the boundary condition at the surface of the particle. For each particle the Newton–Euler equations are solved in the form of differential equations for the particle velocity $\boldsymbol{u}_p$ and angular momentum with respect to the center of mass, $\boldsymbol{h}_p$,

$$\rho_p V_p \frac{\mathrm{d}\boldsymbol{u}_p}{\mathrm{d}t} = \rho_f \oint_{\partial S} \boldsymbol{\tau}\cdot\boldsymbol{n}\,\mathrm{d}\sigma + \boldsymbol{F}_{ext}\,, \tag{21}$$

$$\frac{\mathrm{d}\boldsymbol{h}_p}{\mathrm{d}t} = \rho_f \oint_{\partial S} \boldsymbol{r}\times(\boldsymbol{\tau}\cdot\boldsymbol{n})\,\mathrm{d}\sigma + \boldsymbol{T}_{ext}\,, \tag{22}$$

where ρ_p is the particle density, V_p is the volume of the particle, $\boldsymbol{\tau}$ is the hydrodynamic stress tensor, $\boldsymbol{n}$ is the unit normal vector pointing towards the fluid, $\boldsymbol{r}$ is the position vector of any point in the body with respect to the center of mass and $\boldsymbol{F}_{ext}$ and $\boldsymbol{T}_{ext}$ are external forces and torques, respectively. The latter may include contributions from buoyancy, collisions, lubrication, etc.

In the original method, the equations are solved sequentially, first the fluid equations are solved and this is followed by the particle equations, in what is known as a weakly coupling. The first step is to determine a preliminary velocity field, $\tilde{\boldsymbol{u}}_f$, solution of the momentum Eq. (20) in the absence of immersed boundary forcing. Then, the preliminary velocity is interpolated to the Lagrangian grid. In general, this preliminary velocity will be different from the desired fluid velocity, $\boldsymbol{u}_f^{(d)}$, at each Lagrangian point. The latter is obtained from the no slip boundary condition at the interface, i.e. the desired fluid velocity is equal to the particle velocity at the interface. The forcing term that drives the velocity towards the desired fluid velocity is then defined at each Lagrangian point as

$$\boldsymbol{f}_{ibm} = \frac{\tilde{\boldsymbol{u}}_f - \boldsymbol{u}_f^{(d)}}{\Delta t}, \tag{23}$$

where Δt is the time step. Finally, the forcing term can be spread back to the Eulerian grid, to complete the integration of the Navier–Stokes equations. Once the fluid has been solved, the hydrodynamic forces and torques are easily evaluated and employed as input to solve the Newton–Euler equations of the particle motion (21)–(22).

As pointed out by Zhou and Balachandar (2021), the method "is very popular because it is easy to implement and flexible to simulate various problems". Using this method it is now possible to perform PR-DNS with over one million well-resolved particles (Kidanemariam et al., 2022). Despite its success, the method of Uhlmann has a number of limitations. One of them arises from the weak coupling between the Navier–Stokes equations for the fluid phase and the Newton–Euler equations for the particle motion, leading to a lower stability limit for the density ratio between solid and fluid phase of about 1.2.

Over the years the method of Uhlmann has been modified and improved by several authors. Some modifications have targeted the interpolation and spreading operations (Vanella and Balaras, 2009; Pinelli et al., 2010; Gsell and Favier, 2021). Other modifications have allowed to extend the stability limit to light particles (Kempe and Fröhlich, 2012b; Breugem, 2012; Schwarz et al., 2015). In particular, Tschisgale et al. (2017, 2018) introduced an interface layer with finite thickness to which the rigid body assumption is restricted. They also altered the order in which the equations are solved, leading to a more tightly coupled system. With this approach the authors showed improved stability even in the limit of vanishing particle mass. Using some of the ideas of Tschisgale et al. (2017), a simple modification to the original method of Uhlmann (2005), particularly efficient for neutrally buoyant particles, has been recently proposed (García-Villalba et al., 2023; Schenk et al., 2025).

Using IBM methods to perform PR-DNS simulations physical mechanisms related to the microscale flow can be clarified. For dilute systems, collisions are not very important and simple repulsion models (Glowinski et al., 1999) that ensure no overlap between particles are often employed. Perhaps the simplest dilute system of practical interest that can be studied with these methods is the gravity-induced settling of suspended particles in a quiescent, ambient fluid. For particles of spherical shape, the problem is governed by three parameters: the density ratio between the solid and the fluid phase, the Galileo number, which is a Reynolds number based on the gravitational velocity, and the particle volume fraction. Despite its simplicity, the problem is very rich due to the presence of collective effects. For some values of the parameters, clusters of particles are formed that have a significant impact on the settling velocity (Kajishima and Takiguchi, 2002; Uhlmann and Doychev, 2014). There is indeed experimental confirmation of this observation (Huisman et al., 2016). Also, while the particles settle, the surrounding fluid ceases to be quiescent and pseudo-turbulence is generated. The properties of this pseudo-turbulence remain largely unexplored and deserve further investigation. An additional aspect is that the shape of the particles has proven to have a significant impact on cluster formation, and consequently on the properties of the resulting macroscopic flow. It has been shown that cubes behave very much like spheres (Seyed-Ahmadi and Wachs, 2021) while spheroids have a stronger tendency to cluster formation (Fornari et al., 2018a; Moriche et al., 2023). For large aspect ratio, oblate spheroids tend to pile up (Fornari et al., 2018a), while for moderate aspect ratio the oblate spheroids have been shown to have longer interaction times compared to spheres (Moriche et al., 2023). For prolate spheroids, the results are still not conclusive (Lu et al., 2023; Jiang et al., 2024). A key difference between oblate spheroids, spheres, and cubes is that oblate spheroids do not rotate continuously, while both spheres and cubes do. This suggests that particle rotation may inhibit cluster formation to some extent. A complete understanding of the problem is not yet available, since the parametric space has been sparsely covered and therefore further studies are needed. For other applications of PR-DNS to dilute systems the reader is referred to a recent review (Chouippe et al., 2023).

For dense systems, the contact interactions between particles are increasingly important and deserve more attention (Wachs et al., 2023). Two aspects need to be considered: hydrodynamic interactions (lubrication) and solid–solid contacts. First, when two particles get close to each other, lubrication forces become significant, and they cannot be resolved by the numerical method. These effects may need to be included via sub-grid scale models or lubrication corrections to be added to $\boldsymbol{F}_{ext}$ and $\boldsymbol{T}_{ext}$ in Eqs. (21)–(22). Various lubrication models have been proposed in the literature (Kempe and Fröhlich, 2012b; Costa et al., 2015; Biegert et al., 2017; Jain et al., 2019). They are mainly based on lubrication theories based on the flow in the Stokes regime and the resulting forces that can be computed analytically or using asymptotic expansions. Despite significant advances in lubrication models, debates persist regarding their application within IBM frameworks. One major concern is that lubrication effects only become significant when particles are extremely close to each other, making it difficult to numerically disentangle these effects from the IBM forcing itself. Recall that the IBM forcing term is computed on a Lagrangian grid and then distributed to surrounding Eulerian cells, which in turn influences the hydrodynamic forces incorporated in the Newton–Euler equations of motion. Clarifying this interplay remains an open challenge that requires further investigation.

With respect to the modeling of solid–solid collisions, the literature on this topic is very extensive. There is a main distinction between soft-sphere collision models and hard-sphere collision models. In the latter, the collision is treated as an instantaneous event, the particles are assumed to be rigid and no overlap is allowed. The collision is resolved using impulse-based methods. At the moment of collision, an instantaneous change in momentum is applied to each particle based on conservation laws and a restitution coefficient, which quantifies the energy loss during the impact. Due to this simplicity, hard-sphere models do not capture the detailed physics of deformable contacts or simultaneous multi-particle interactions. As a consequence, they are not often used for dense systems. Instead, soft-sphere collision models are typically employed (Kempe and Fröhlich, 2012a; Kidanemariam and Uhlmann, 2014; Biegert et al., 2017). In this approach collisions are treated as continuous processes. When particles come into contact, they are allowed to slightly overlap. The overlap is used to calculate contact forces via spring–dashpot or viscoelastic models. The spring component represents elastic deformation, while the dashpot accounts for dissipative effects, capturing energy losses during the collision. Because the collision force is computed over a finite time interval, soft-sphere models require time-resolved simulations where the collision process is integrated alongside the overall dynamics, often requiring sub-stepping for improved accuracy. Other effects may be incorporated via the particle interaction terms, such as agglomeration and break-up, and these are the subject of intense research (Vowinckel et al., 2019, 2023).

5.1. Turbulent, particle-laden wall-bounded flows

In turbulent wall-bounded flows containing a dispersed solid phase, the key questions pertain to how turbulence is modulated and where the particles are transported. Among the various parameters governing the system, particle concentration — expressed as volume and/or mass fraction — plays a crucial role. In highly dilute systems, the global influence of the solid phase on the flow is negligible, allowing the focus to be solely on particle transport. Restricting on particles smaller than the characteristic hydrodynamic length scales, the problem was numerically addressed in the 1990s through direct numerical simulations employing the point-particle approximation in the one-way coupling regime. For a recent review, see Brandt and Coletti (2022). A key phenomenon in wall-bounded turbulence is the preferential transport of inertial particles towards the wall, driven by inhomogeneous turbulence, commonly referred to as turbophoresis (Marchioli and Soldati, 2002). As particle concentration increases, whether in terms of mass or volume, the impact of dispersed phase on flow becomes significant, requiring two-way or four-way coupling models. This introduces several critical challenges related to the small-scale modeling of particle dynamics and back-reaction (Gualtieri et al., 2015; Evrard et al., 2021; Balachandar and Liu, 2023). For instance, it remained unclear whether and under what conditions particles increase drag and/or enhance wall turbulence due to conflicting results. Over the past decade, particle-resolved direct numerical simulations (PR-DNS) have provided valuable insights into these cases. This technique enables a detailed simulation of all relevant scales in the physical process of particle-laden flows. However, since resolving the typical particle scale on the computational mesh requires approximately 10 or more grid points per particle diameter, PR-DNS of channel flows at low Reynolds numbers may involve a total grid point count reaching several billion (Prosperetti, 2015; Costa et al., 2021).

In turbulent channel flow with neutrally buoyant spherical particles, two key parameters govern the system: the volume fraction and the particle size relative to the wall viscous length (Picano et al., 2015). In viscous suspensions, the increase in apparent viscosity due to particle-induced stresses is well established (Stickel and Powell, 2005). However, even when this effect is incorporated by adjusting the effective Reynolds number, the dynamics of wall turbulence remains modified in the presence of particles of finite size, i.e., those larger than the viscous length (Costa et al., 2016). This effect is particularly relevant in high Reynolds number flows, where the viscous length is small. Under dense conditions, particle-induced stresses can dominate the overall dynamics, potentially reducing turbulent activity and turbulent Reynolds shear stress while still increasing total drag. In this regime, the suspension dynamics in channel flows deviates from conventional turbulence, exhibiting much slower dispersion rates, distinctive particle migration towards the bulk, and the formation of a particle layer near the wall. Given the moderate Reynolds numbers typically explored in current PR-DNS studies, the behavior at high inertia remains uncertain. In this regime, the classical Bagnoldian model — where particle collisions dominate — would traditionally be expected, yet recent studies have challenged this assumption (Hunt et al., 2002; Yousefi et al., 2023).

At the opposite limit, relatively dilute suspensions can consist of particles with a density much higher than that of the carrier fluid. In this regime, despite the low volume fraction — such that particle interactions are negligible and the fluid viscosity remains essentially unchanged — the mass fraction can be sufficiently high to modulate turbulence through the dispersed phase. Notably, particle back-reaction has been observed even at mass fractions on the order of 10^{-2}, leading to a 10% increase in overall drag (Peng et al., 2019; Costa et al., 2021). Analysis of PR-DNS data has revealed that the mechanism behind the observed drag increase differs significantly from that in concentrated suspensions. In this case, the particles are dilute but much denser and more inertial, which enhances the turbulent shear Reynolds stress of the suspension, leading to increased drag. Notably, the particle shear Reynolds stress exhibits a pronounced peak in the near-wall region, attributed to a combination of inertia and lift effects. This results in a drag increase greater than what would be expected based on dimensional arguments (Costa et al., 2021). Even under highly dilute conditions, discrepancies have been observed between PR-DNS results and predictions from standard point-particle simulations regarding near-wall particle dynamics (Costa et al., 2020). This highlights the need for further investigations into these configurations.

5.2. Future work

Regarding the open issues that will define the next challenges in numerical methods, physical understanding, and modeling, we can outline the following key points:

1. Compressible gas-particle flows introduce new physical phenomena, such as shock waves and acoustic waves interacting with particles. Despite their significance, only a few recent studies have explored these aspects in the context of PR-DNS (Capecelatro and Wagner, 2024). This highlights the need for further investigations to develop improved models that accurately capture shock–particle interactions, drag laws incorporating Mach number effects and collective behaviors.
2. Polydispersity is another aspect that has not been extensively investigated. Despite its importance in environmental and engineering applications, only a few studies have accounted for its effects (Fornari et al., 2018b; Rahmani et al., 2018). The preferential transport, collisions and close interactions in polydisperse systems pose a significant challenge, particularly for PR-DNS, due to the intrinsic variation in particle length scales that must be fully resolved.
3. All these features should be properly modeled within the Euler–Euler and Euler–Lagrange frameworks, which involve several unclosed terms, particularly in highly coarse-grained approaches such as Wall-Modeled Large Eddy Simulations (WMLES) and Reynolds-Averaged Navier–Stokes (RANS) methodologies (Johnson et al., 2020; Osnes et al., 2023). In these context the new tools provided by Artificial Intelligence can provide new opportunities in this field.
4. Lubrication–collision coupling in dense systems. The interplay between IBM forcing and lubrication physics at sub-grid separations remains poorly quantified. Future methodologies should integrate analytical lubrication solutions for gaps below $2\Delta x$, coupled with data-driven corrections for finite Reynolds number effects. Experimental validation to separate numerical artifacts from true near-contact dynamics in dense suspensions is highly desirable.
5. Multiphysics coupling. New applications require IBM extensions to solve coupled transport equations (e.g., species concentration, temperature). Developing conserved quantity exchange protocols at fluid–particle interfaces will be essential for simulating, for example, catalytic or reactive particles.

6. Multi-fluid models

6.1. Fundamental equations and closure models

The multi-fluid approach, which bases on an Eulerian representation of all phases, is frequently used to simulate multiphase flows involving bubbles, droplets or particles in medium and large domain sizes. The latter scales are typical for industrial processes such as bubble column reactors, stirred tank reactors, flotation cells, steel casting and nuclear reactor cooling systems, to name only a few examples. It allows to use relatively coarse numerical meshes, making it often the only feasible numerical approach. In the averaging procedures used to

obtain separate balance equations for each phase α, Eqs. (24)–(26), information about the precise location and shape of interfaces is lost and interpenetrating phases are assumed to be present with a certain probability.

The basic equations are the mass conservation

$$\frac{\partial r_\alpha \rho_\alpha}{\partial t} + \nabla \cdot (r_\alpha \rho_\alpha \boldsymbol{u}_\alpha) = \Gamma_\alpha, \tag{24}$$

and the momentum conservation

$$\frac{\partial r_\alpha \rho_\alpha \boldsymbol{u}_\alpha}{\partial t} + \nabla \cdot (r_\alpha \rho_\alpha \boldsymbol{u}_\alpha \boldsymbol{u}_\alpha) = -r_\alpha \nabla p + \nabla \cdot (2 r_\alpha \mu_{\alpha,eff} \boldsymbol{S}_\alpha) + r_\alpha \rho_\alpha \boldsymbol{g} + \boldsymbol{f}_\alpha + \boldsymbol{\Gamma}'_\alpha, \tag{25}$$

with the transfer terms

$$\boldsymbol{f}_\alpha = \sum_{\beta \neq \alpha} \boldsymbol{f}_{\alpha\beta}, \quad \Gamma_\alpha = \sum_{\beta \neq \alpha} \Gamma_{\alpha\beta}, \quad \boldsymbol{\Gamma}'_\alpha = \sum_{\beta \neq \alpha} \Gamma_{\alpha\beta} \boldsymbol{u}_{\alpha\beta}. \tag{26}$$

Here r_α, $\boldsymbol{u}_\alpha$, ρ_α, $\mu_{\alpha,eff}$, Γ_α, $\boldsymbol{\Gamma}'_\alpha$, $\boldsymbol{S}_\alpha$ and $\boldsymbol{f}_\alpha$ are the volume fraction, the velocity, the density, the effective viscosity, the mass source due to phase transfer between phase α and β, $\Gamma_{\alpha\beta}$, the momentum source connected to this mass source computed from the velocity of the reduced phase, $\boldsymbol{u}_{\alpha\beta}$, the stress tensor and the interfacial momentum transfer of phase α. p is the pressure and $\boldsymbol{g}$ the acceleration due to gravity.

All information on local structure of the interfaces and phase interaction (as $\boldsymbol{u}_{\alpha\beta}$ and $\Gamma_{\alpha\beta}$) has to be considered by closure models. Disregarding mass and heat transfer for now, such models are required for the momentum transfer between the phases, usually expressed in terms of bubble, droplet or particle forces and coalescence and breakup of the disperse entity. To account for the latter a coupling with a population balance model, e.g. the method of classes (Lehnigk et al., 2023) or method of moments (Passalacqua et al., 2018) is required. In addition the modification of the carrier phase turbulence needs to be considered in general.

The main issue of the approach concerns these closure models. There are many model proposals in literature and often such models include adjustable parameters. Many papers present model validations based on data from only one or a few experiments. To achieve good agreement with these data, in most cases a result-oriented selection of models and tuning of parameters is made. However, this leads to model setups that are hardly transferable to modified flow situations (i.e. geometrical variations or other boundary conditions) and limits the needed predictive capabilities. Suitable closure models should only depend on local flow characteristics. Therefore, the same closure models should also apply to flows within a certain parameter range of the local flow characteristics, regardless of the specific geometric configuration.

6.2. Baseline model development and validation framework

This consideration led to the proposal to establish baseline models. As part of this baseline strategy well-defined closure models including all parameters are tested on various data from experiments (Lucas et al., 2016). Such a baseline model was first developed and validated for bubbly flows (Rzehak et al., 2017). Later, the set of models was updated several times based on a well-defined strategy (Liao et al., 2018). Based on the multiphaseEuler solver module of the OpenFOAM Foundation software, simulation setups are collected and maintained in an open-source case repository containing more than 250 experimental datasets for various flow situations of bubbly flows (Hänsch et al., 2024). A fully automated workflow management has been established (Hänsch et al., 2021), which allows to simulate all these cases or subsets of them (in the standard validation run about 80 cases are used) in a reproducible manner. The workflow can be executed with one command, runs in a containerized environment, and creates a report from hundreds of results, including various plots of parameters (Lehnigk et al., 2023). The quality of the CFD prediction can further be quantified using a recently developed fuzzy logic controller operating on error metrics that describe the deviation of the CFD result from the experimental data. This allows a systematic comparison of the performance of the baseline model set with a modified model setup. The whole procedure, including the choice of criteria for the fuzzy logic controller, is still in its infancy, but modern AI tools make it possible to take model development and validation to a new level and are likely to boost the necessary consolidation of a reliable set of closure models for the multi-fluid approach.

In addition to the framework, the improvement and generalization of the closure models themselves is of course an important task. This should not only be driven by improving the agreement with experimental data sets, but should preferably be based on a better understanding of the local flow phenomena, relying on theoretical considerations, high-fidelity experimental data and direct numerical simulations (DNS). Here, improved measurement techniques and computational resources enabling DNS for increasingly complex multiphase flows, both combined with machine learning methods (Hessenkemper et al., 2024), will be the basis for strong progress in the years to come.

However, there is still a long way to go. To give an example, the lateral lift force on bubbles is crucial for the distribution of the bubbles e.g. at a pipe cross section or a bubble column. The widely used correlation by Tomiyama et al. (2002) was obtained for highly viscous systems (glycerol solution), in a linear laminar shear flow for a single bubble. This is far away from real flow situations. Recently, a correlation has been obtained for a bubble in water (Hessenkemper et al., 2021), but the other limitations remain. Shi et al. (2023) showed that the lift force coefficient is already significantly different when the main flow direction and the relative velocity are not parallel. It is very important to extend the available correlations for such flows, flows with non-linear shear and rotation, turbulent flows, bubble swarms and others. Similar tasks need to be solved for other bubble forces, coalescence and breakup models and turbulence modulation by bubbles. And, of course, the whole procedure has to be repeated for flows with droplets and particles.

6.3. Morphology-adaptive modeling approaches

In many medium and large scale industrial flows, the size of the interfaces varies over a wide range of scales. There may be very small droplets or bubbles at one end and large interfaces at the other. In addition, transitions between these different morphologies need to be considered, such as entrainment and detrainment processes. Typically, different numerical approaches are used for the different scales. While large interfaces can be treated in a resolved manner in one-fluid approaches such as Volume of Fluid (VoF) or Level Set methods, disperse phases are considered unresolved in the multi-fluid model. Mixed regimes or transitions between the scales are not captured. To overcome this limitations, there are a few proposals in the literature aiming to bring these two strategies together. Some of them are based on a combination of VoF-like methods with Lagrangian particle tracking, while others are purely based on the multi-fluid approach. Some of them use a two-field approach and a morphology-specific blending of closure models: AIAD (Höhne et al., 2020), FF-LIS (Mathur et al., 2019), others introduce more fields to strictly separate the different morphologies with their own set of conservation equations. Examples for the latter are GENTOP (Hänsch et al., 2012), GEMMA (Colombo et al., 2022), FF-LIS (Frederix et al., 2021), LBM (Mer et al., 2018) and MultiMorph (Meller et al., 2021). The Dresden6 group brings together a number of international organizations (Helmholtz-Zentrum Dresden-Rossendorf, University of Sheffield, VTT Technical Research Center, NRG Petten, Jožef Stefan Institute, University of Santa Catarina, Siemens Industry Software, Ansys Germany) working on such concepts with the aim of advancing and maturing the various approaches in a consistent way.

The MultiMoph model (Schlegel et al., 2023, 2024), see Fig. 6, is based on the multiphaseEuler module of the OpenFOAM Foundation software with a modification regarding the numerical scheme (compact

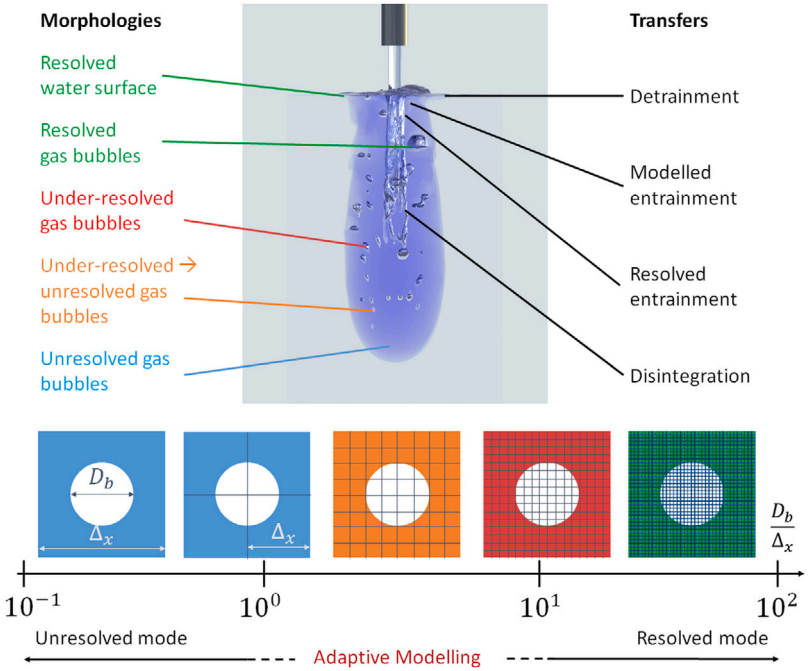

Fig. 6. Morphology-adaptive modeling of gas entrainment by plunging jet. Interfaces that are much larger than the grid size are resolved, while a statistical approach is used for interfaces smaller than the grid size. Adaptive modeling is used in between.

momentum interpolation). A consistent formulation of the drag and virtual mass forces is adopted to allow for a good representation of resolved interfaces between continuous phases. If the resolution is fine enough, the results, e.g. for the simulation of a resolved bubble, agree with VoF-like one-fluid methods, but having separated fields for the phases. If the resolution is too low, an under-resolution parameter is determined based on the local shear (Meller et al., 2023). This parameter is the basis to blend in a slip between the phases. If the bubble is represented only by a few grid cells, the gas will be transferred to the disperse gas phase. Recently, to capture the reverse scenario, a mass and bubble number consistent sub-model has been established to generate resolved bubbles out of the disperse gas phase in case of an over-resolution. Empirical transfer mechanisms such as entrainment and detrainment can be considered as well as numerically initiated transitions at regions with under- or over-resolution. One of the next steps will be the inclusion of wall film models. The MultiMorph model has been verified by numerous test cases and was also validated for some applications. However, even though the basic framework is now available as open-source code (Schlegel et al., 2024), there are still many open questions, especially regarding the consistent simultaneous modeling of empirical transitions, which represent a major challenge for the future work.

6.4. Future work

The main challenges for the further development of the multi-fluid approach are:

1. **Consolidation of closure models**. It requires generalized closure models that are applicable in a wider range of flow conditions and with a better physical basis. The development of new or improved models should be based on theoretical considerations, high-fidelity experimental data and DNS data. Modern IT-tools and machine learning methods are promising for progress.
2. **A generalization of the modeling to extend the applicability**. Since different morphologies can occur in one flow domain, and the morphology is often not known a priori, frameworks need to be established that can handle such situations. There are some promising methods under development, but it will be a long way to consolidate them together with appropriate transition mechanisms.

7. Population balance models for reactive multiphase flows

In the context of the multi-fluid models, described in the previous section, the phases are represented within an Eulerian framework, via volume fractions and mean velocities, as interpenetrating media. Governing equations, based on mass, momentum and energy conservation principles, are solved for each phase, and key terms in these equations are those quantifying the rate of exchange of relevant properties, namely mass, momentum and energy, between the involved phases. In the case of poly-disperse multiphase systems, where there is a continuous phase (gas or liquid) and one or multiple disperse phases (solid particles/crystals/aggregates, liquid droplets or gas bubbles) a key property in defining these rates of exchange (known as phase coupling terms) is the size distribution of the elements of the disperse phase (Buffo and Marchisio, 2014). This is the so-called particle or crystal size distribution (PSD or CSD), the droplet size distribution (DSD) or the bubble size distribution (BSD), depending on the multiphase system of interest (Marchisio and Fox, 2013).

These size distributions change with time in the multiphase systems, and with space, as they are often spatially heterogeneous, due to a number of phenomena, particularly relevant in the case of reactive multiphase systems and flows. Examples of these phenomena are: combustion processes and turbulent flames with (soot) particles formation (Pollack et al., 2019), reacting fluidized beds, reacting bubble columns and gas-liquid stirred tank reactors (Gemello et al., 2018; Maluta et al., 2021; Allio et al., 2023), multiphase packed-beds reactors and porous media (Crevacore et al., 2016; Messina et al., 2015; Icardi et al., 2023), reacting emulsions and liquid–liquid dispersions (Ferrari et al., 2023), as in the case of emulsion polymerization and food emulsions, and reactive crystallization (also known as precipitation) (Raponi and Marchisio, 2024; Para et al., 2022; Raponi et al., 2023a; Para et al., 2023; Morgeneyer et al., 2022).

In all these cases chemical reactions (or other physical phenomena, such as boiling) can generate the disperse phase. Solid crystals and particles, liquid droplets or gas bubbles can be formed spontaneously in what is known as nucleation, and the nucleation rate, often estimated by resorting to the classical nucleation theory, defines the rate with which these elements are formed per unit volume and unit time. Chemical reactions can moreover induce or enhance mass transfer between phases, enlarging or reducing the size of the elements of the disperse phase, resulting in what is known as continuous molecular growth (or shrinkage). Eventually chemical reactions, or other phenomena can induce aggregation or breakage of the elements of the disperse phase(s), resulting in their "discrete" size enlargement or reduction, with specific rates, often expressed in terms of "kernels", whose functional form is often derived, via a parallelism with the gas kinetic theory.

These phenomena, overall known as particulate processes, cause continuous and discrete changes of the above-mentioned size distributions, namely PSD, CSD, DSD, BSD, which can in turn be described by population balance equations (PBEs). The PBE is a continuity statement written in terms of these size distributions and it accounts for the effects of all these phenomena, all these particulate processes, classified as: continuous drift (molecular growth), zero-order (nucleation), first-order (breakage) and second-order (aggregation) (Soos et al., 2013) processes. In its mathematical formulation the PBE resembles the Boltzmann transport equation, derived in the context of statistical mechanics and kinetic gas theory, to describe molecular velocity distributions for systems far away from the Maxwell–Boltzmann equilibrium (Icardi et al., 2012), but also the Williams master equation for sprays or the Smoluchowski equation for colloidal systems (Shiea et al., 2020b).

Coupling strategies and numerical methods. Several strategies have been developed for the solution of this equation, in the context of computational fluid dynamics (CFD) multifluid models. These can be roughly classified into two categories: (1) on-the-fly/on-line coupling (Feng et al., 2023; Li and Marchisio, 2022; Li et al., 2021) and (2) off-line coupling (De Bona et al., 2016; Romano et al., 2023; Raponi et al., 2023b).

7.1. On-the-fly coupling

In the first category the PBE is solved together with the other governing equations within the numerical framework of the CFD code, very often based on the finite-volume method. For this strategy two main numerical methods have been proposed and have been used: the method of classes (MoC) and the method of moments (MoM) (Salenbauch et al., 2019). With the MoC the size distribution is discretized into finite "size bins" or "classes" and the PBE is transformed into a set of balance equations, quantifying the rate of appearance or disappearance, in each size class, of the number, volume or mass (per unit volume) of particles/crystals/droplets/bubbles belonging to that specific class. The method is quite intuitive and very robust, however it suffers from the fact that the overall size distribution range (or width) needs to be known a priory, that dealing with aggregation and breakage is not easy, and that the extension of the method to multi-variate problems, where not only size, but also other internal coordinates (e.g. composition or shape) are considered, is not easy.

With the MoM the PBE is broken down into a finite-set of transport equations for the moments of the size distribution, PSD, CSD, DSD or PSD, exactly as done with the Grad moment method (for molecular velocity distributions) in the context of the gas kinetic theory. The different moments of the size distribution have different physical meaning, depending on the details of its formulation. In general the moment of order zero represents the total particle/crystal/droplet/bubble number density, the moment of order one the total length density, the moment of order two and three are respectively proportional to the total surface area per unit volume and the total volume fraction of the disperse phase. Moreover ratios of these moments corresponds to different mean particle/crystal/droplet/bubble size. Namely the ratio between the moments of order one and zero is the number-averaged size, between three and two is the area-averaged size (or Sauter diameter) and between four and three is the volume-averaged size. The distance between these three characteristic sizes is a measure of how polydisperse the multiphase system is, as for a perfectly monodisperse system all the averages collapse into one single value! The MoM has the advantage of being generally cheaper than the other methods, as a small number of moments is required to describe the size distribution (i.e. typically no more than four or six) and no a-priori knowledge on the width of the size distribution is needed. However, the solution of the moments transport equation in CFD codes, based on the finite-volume method, requires the use of specific time and space integration and discretization schemes, that combine the efficiency of numerical CFD schemes and the preservation of the moments realizability (Shiea et al., 2020a; Li et al., 2019). In essence the introduction of these moments equations add more constraints for their numerical solution to the ones usually encountered in CFD (i.e. boundedness and stability).

Monokinetic versus polykinetic approaches. As already mentioned, with multifluid models the multiphase system is represented by a number of interpenetrating continua, one constituting the continuous phase and the other representing the disperse phase(s). Mass balance (continuity) and momentum balance equations are solved for each phase. If only one disperse phase is present (e.g. solid particle or crystals, liquid droplets or gas bubbles) the entire disperse phase can be represented by one single "phase" with one momentum balance equation attached. In this case all the elements of the disperse phase move with the same velocity, which is the average velocity. Alternatively (for relatively small Stokes number flows) one single momentum balance equation for the mixture of the continuous and disperse phase can be solved, and then the velocities of the two phases can be back calculated with an algebraic approach (Tronci et al., 2021). In both cases it is straightforward to assume that all the elements of the disperse phase move with the same velocity, this is called the monokinetic approach. Both with the MoC and with the MoM all the classes or all the moments move with the same average velocity. When the size distribution is however very wide it is more realistic to assume that elements of the disperse phase characterized by different sizes move with different velocities. This can be done in a number of different ways, will result in classes and moments moving with different velocities, and is usually called the polykinetic approach (Li et al., 2020; Buffo and Marchisio, 2014). Among different strategies it is worth mentioning the velocity polynomial approximation (VPA), employed in the context of the MoM, in which the size-conditional velocities are modeled with the velocity polynomial coefficients (VPCs) that can be in turn obtained from the moments themselves (Marchisio and Fox, 2013).

What are the typical pros and cons of the MoC and the MoM?

- MoC requires knowledge of the width of the size distribution whereas MoM does not
- MoC can be solved with standard time and space discretization and integration numerical schemes subjected to the usual boundedness and stability constraints, whereas the MoM requires the use of ad-hoc numerical schemes
- MoM usually can be employed with a very small number of additional transport equations (four or six) whereas the MoC requires more equations and results in larger computational times

Parallelization in HPC implementations and speed-up strategies. When dealing with real scale, industrial applications, of reacting multiphase flows, the necessity of accounting for detailed kinetics (as in combustion) (Salenbauch et al., 2017), co-existence of complex chemical equilibria (as in precipitation), cause a rise in computational costs that can be addressed only resorting to High Performance Computing (HPC) resources. It is also worth to mention that since most applications involve turbulent flows, a turbulent model needs to be used. In

the context of Reynolds-averaged Navier–Stokes equations (RANS) or Large-Eddy Simulation (LES) models (Maniscalco et al., 2021) a molecular mixing or micro-mixing model must be included (Marchisio and Fox, 2016). This causes an additional burden to the CFD calculation.

In this context the strategies adopted for parallelization are crucial. One standard strategy is to divide the computational domain into regions and assign each region to a parallel process and a specific core. Since however the reactive multiphase system is spatially heterogeneous, different phenomena characterized by different rates occur in different regions, resulting in a large load unbalance between the different parallel processes and corresponding cores. Since to move to the subsequent task, all the processes needs to be finished, typically one region constitutes the bottleneck, resulting in very inefficient parallelization, poor speed-up, bad scaling and unsatisfactory overall performances. To overcome this issue, together with another issue, related to the fact that the characteristic timescale for fluid physical transport might be very different from those of relevant particulate processes (i.e. nucleation, growth, aggregation and breakage), operator splitting (OS) can be adopted. OS integrates transport equations (for all the relevant properties) by separating each single time step (or iteration) in two parts: first physical transport is solved and then the particulate processes (i.e. nucleation, growth, aggregation and breakage) appearing in the source terms of the transport equations are solved. This decoupling allows to use large time steps, accelerate convergence, resulting in smaller computational times, but allows also to parallelize independently and synergistically physical transport (with a regional approach) and source terms for particulate processes. This results in much faster and more robust computations.

7.2. Off-line coupling

When the timescales associated with physical transport, namely the rate with which the phases move around in the multiphase systems, are very different from those associate with the particulate processes, namely nucleation, growth, aggregation and breakage, the off-line coupling method can be used. With these techniques (usually in the context of the multifluid models) CFD is used to determine the flow and turbulent fields in the multiphase systems, by adopting a first-approximation size distribution. These flow and turbulent fields are then employed to solve the PBE decoupled and separated from the main CFD code and the size distribution is determined. This is fed back to the CFD multifluid model and the process is iterated until convergence is reached. Several ways to solve off-line the PBE can be identified. They are listed and described below.

Volume-averaged models. When the timescales associate with physical transport are faster then those associated with particulate processes, or in other words mixing is faster than nucleation, growth, aggregation and breakage, a volume-averaged approach can be used. Very often the ratio between these timescales is referred to as the Damkhöler number (Marchisio, 2024). The PBE can, in fact, in this case, be averaged out resulting in a volume-averaged PBE, in which the particle/crystal/droplet/bubble size distribution depends only on time and not or space. This requires special attention to the source terms related to the particulate processes involved. In fact, the fact that mixing is faster than the particulate processes, implies that the size distribution is quite spatially homogeneous in the system, and does not change from point to point in the system, but it does not imply that the rate with which particles/crystals/droplets/bubbles nucleate, growth, aggregate and break, is spatially homogeneous. There will be likely regions where particles/crystals/droplets/bubbles nucleated, grow, aggregate or break more than in others. The volume-averaged PBE must be therefore properly solved.

Compartment models. In this second case the computational domain, representing the system/flow or reactor, is divided into compartments. The number of compartments can be freely defined by the modeler and can range from one (resulting in the volume-averaged model) to the number of cells employed in the finite-volume CFD simulation (resulting in the on-the-fly on-line coupling). The compartments are identified with different algorithms, such as the reactor network model of Fluent and the agglomerative-clustering of scikit-learn (Pedregosa et al., 2011). The general concept is to group together computational cells from the finite-volume CFD calculation which are neighboring and share similar values of specific flow properties. In the context of RANS/LES simulations this could be the value of the turbulent dissipation rate, which is the driving force for molecular mixing, particle/crystal/droplet/bubble aggregation and breakage, or of the concentration of a key chemical species, which is the driving force for the involved chemical reactions. This is schematically represented in Fig. 7. It is important to remind the reader that some fundamental questions still need to be answered, as the transport equations for the CFD multifluid model and the compartment model are not identical, as in the compartment model only convective fluxes are computed and no diffusion (either molecular not turbulent) is present.

7.3. Future work

Future work should focus on the main challenges related to the use of population balances in the context of multifluid models, namely:

1. Applicability of the closure models: the different particulate processes are described via rate equations and kernels that have limited applicability and contain empirical parameters.
2. Identification of the model parameters: the population balance model contains many unknown parameters which needs to be fitted with experiments. Novel and faster techniques for parameter identification needs to be developed and machine learning can be a game changer (Raponi and Marchisio, 2024).
3. More efficient parallelization and acceleration: simulations are still computationally very expensive and innovative strategies to make them faster are urgently needed.

8. Sub-grid scale modeling

Subgrid-scale models become necessary when essential features have length scales smaller than the grid size. Such features are common whenever interfaces are substantially deformed and break up, as is the case in atomizing flows. The pinching of thin threads (either liquid or gas) is known to occur in finite time as shown from the work of Eggers (1993). On the other hand topology change by the piercing or perforation of thin sheets is not occurring in finite time if a continuum sharp interface model is used. The sheet will simply stretch and thin indefinitely. Experimental observations (Opfer et al., 2014; Kant et al., 2023) show however hole formation and subsequent rapid expansion following the Taylor–Culick rim dynamics (Taylor and G.I, 1959; Culick, 1960). (For a discussion of the possible physical causes of breakup see Villermaux (2020) and Poulain et al. (2018).) The Taylor–Culick speed provides a convenient manner to estimate the sheet thickness h_c at breakup time. Perhaps surprisingly, this thickness is not nanometric, but much larger, on the scale of a hundred nanometers to a hundred microns depending on the flow. A much-studied example is a floating bubble, whose "death" has been abundantly studied starting with the work of Debrégeas et al. (1998). Other small structures arising in multiphase flow are thin thermal or mass transfer boundary layers, electrical double layers and Debye layers, compound droplets and so on. The dynamic contact line requires subgrid modeling whenever the grid is larger than the regularization scale of the singularity (Kulkarni et al., 2023) although it is beyond the scope of this paper.

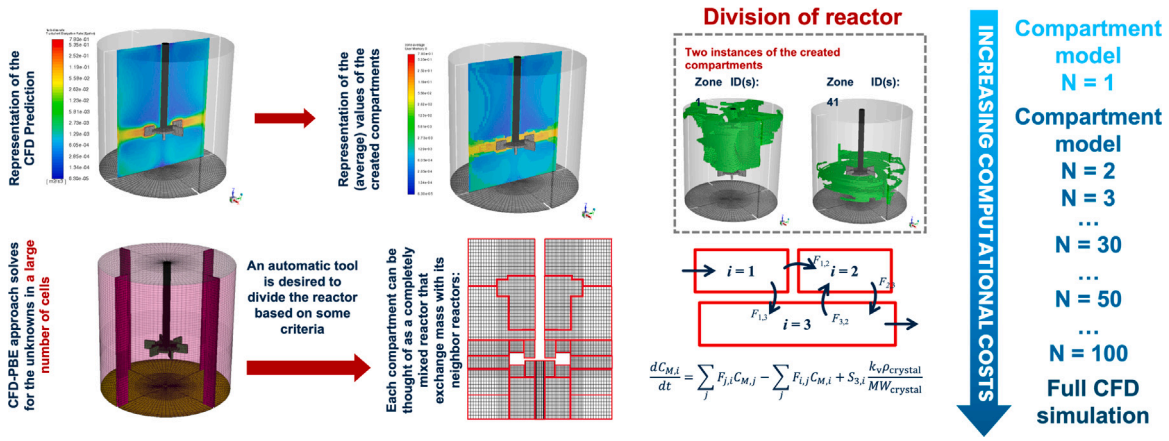

Fig. 7. Development of a compartment model. From one single CFD simulation by using different algorithms computational cells are grouped together in compartments, exchanging mass with each other, via convective fluxes. The modeler can freely set the number of compartments ranging from one (volume-averaged model) to a full CFD simulation.

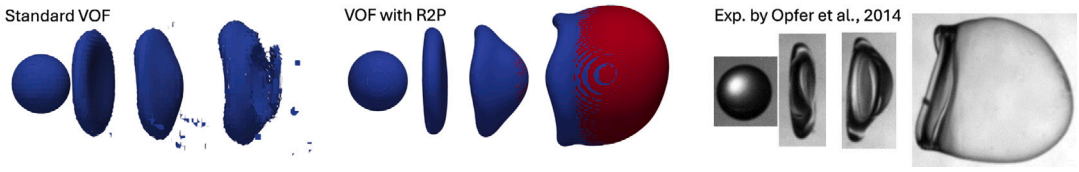

Fig. 8. Bag formation when a liquid droplet is exposed to a gas cross-flow at a Weber number of about 15: standard VOF with PLIC breaks up right away into meaningless droplets (left), while VOF with R2P preserves the thin liquid film without any spurious break-up as the film falls below the mesh resolution (middle), in agreement with experiments (Opfer et al., 2014) (right).

8.1. Topology changes

In most scenarios, Eulerian interface capturing methods such as VOF will exhibit mesh-dependent behavior when predicting topology changes: this is due to the mesh size providing a minimal length scale for interface folding below which topology change is triggered. This is most obvious in the case of bag break-up, wherein a fast gas penetrates a liquid structure and inflates a thin liquid film into a large bag-like shape. From theory and experimental observations, the thin liquid film is expected to have a thickness close to or below a micron by the time the bag breaks. In simulations, however, the bag always ruptures when the film reaches the mesh resolution. To address this issue head on, a new interface reconstruction method for geometric VOF called Reconstruction with 2 Planes (R2P) (Chiodi, 2020; Han et al., 2024a) was recently developed. As its name indicates, R2P represents the liquid–gas interface as two planes that co-exist within a single computational cell. In comparison to the widely used Piecewise Linear Interface Calculation (PLIC) (Youngs, 1982), this new algorithm greatly improves the accuracy of the reconstruction, in particular when dealing with thin structures such as films. The placement of the two planes requires the solution of a non-linear optimization problem in six dimensions, which can be solved efficiently thanks to an excellent initial guess formulated from transported surface data, and an efficient and mass-conserving distance-finding algorithm that accounts for two planes with arbitrary orientation. The ability of R2P to capture the formation and transport of SGS liquid films in a two-phase flow simulation is illustrated in Fig. 8: in that example, the droplet is discretized with about 20 cells per diameter, which means that the film thickness is orders of magnitude smaller than the mesh, yet no spurious break-up is seen with R2P.

Exploiting this SGS film capturing capability, Han and Desjardins (2024) introduced a SGS film break-up model. First, it is assumed that the film ruptures whenever its thickness falls below 2 μm, in accordance with experimental observations by Jackiw and Ashgriz (2022). When rupture happens, the SGS film retracts from its rim according to Taylor–Culick theory and sheds droplets, as described in the work by Wang and Bourouiba (2018). In the simulations, this is modeled by progressively converting the SGS film into Lagrangian droplets in a mass-conserving manner, using a recently proposed model for the drop size pdf (Jackiw and Ashgriz, 2022). Finally, the ligament break-up model of Kim and Moin (2020) is used to predict the outcome of the fragmentation of the left-over large rim. This strategy is demonstrated in Fig. 9 with the problem of a droplet at a Weber number of approximately 15 undergoing bag break-up in a cross-flow: a thin liquid sheet is formed, and bursts into $\mathcal{O}(10^4)$ droplets, while the rim forms a ligament that survives longer and undergoes a slower Rayleigh–Plateau break-up process. The modeled break-up process is in excellent qualitative agreement with experimental images by Opfer et al. (2014), and the resulting drop size pdf is found to be in excellent agreement with recent holographic measurements by Guildenbecher et al. (2017). Again, since the bag is entirely tracked at the sub-grid scale, a mesh size of only about 20 cells per drop diameter is sufficient to achieve convergence of the bag and drop statistics.

8.2. Manifold death

Various interface tracking methods react in different ways when the thickness of the sheet reaches a few multiples, typically two or three, of the grid scale. Typically, Level-Set methods evaporate the thin phase and lose the associated mass. This transformation is called numerical evaporation. Volume-of-Fluid methods conserve mass and thus transform the thin sheets into a complex array of ligaments and droplets as shown by Kulkarni et al. (2025). This transformation is called numerical breakup. The size of these ligaments and drops is related to the size of the sheet, which may lead to a population of droplets much larger than the physical ones if the numerical breakup of the sheet occurs for sheet thicknesses much larger than the ones observed in the experiments. Numerical breakup also prevents the observation of convergence of the PDF of droplet sizes, since refining the grid leads to a change in the droplet production after numerical breakup or evaporation. Upon grid refinement, Level-Set methods seem to converge to a limiting PDF *from below* as shown by Herrmann (2011), while VOF methods seem to converge to a limiting PDF *from above* as

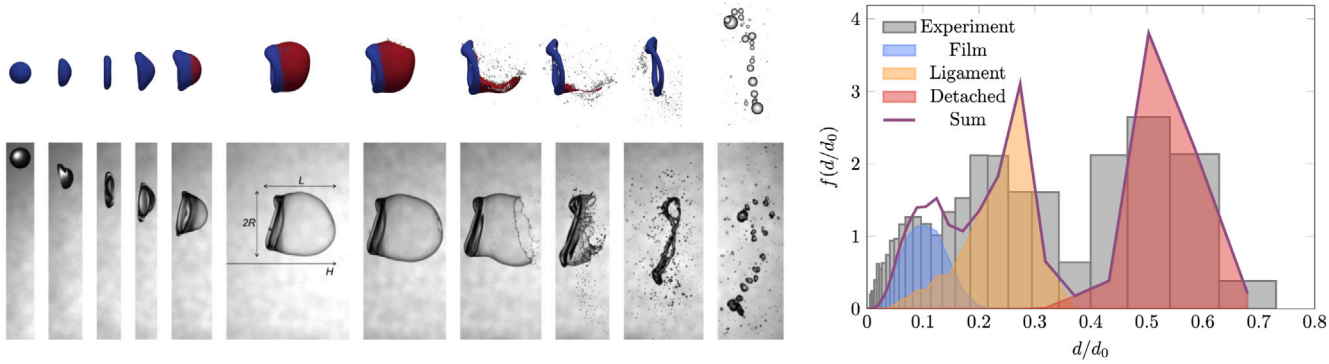

(a) Time sequence comparison: VOF with R2P and break-up model on top, experiments by Ofper et al. (2014) on the bottom

(b) Drop size pdf from simulation (purple line) and exp. by Guildenbecher et al. (2017) (grey bars)

Fig. 9. Bag break-up model based on R2P: (a) compares qualitatively the simulated film break-up with experimental images by Opfer et al. (2014), while (b) compares quantitatively the resulting droplet size distribution against measurements by Guildenbecher et al. (2017).

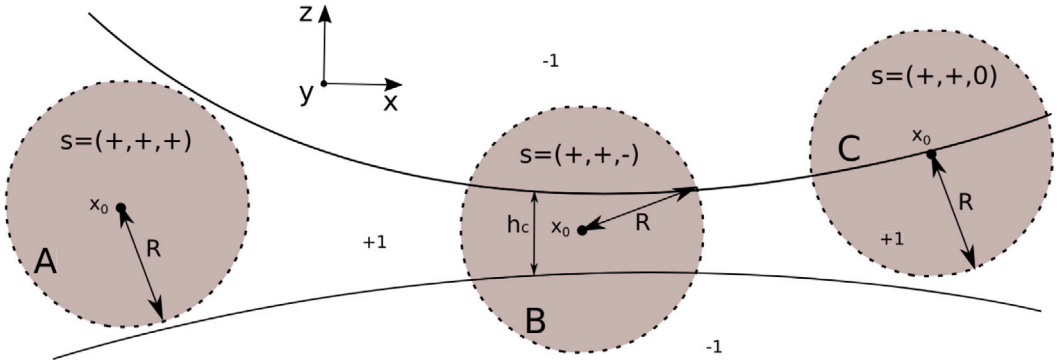

Fig. 10. Illustration of the signature method for a thin sheet.
Source: Reproduced from Chirco et al. (2022).

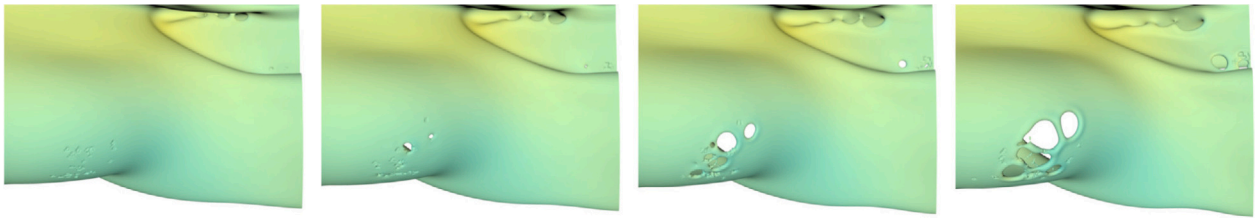

Fig. 11. Evolution of a thin sheet under the action of the Manifold Death algorithm. The holes shown are pierced at random in the regions detected by the signature method of Fig. 10.
Source: Reproduced from Chirco et al. (2022).

seen in the PDFs of Ling et al. (2017). This seems clearly caused by the mass loss in the Level-Set method and the mass conservation in the VOF method.

The Front-Tracking methods can maintain the existence of the thin objects indefinitely resulting in the absence of topology change and droplet production via hole perforation. To control these various thin-sheet-related unphysical numerics, a simple solution is to perforate a hole in the thin sheet when it reaches a specified *critical thickness* h_c. For Level-Set and Front-Tracking methods it is sufficient to arbitrarily change the phase of the sheet to the opposed phase in a region or ball of size ℓ_b. That size must be larger than h_c for the hole to expand rather than "healing" according to the energetic argument of Taylor and Michael (1973). In the Front-Tracking method, a more complex reconnection algorithm must be used to change the topology of the front. (For a description of how this can be performed, see Razizadeh et al. (2018).) The Front reconnection method has been used by Afanador et al. (2021) to study atomizing 2D flow. Droplet size PDFs where however not investigated using the Front-Tracking method. Controlled hole perforation for Volume-of-Fluid methods was first described by Chirco et al. (2022) who called it the Manifold Death (MD) method to emphasize that hole formation results in the quick disappearance of the thin sheet by Taylor–Culick expansion. The method allows to obtain convergence of the PDF in at least a range of droplet sizes. The method of Chirco et al. (2022) is based on the analysis of the topology of the neighborhood of a cell to detect various configurations of the phase distribution. This analysis is performed by the computation of a quadratic form, a CPU-efficient procedure that does not require complex analysis such as skeletonization. The signature of the quadratic form is then computed to distinguish the various configurations as shown on Fig. 10. The scale at which the quadratic form is computed controls the critical sheet thickness h_c for breakup. This thickness is approximately $h_c = 3\Delta_{MD}$ where Δ_{MD} is the octree grid size at which the quadratic form is estimated. The method was first tested on the *phase inversion problem*, a kind of atomization-in-a-box for which the droplet size distribution is known not to converge (Estivalezes

et al., 2022). A clear convergence of the PDF is seen. The method was subsequently tested by Tang et al. (2023) and Kulkarni et al. (2025) who also observe improvements in the convergence of the PDF, although at least in the case of Kulkarni et al. (2025). The number of droplets below the critical sheet thickness h_c also increases with grid refinement while keeping h_c constant. The method clearly needs improvement, which could simply be realized by a better control of the "hidden parameters" of the algorithm. Indeed the MD algorithm has a clearly defined parameter, the critical sheet thickness h_c and two less understood parameters, the time interval between attempts at hole formation, and the maximum number of holes perforated at this time step. Both of these parameters control the hole perforation frequency. It seems likely from the visualizations of Fig. 11 and from the excess of very small droplets that the perforation frequency is too high and should be somehow adjusted. A more complex improvement of the method would be to include some physical knowledge about the hole formation process. Both perspectives should lead to an improved capability of simulations to predict the droplet size distribution.

8.3. Future work

The main areas of future work can be categorized as follows

1. The R2P method could be supplemented with a Taylor–Culick rim retraction model and a ligament formation model.
2. Specific subgrid ligament models could be developed to supplement the subgrid liquid sheet R2P model.
3. The manifold death method requires numerous improvements. The main one is that the "hidden parameters" of the method are not well controlled. They should be tuned, or replaced by other controls, to limit the number of holes in any given bag or membrane, to match experimental observations. A first discussion of that can be found in Kulkarni et al. (2025).

9. Coupled multiphysics simulations

9.1. Fluid–solid with hydraulic fracturing and damage

Fluid–Structure Interaction (FSI) arises from the interaction between deformable solid structures and surrounding or internal fluid flows. This complex, non-linear phenomenon involves coupling fluid dynamics and solid mechanics through momentum exchange across evolving interfaces. Deformation of immersed structures alters these interfaces, tightly linking fluid and solid dynamics. Key challenges in modeling FSI include lubrication forces, solid–solid contact forces, and boundary layer dynamics near solid–fluid interfaces.

The complexity of the problem increases significantly when fracture mechanics is considered. For instance, predicting the initiation and propagation of cracks in airplane wings due to fatigue from aerodynamic forces, soil fracturing, erosion, planetary surface morphology and geotechnics. In the latter examples, the FSI problem is often complicated by a multiphase solid–liquid flow that acts on the solid structure.

To model FSI problems involving flow-induced fracturing, it is crucial to consider fluid dynamics, solid mechanics, and fracture mechanics simultaneously making it a very complex task from theoretical and numerical point of views.

Numerous attempts have been made to tackle the problem numerically (Wang et al., 2023; Zhang et al., 2023; Nguyen and Indraratna, 2020; Yang et al., 2024; Dalla Barba et al., 2022). Among them, popular and innovative techniques are based on the so-called Enriched (or Extended) Finite Element Method (XFEM), Phase Field Method (PFM), Distinct Element Method (DEM) and peridynamics (PD). These are often coupled with simplified fluid models to account for hydraulic stresses and lubrication forces. Typically, Poiseuille or cubic laws are used to describe the flows in thin fractures together with Darcy law to account for the leakage fluxes into the porous matrixes generated by fracture networks.

XFEM (Moës et al., 1999) was initially developed to solve problems where localized features cannot be efficiently resolved by mesh refinement. The basic idea is to enhance the standard polynomial nodal shape functions used in classical finite element modeling with appropriate discontinuous basis functions for nodes belonging to elements that intersect a crack or other localized discontinuous features, such as voids or inhomogeneities (Wang et al., 2023; Shi and Liu, 2021; Jafari et al., 2021; Yoshioka et al., 2019). The technique has been used to simulate laminar flow in fractures, also representing non-planar 3D cases and the interference effect of multiple fractures and fracture propagation. On the other hand, PFM has become quite popular for describing cracks and differs from other numerical methods in that a scalar field is used to solve the diffusion equation to characterize crack growth. In PFMs minimizing the total energy function of cracked solids is the basis. The elastic strain energy is divided into tensile and compressive parts. The crack propagation process is dominated by tensile strain, that is, tensile strain energy drives the phase field evolution (Zhang et al., 2023; Xing and Zhao, 2023; Ambati et al., 2015). The technique has been used to capture complex fracture behaviors also with different level of saturation.

The Discrete Element Method (DEM) (Cundall, 1971) is widely used for simulating discontinuous solid media, such as rock aggregates, by dividing them into finite-size polyhedral or spherical blocks. Each element's mechanical behavior is typically resolved using Newton's equations for rigid body motion, though deformability and complex behaviors can be included by coupling DEM with the Finite Element Method (FEM). Contact-force models handle interactions like impact forces, Coulomb friction, and lubrication. Coupled DEM-Navier–Stokes models simulate multiphase flows with discontinuous solids, such as sand with fluids (Nguyen and Indraratna, 2020; Damjanac and Cundall, 2016; Yan et al., 2016). However, DEM requires prior knowledge of block shapes, affecting system response, and cracks can only form between distinct elements, not within a single block, following solid–solid contact regions.

Peridynamics (PD) has also been recently employed to numerically tackle the fluid-induced fracture problem. Peridynamics relies on a novel theory of solid mechanics based on integral equations (Silling, 2000). In peridynamics, a solid is represented as a set of Lagrangian particles mutually interacting though short-range, micro-potentials and fracture mechanics is intrinsically accounted for within the theory by deactivations of pair interactions. This reformulation of continuum mechanics provides a robust mathematical framework that inherently incorporates discontinuities such as cracks, unlike traditional continuum mechanics approaches that require supplementary criteria and adjustments to handle these phenomena. This relies on the major advantage of peridynamics: it can reliably account for crack formation and propagation without the need for empirical models. By avoiding the latter, peridynamics eliminates many of the uncertainties and assumptions that can compromise the reliability of conventional fracture mechanics, leading to more precise and dependable results in various engineering applications, from aerospace to geotechnics. Some innovative approaches have been recently using peridynamics to tackle fluid induced fracture problems (Yang et al., 2024; Dai et al., 2023; Dalla Barba and Picano, 2021; Dalla Barba et al., 2022). In particular, the major advantage of such approaches relies on a accurate description of fluid mechanics even in interstitial cavities by directly solving Navier–Stokes equations or by using a Spherical Particle Hydrodynamics (SPH) approach together with Immersed Boundary Methods (IBM). These methods have also the possibility of a simpler description of a resolved particle-laden multiphase flow interacting with the solid structures (Dalla Barba et al., 2022).

To conclude, in perspective, these models offer significant contributions to advancing our ability to numerically address fluid-induced fracturing. Different examples demonstrate their broad applicability,

ranging from predicting crack formation and propagation due to fatigue in aircraft wings to addressing geotechnical and environmental processes such as soil fracturing, erosion, and fracking. In geotechnics and environmental engineering, these models can simulate soil fracturing and erosion processes, which are essential for understanding and mitigating land degradation and instability. For instance, predicting how soil fractures under various environmental conditions can help in developing effective erosion control measures and maintaining soil health. It should be noted that in these applications the flow is often laden of particles that directly interact with the solid structure, i.e. soil or porous media. This critical aspect represents a challenging task for accurate scale-resolved numerical algorithms and simulations. Overall, these numerical models are indispensable tools in a wide range of engineering applications, offering the potential for more efficient, safe, and environmentally responsible practices and for developing reliable large-scale models.

9.2. Surfactant-laden interfaces

Surface-active agents, or 'surfactants', are chemicals that adsorb at interfaces lowering the interfacial tension. Surfactants and their applications abound in industrial, environmental, and daily-life settings (Manikantan and Squires, 2020). They are central to detergency, cleaning, decontamination, and personal care products as emulsifiers and foaming agents (Eggleton and Stebe, 1998). Surfactants also feature in inkjet printing (Lohse, 2022), agrichemical applications as pesticide chemicals, in paints and coating flows, in enhanced oil recovery and oil spill clean-up operations, and in biomedical applications wherein they are delivered to the airways of neonatals to counteract Respiratory Distress Syndrome (Rosen and Kunjappu, 2012; Myers, 2020). In environmental applications, surfactants influence bubble bursting through interfaces (Constante-Amores et al., 2021; Pico et al., 2024), which leads to aerosol formation, and affect breaking (Deike, 2022) and smoothing (Lohse, 2023) of ocean waves; the latter highlights the crucial role of Marangoni stresses brought about by surface tension gradients induced by variations in the surfactant interfacial concentration. For an excellent summary of studies featuring the effects of surfactants on interfacial flows over the past five decades (see Farsoiya et al. (2024) and references therein).

Tackling multiphase flow problems featuring surfactant-laden interfaces involves solving the following equations for the interfacial surfactant species, Γ, and bulk concentration, C_b:

$$\frac{\partial \Gamma}{\partial t} + \nabla_s \cdot (\Gamma \mathbf{u}_t) = D_s \nabla_s^2 \Gamma + j_n, \qquad \frac{\partial C_b}{\partial t} + \mathbf{u} \cdot \nabla C_b = D_b \nabla^2 C_b, \tag{27}$$

where $\mathbf{u}_t = (\mathbf{u}_s \cdot \mathbf{t})\mathbf{t}$ denotes the tangential velocity vector wherein $\mathbf{u}_s$ represents the surface velocity at the interface and $\mathbf{t}$ is the unit vector tangent to the interface; D_s is the surface diffusion coefficient, D_b denotes the surfactant diffusivity in the bulk, and j_n is the mass flux exchange between the bulk and the interface related to the diffusive flux via (Eggleton and Stebe, 1998):

$$j_n = k_a C_s(\Gamma_\infty - \Gamma) - k_d \Gamma = -D_b \mathbf{n} \cdot \nabla C_b|_{\text{interface}}, \tag{28}$$

where k_a and k_d are the adsorption and desorption coefficients, respectively, C_s is the surfactant bulk concentration in the region immediately adjacent to the interface, and Γ_∞ is the interfacial surfactant concentration at saturation. For a soluble surfactant, bulk-interface equilibrium leads to $j_a = j_d$ and $j_n = 0$. A modified Langmuir–Szyszkowski equation of state is used for $\sigma = \sigma(\Gamma)$: (Shin et al., 2018; Muradoglu and Tryggvason, 2014): $\sigma = \sigma_{cl}\left[1 + \frac{\mathcal{R}T\Gamma_\infty}{\sigma_{cl}} \ln\left(1 - \frac{\Gamma}{\Gamma_\infty}\right)\right]$, where σ_{cl} is the interfacial tension of the surfactant-free interface, $\mathcal{R}$ is the ideal gas constant, and T is the temperature. Soluble surfactant simulations are initialized with a bulk concentration C_∞ in equilibrium with an initial surface coverage, Γ_0, set as a parameter and C_∞ is then obtained

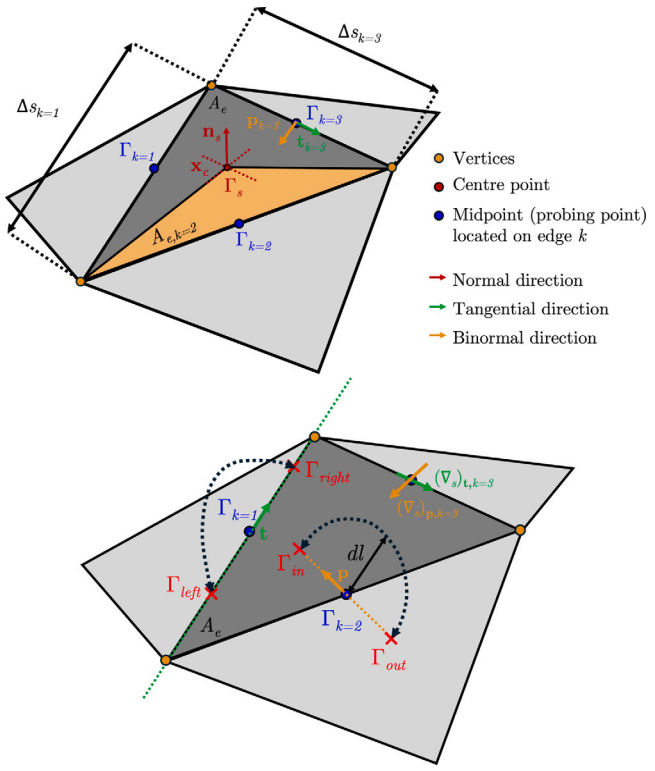

Fig. 12. Lagrangian triangular surface element: (a) depicts the normal, binormal, and tangential vectors to the interface, edge lengths and sectional area $A_{e,k}$, and the central ($\mathbf{x}_c$) and edge (k) midpoint values; (b) depicts the direction of the surface gradients at an edge showing the probing technique in the tangential and binormal directions. *Source:* Adapted from Shin et al. (2018).

from Eq. (28) by setting $j_{a/d} = 0$ and solving for $C_s = C_\infty$. When modeling insoluble surfactants, we set $j_n = 0$ in Eq. (27).

Farsoiya et al. (2024) have highlighted the need for a robust numerical technique for high-fidelity simulations of complex interfacial flows whilst accounting for surfactant transport at deforming interfaces that can undergo topological transitions; examples of the latter include the breakup and coalescence of bubbles and drops, and the fragmentation of jets. A number of techniques have been used to this end, which include algebraic (Antritter et al., 2024) and geometric (James and Lowengrub, 2004) VoF approaches with structured and unstructured adaptive mesh refinement, phase field (Teigen et al., 2011) and hybrid algebraic (Cannon et al., 2024) and geometric (Farsoiya et al., 2024) methods, front-tracking (Muradoglu and Tryggvason, 2014) and level set (Atasi et al., 2018) techniques, and hybrid level sets and front-tracking methods (Shin et al., 2018).

One way to solve the above equations is by using the interface tracking methodology discussed in Section 4 as outlined in the work of Muradoglu and Tryggvason (2014) and Shin et al. (2018). In particular, for surfactant-laden interfaces, the surface force $\mathbf{F}_\sigma = \mathbf{F}_n + \mathbf{F}_s$ appearing in the Navier–Stokes equations (see Section 4) incorporates capillary and surfactant-induced Marangoni-driven forces, $\mathbf{F}_n$ and $\mathbf{F}_s$:

$$\mathbf{F}_n = \int_{A_e} \sigma\kappa\mathbf{n}\delta(\mathbf{x} - \mathbf{x}_s)\mathrm{d}A = \sigma\kappa_H \nabla\mathcal{H}, \qquad \mathbf{F}_s = \int_{A_e} \nabla_s\sigma\delta(\mathbf{x} - \mathbf{x}_s)\mathrm{d}A. \tag{29}$$

The treatment of $\mathbf{F}_n$ was dealt with in Section 4. The evaluation of $\mathbf{F}_s$ commences by resolving $\nabla_s\sigma$ into its binormal, $\mathbf{p}$, and tangential, $\mathbf{t}$, components:

$$\nabla_s\sigma = (\nabla_s\sigma)_\mathbf{p}\mathbf{p} + (\nabla_S\sigma)_\mathbf{t}\mathbf{t}. \tag{30}$$

To compute $\mathbf{F}_s$, Eq. (30) is re-expressed as follows

$$\mathbf{F}_s = \sum_{k=1}^{3}[(\nabla_s\sigma)_{\mathbf{p},k}\,\mathbf{p}_k + (\nabla_s\sigma)_{\mathbf{t},k}\,\mathbf{t}_k]\delta(\mathbf{x} - \mathbf{x}_k)A_{e,k}, \tag{31}$$

where $A_{e,k}$ denotes one-third of the triangular interfacial element's area, bounded by two vertices and the center point, $\mathbf{x}_c$, as shown in Fig. 12(a). The surface tension gradients $\nabla_s\sigma$ can be recast in terms of $\nabla_s\Gamma$ using the Langmuir–Szyszkowski equation of state, and Fig. 12(b) demonstrates the 'probing' procedure used to compute $\nabla_s\Gamma$; further details are in the work of Shin et al. (2018). Lastly, the ghost fluid method can be used to treat the flux term j_n.

The reader is also referred to the recent paper of Farsoiya et al. (2024) who have solved the equations governing the dynamics of surfactant-laden interfaces using a promising approach which combines geometric VOF and the phase field method. This technique was used to demonstrate the reduction in the terminal velocities of rising bubbles due to surfactant-induced Marangoni stresses for the case of insoluble surfactants. Farsoiya et al. (2024) also showed that Marangoni effects can lead to a transition from spiraling to zig-zagging rise trajectories depending on the values of the Bond and Galileo numbers that characterize the system dynamics in agreement with experimental observations.

9.3. Future work

The main challenges related to the coupled multiphysics simulations are:

1. Concerning fluid–structure fracturing problems, sub-models for the unresolved viscous flow entering into a propagating crack should be developed in order to accurately represent this complex phenomenon
2. Multiscale models for hydraulic fracturing should be developed in order to be incorporated in large-scale simulations involving porous media fracturing, particle/aggregate break-up, erosion processes which often occur in environmental and industrial problems
3. Future work in surfactant-laden interfacial flows will focus on developing predictive models for flow dynamics above the critical micelle concentration and wherein interfacial viscous effects play an influential role. Furthermore, incorporating the influence of surfactants on contact angle hysteresis will help to develop models of contact line motion that account for local surfactant concentration arising from local sorption kinetic processes. These advances will bring the current state-of-the-art closer to being able to address industrial challenges.

10. Data-driven models for multiphase flows

The past decade has witnessed an increase in the use of machine learning (ML) algorithms in making predictions in various branches of science and engineering. These algorithms have also found use in fluid mechanics, although the focus has been mainly on single-phase flows rather than two- and multiple-phase flows, as highlighted by recent reviews (Brunton et al., 2020; Wang and Wang, 2021; Zhu et al., 2021). Since then, a number of papers have been published on machine learning in multiphase flows; we provide a brief summary of some of these papers with a focus on modeling and prediction.

Traverso et al. (2023) developed a data-driven surrogate model for rapid estimates of drop size distributions (DSD) of sprays and dispersed flows from control parameters such as fluid properties and flow rates, and geometrical designs, e.g., nozzle diameter and spray angle. The DSD is inferred by combining observations of its integrals and first moments values for a set of drop diameters. This is done by training a Gaussian Process regression model on data from numerical simulations of sprays obtained using Basilisk (Popinet, 2009) and by assuming that the prior distribution of observations also follows a Gaussian distribution. Following model training, the optimized model was used to predict the DSD (see Fig. 13), and the model covariance enabled the design of further 'experiments' (physical or numerical), to minimize uncertainty.

Cundy et al. (2024) used physics-informed ML to predict drop breakup in two-phase flows, accounting for local and instantaneous information on interfacial geometry and flow fields. The models were trained on high-fidelity simulation of three-dimensional Taylor–Green vortices and homogeneous isotropic turbulence and provided accurate and efficient predictions of the breakup probability and DSDs. The results of this work could be embedded within large-scale simulations to improve their accuracy and computational efficiency. Cahaly et al. (2024) developed a ML model, PLIC-Net, for accurate reconstruction of interfaces in two-phase flows within VOF methods that would otherwise have required the use of costly complex optimization algorithms and heuristics. PLIC-Net employed feed-forward deep neural networks which were trained on a broad range of interfacial shapes generated analytically from randomized paraboloidal surfaces. The PLIC-Net predicted the normal vectors to the interface accurately and provided more efficient interfacial reconstruction than traditional alternatives such as LVIRA and ELVIRA.

Liu et al. (2024) developed an unsupervised parameterized physics-informed neural network (P-PINNs) for the solution of the flow past a spinning sphere in uniform flow. This study was motivated by the need to circumvent computationally expensive CFD simulations for various combinations of parameters. The P-PINNs model was trained using random sampling points within the flow domain and boundary conditions and predicted the flow field accurately and efficiently (as benchmarked against particle-resolved direct numerical simulations) whence the drag, lift, and torque on the sphere were calculated. Elmestikawy et al. (2024) used particle-resolved direct numerical simulation data to train graph neural networks (GNNs) to learn the pairwise interactions of neighboring particles in Stokes flow; this is in an effort to overcome the failure of traditional models that do not account for drag variations on particles in random arrangements. The data from GNNs were converted to algebraic expressions that facilitated 'interpretability' of the ML model and enhanced its computational efficiency. The accuracy of the GNN-based model ranged from 74% to 84.7% as benchmarked against particle-resolved simulations.

ML models were also developed by Cheng et al. (2024) to predict the spatiotemporal dynamics of multiphase compressible flows using a physics-aware recurrent convolutional (PARC) neural network. PARC was trained using simulations of the Burger's equation, of flow past a cylinder, and of interactions with particles featuring shocks. The results of Cheng et al. (2024) have demonstrated that PARC can provide accurate flow characteristics and is capable of capturing transient features and sharp gradients with a significant reduction in computational cost as compared to traditional CFD approaches based on DNS.

Lastly, Basha et al. (2024) highlighted the work of a multi-university collaboration that brought together multi-physics and ML modeling as well as experiments to provide accurate, reliable, and efficient predictive capabilities for a wide range of multiphase flows. The programme demonstrated the use of Bayesian regularized artificial neural networks, extreme gradient boosting for drop formation prediction in microfluidic channels, generalized latent assimilation for predictive models of drop coalescence, and design of experiments for the optimization of lipid nanoparticle synthesis in microchannels. Gradient boosting machines were also used to invert acoustic emission signals for fluidized beds particle size distribution characterization, and a sub-sampling based adversarial neural network was used to predict slug flow dynamics in long horizontal pipelines. Lastly, long short-term memory networks were employed for predicting mixing performance in stirred and static mixers, and active learning via Bayesian optimization was used to recover coalescence model parameters with applications in green hydrogen electrolyzers.

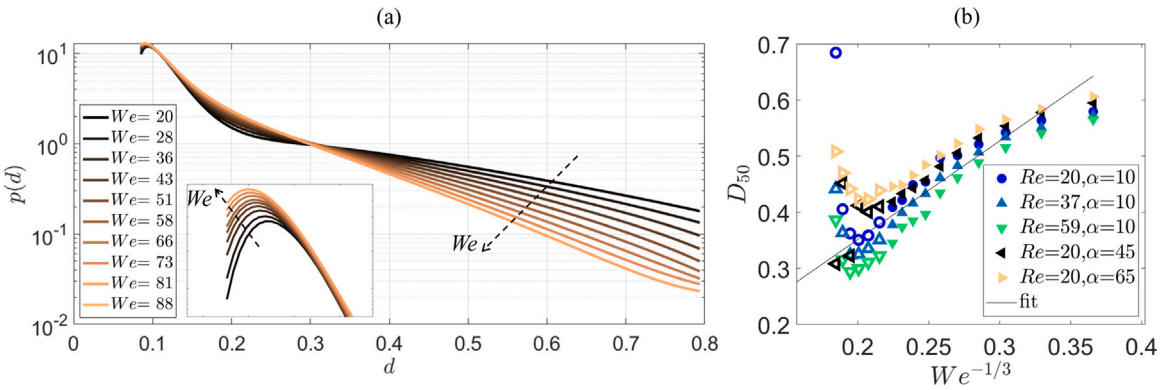

Fig. 13. (a) DSDs predicted by the GPR-based method for various We with the inset showing an enlarged view of the peaks for small d; (b) volume mean diameter D_{50} vs $We^{-1/3}$ for various α and Re.
Source: Reproduced from Traverso et al. (2023).

10.1. Future work

1. The method of Traverso et al. (2023) highlighted above can be readily applied to other multiphase flows whose features can be characterized by a probability density function that varies with changes in global, control parameters. These flows include drop size distributions in mixer-settler tanks and static mixers and bubble size distributions in chemical reactors, which are used in the energy, manufacturing, and pharmaceutical industries.
2. A future research avenue should focus on the creation of an autonomous optimization framework for multiphase flows that integrates CFD simulators with data-driven surrogate models, and analytical and/or statistical models into a single predictive flow emulator within an optimization workflow (that also includes geometry optimization). Within such a framework, the optimization algorithm learns from information/data provided by the emulator and adjusts its parameters as necessary. Critically, this algorithm should select the fidelity level (from high-fidelity, expensive CFD simulations to low-fidelity, cheap data-driven model predictions) for efficient exploration of the relevant design spaces. Use of Deep Reinforcement Learning lends itself naturally for use as an outer-loop for the optimization framework.
3. Future ML modeling of multiphase flows should make use of Explainable AI techniques such as SHapley Additive exPlanations (SHAP) to explain the features underlying an ML model and elucidate the mechanisms underlying its decision-making processes. The work of Hu et al. (2024) provides an example of using SHAP to interpret the decisions of ML models used to predict drop coalescence in microfluidic devices.

11. Other topics

In this section, we briefly comment on topics that have not been covered in the sections above.

- **Contact line methods.** Static contact lines have been covered for quite a while. In level-set methods, the boundary condition $\nabla\phi \cdot \mathbf{n_S} = \cos\theta$ where $\mathbf{n_s}$ is the normal to the solid gives good results. In dynamics situations the methods are more complex. Recently both Navier slip boundary condition (Fullana et al., 2020), the Generalized Navier Slip Boundary Condition (Qian et al., 2003; Gerbeau and Lelievre, 2009; Fullana et al., 2024) and the superslip condition (Devauchelle et al., 2007; Kulkarni et al., 2023) have been advocated. The phase field and the sharp interface approaches have been compared to each other and to molecular dynamics (Lācis et al., 2022; Fullana et al., 2025). Finite element methods have also seen interesting advances (Liu et al., 2016; Diddens, 2017; Sprittles, 2015).
- **Phase change and boiling.** Phase change implies often a volume source in the form $\nabla \cdot \mathbf{u} = (\rho_g^{-1} - \rho_l^{-1})\dot{m}\,\delta_I$ where $\dot{m}$ is the mass per unit interface area changing phase. It has been coupled with sharp interface methods (whether level-set, front-tracking or VOF) in several distinct ways, which mostly differ in the manner in which the singular volume source is treated, see Long et al. (2024), Darshan et al. (2024), Cipriano et al. (2024), Long et al. (2025) and references therein. Phase field models may also be used for phase change in which case the singularity is relieved at the cost of the additional computational expense caused by the finite thickness interface.
- **Three-phase and n-phase flow**. This topic has also witnessed some recent progress. In particular, modeling three-phase or n-phase flow with surface tension effects has been investigated in detail only recently (Zhao et al., 2024; Maës et al., 2025).
- **Cahn–Hilliard and Van der Waals methods.** Most of this review addresses Allen–Cahn type diffuse interface methods. Many multiphase flow problems have been investigated using Cahn–Hilliard type (Carlson et al., 2011) and Van der Waals type methods (Laurila et al., 2012; Zhao et al., 2023).
- **Improvements in surface tension methods.** Recent work (until 2018) is summarized in Popinet (2018). Popinet and coworkers have pursued "integral methods" which are both momentum conserving and well-balanced. Better representation of Marangoni stresses may also be obtained by these methods. References can be found in Saini et al. (2025). Denner and coworkers have investigated implicit surface tension methods, that address a critical issue, such as the small time step of explicit methods (Denner et al., 2022).
- **Energy stable methods.** Energy stability is a technique for achieving numerical stability by conservation of the energy in the time and space discretized equations. It is often realized by using skew-symmetric schemes. This approach has probably not been sufficiently tried for multiphase flow, despite some interesting recent work by Fuster (2013) and Nordström and Malan (2025).
- **Elasto-visco-plastic multiphase flows.** have seen a burst of activity using various methods, phase field, finite element or VOF, see for example Zinelis et al. (2024), Dixit et al. (2025), Deoclecio et al. (2023), and Balasubramanian et al. (2024).
- **Particle methods.** We have been relatively silent about methods such as Smoothed Particle Hydrodynamics or lattice Boltzmann, although these have enjoyed success in sloshing studies (Colagrossi et al., 2010; Calderon-Sanchez et al., 2021) and boiling (Das and Das, 2015).

12. Closing remarks

The field of multiphase flow modeling is undergoing a transformative phase, driven by the complexity of real-world applications and the increase of computational resources. Recent advances in numerical methods for multiphase flow have markedly improved our ability to simulate complex interfacial dynamics and multiscale phenomena. Yet, significant challenges remain in faithfully capturing the intricate evolution of interfaces during processes such as breakup, coalescence, and topology changes. Many established approaches — ranging from Volume-Of-Fluid and Level-Set methods to Front-Tracking and diffuse-interface schemes — still rely on approximations that restrict their accuracy and lead to grid-dependent behavior. In particular, the treatment of subgrid-scale physics, interfacial instabilities, and non-equilibrium phase-change processes often requires further refinement. These limitations underscore the need for higher-order reconstruction techniques, robust integration schemes, and advanced subgrid models that can more accurately bridge the gap between microscale physics and macroscopic flow behavior.

Looking ahead, the community must focus on developing unified, adaptive frameworks that combine the strengths of physics-based modeling with emerging data-driven and machine learning approaches. Such integrated methods promise to enhance the predictive capabilities of multiphase flow simulations by providing robust closure models informed by high-fidelity experimental data and direct numerical simulations. Moreover, ensuring computational efficiency and scalability — especially as we approach the exascale computing era — remains a critical issue; novel algorithms and optimized parallel implementations will be required to fully exploit the architectures of future supercomputers. Future research should target the coupling of microscale interfacial phenomena with macroscale dynamics, enabling simulations that are both computationally efficient and physically accurate. These endeavors will be essential for overcoming current bottlenecks and will pave the way for next-generation simulations capable of reliably tackling the complexities of industrial and natural multiphase systems.

CRediT authorship contribution statement

Manuel Garcia-Villalba: Writing – original draft. **Tim Colonius:** Writing – original draft. **Olivier Desjardins:** Writing – original draft. **Dirk Lucas:** Writing – original draft. **Ali Mani:** Writing – original draft. **Daniele Marchisio:** Writing – original draft. **Omar K. Matar:** Writing – original draft. **Francesco Picano:** Writing – original draft. **Stéphane Zaleski:** Writing – original draft.

Acknowledgments

AM gratefully acknowledges Dr. Makrand Khanwale and Mr. Henry Collis for proof editing a draft of Section 3 and offering new additions. SZ has received funding from the European Research Council (ERC) under the European Union's Horizon 2020 research and innovation programme (TRUFLOW project, grant agreement number 883849).

The authors acknowledge TU Wien Bibliothek for financial support through its Open Access Funding Programme.

Declaration of competing interest

The authors declare that they have no known competing financial interests or personal relationships that could have appeared to influence the work reported in this paper.

Data availability

No data was used for the research described in the article.

References

Abels, H., Garcke, H., Grün, G., 2012. Thermodynamically consistent, frame indifferent diffuse interface models for incompressible two-phase flows with different densities. Math. Models Methods Appl. Sci. 22, 1150013.

Aboulhasanzadeh, B., Thomas, S., Taeibi-Rahni, M., Tryggvason, G., 2012. Multiscale computations of mass transfer from buoyant bubbles. Chem. Eng. Sci. 75, 456–467.

Afanador, A.R., Zaleski, S., Tryggvason, G., Lu, J., 2021. Effect of topology changes on the breakup of a periodic liquid jet. Comput. & Fluids 228, 105059.

Ahn, H.T., Shashkov, M., 2009. Adaptive moment-of-fluid method. J. Comput. Phys. 228, 2792–2821.

Allen, S.M., Cahn, J.W., 1979. A microscopic theory for antiphase boundary motion and its application to antiphase domain coarsening. Acta Met. 27, 1085–1095.

Allio, A., Buffo, A., Marchisio, D., Savoldi, L., 2023. Two-fluid modelling for polydisperse bubbly flows in vertical pipes: Analysis of the impact of geometrical parameters and heat transfer. Nucl. Eng. Tech. 55, 1152–1166. http://dx.doi.org/10.1016/j.net.2022.12.005.

Ambati, M., Gerasimov, T., De Lorenzis, L., 2015. A review on phase-field models of brittle fracture and a new fast hybrid formulation. Comput. Mech. 55, 383–405.

Antritter, T., Josyula, T., Maric, T., Bothe, D., Hachmann, P., Buck, B., Gambaryan-Roisman, T., Stephan, P., 2024. A two-field formulation for surfactant transport within the algebraic volume of fluid method. Comput. & Fluids 275, 106231.

Arranz, G., Martinez-Muriel, C., Flores, O., Garcia-Villalba, M., 2022. Fluid–structure interaction of multi-body systems: Methodology and applications. J. Fluids Struct. 110, 103519. http://dx.doi.org/10.1016/j.jfluidstructs.2022.103519.

Atasi, O., Haut, B., Pedrono, A., Scheid, B., Legendre, D., 2018. Influence of soluble surfactants and deformation on the dynamics of centered bubbles in cylindrical microchannels. Langmuir 34, 10048.

Baer, M.R., Nunziato, J.W., 1986. A two-phase mixture theory for the deflagration-to-detonation transition (DDT) in reactive granular materials. Int. J. Multiph. Flow 12, 861–889.

Balachandar, S., Liu, K., 2023. A correction procedure for self-induced velocity of a finite-sized particle in two-way coupled Euler–Lagrange simulations. Int. J. Multiph. Flow 159, 104316.

Balasubramanian, A.G., Sanjay, V., Jalaal, M., Vinuesa, R., Tammisola, O., 2024. Bursting bubble in an elastoviscoplastic medium. J. Fluid Mech. 1001, A9.

Basha, N., Arcucci, R., Angeli, P., Anastasiou, C., et al., 2024. Machine learning and physics-driven modelling and simulation of multiphase systems. Int. J. Multiph. Flow 179, 104936.

Beig, S.A., Johnsen, E., 2015. Maintaining interface equilibrium conditions in compressible multiphase flows using interface capturing. J. Comput. Phys. 302, 548–566.

Biegert, E., Vowinckel, B., Meiburg, E., 2017. A collision model for grain-resolving simulations of flows over dense, mobile, polydisperse granular sediment beds. J. Comput. Phys. 340, 105–127.

Brackbill, J., Kothe, D., Zemach, C., 1992. A continuum method for modeling surface tension. J. Comput. Phys. 100, 335–354. http://dx.doi.org/10.1016/0021-9991(92)90240-Y.

Brandt, L., Coletti, F., 2022. Particle-laden turbulence: progress and perspectives. Annu. Rev. Fluid Mech. 54, 159–189. http://dx.doi.org/10.1146/annurev-fluid-030121-021103.

Brassel, M., Bretin, E., 2011. A modified phase field approximation for mean curvature flow with conservation of the volume. Math. Methods Appl. Sci. 10, 1157–1180.

Breugem, W.P., 2012. A second-order accurate immersed boundary method for fully resolved simulations of particle-laden flows. J. Comput. Phys. 231, 4469–4498. http://dx.doi.org/10.1016/j.jcp.2012.02.026.

Brunton, S.L., Noak, B.R., Komoutsakos, P., 2020. Machine learning for fluid mechanics. Annu. Rev. Fluid Mech. 52, 477–508.

Buffo, A., Marchisio, D., 2014. Modeling and simulation of turbulent polydisperse gas-liquid systems via the generalized population balance equation. Rev. Chem. Eng. 30, 73–126. http://dx.doi.org/10.1515/revce-2013-0015.

Cahaly, A., Evrard, F., Desjardins, O., 2024. PLIC-Net: A machine learning approach for 3D interface reconstruction in volume of fluid methods. Int. J. Multiph. Flow 178, 104888.

Cahn, J.W., Hilliard, J.E., 1958. Free energy of a nonuniform system. I. Interfacial free energy. J. Chem. Phys. 28, 258–267.

Calderon-Sanchez, J., Martinez-Carrascal, J., Gonzalez-Gutierrez, L.M., Colagrossi, A., 2021. A global analysis of a coupled violent vertical sloshing problem using an SPH methodology. Eng. Appl. Comput. Fluid Mech 15, 865–888.

Cannon, I., Soligo, G., Rosti, M.E., 2024. Morphology of clean and surfactant-laden droplets in homogeneous isotropic turbulence. J. Fluid Mech. 987, A31.

Capecelatro, J., Wagner, J.L., 2024. Gas–particle dynamics in high-speed flows. Annu. Rev. Fluid Mech. 56, 379–403.

Carlson, A., Do-Quang, M., Amberg, G., 2011. Dissipation in rapid dynamic wetting. J. Fluid Mech. 682, 213–240.

Chen, X., Hilhorst, D., Logak, E., 2011. Mass conserving Allen–Cahn equation and volume preserving mean curvature flow. Interfaces Free Boundaries 12, 527–549.

Chen, Y., Shen, J., 2016. Efficient, adaptive energy stable schemes for the incompressible Cahn–Hilliard Navier–Stokes phase-field models. J. Comput. Phys. 308, 40–56.

Chen, D., Xie, B., 2022. Revisit to the THINC/QQ scheme: Recent progress to improve accuracy and robustness. Int. J. Numer. Meth. Fluids 94, 719–755.
Cheng, X., Nguyen, P.C.H., Seshadri, P.K., Verma, M., Gray, Z.J., Beerman, J.T., Udaykumar, H.S., Baek, S.S., 2024. Physics-aware recurrent convolutional neural networks for modeling multiphase compressible flows. Int. J. Multiph. Flow 177, 104877.
Chiapolino, A., Saurel, R., Nkonga, B., 2017. Sharpening diffuse interfaces with compressible fluids on unstructured meshes. J. Comput. Phys. 340, 389–417.
Chiodi, R., 2020. Advancement of Numerical Methods for Simulating Primary Atomization (Ph.D. thesis). Cornell Univ.
Chiodi, R., Desjardins, O., 2022. General, robust, and efficient polyhedron intersection in the Interface Reconstruction Library. J. Comput. Phys. 449, 110787. http://dx.doi.org/10.1016/j.jcp.2021.110787.
Chirco, L., Maarek, J., Popinet, S., Zaleski, S., 2022. Manifold death: A volume of fluid implementation of controlled topological changes in thin sheets by the signature method. J. Comput. Phys. 467, 111468. http://dx.doi.org/10.1016/j.jcp.2022.111468.
Chirco, L., Zaleski, S., 2022. An edge-based interface-tracking method for multiphase flows. Int. J. Numer. Meth. Fluids 1–7. http://dx.doi.org/10.1002/fld.5144.
Chiu, P.H., Lin, Y.T., 2011. A conservative phase field method for solving incompressible two-phase flows. J. Comput. Phys. 230, 185–204.
Chouippe, A., Kidanemariam, A.G., Derksen, J., Wachs, A., Uhlmann, M., 2023. Results from particle-resolved simulations. In: Subramaniam, S., Balachandar, S. (Eds.), Modelling Approaches and Computational Methods for Particle-Laden Turbulent Flows. Academic Press, pp. 185–216.
Cipriano, E., Frassoldati, A., Faravelli, T., Popinet, S., Cuoci, A., et al., 2024. Multicomponent droplet evaporation in a geometric volume-of-fluid framework. J. Comput. Phys. 507, 112955.
Colagrossi, A., Colicchio, G., Lugni, C., Brocchini, M., 2010. A study of violent sloshing wave impacts using an improved SPH method. J. Hydraul. Res. 48, 94–104.
Collis, H., Brzgin, A., Mirjalili, S., Mani, A., 2025. A thermodynamically consistent and robust four-equation model for multi-phase multi-component compressible flows using ENO-type schemes including interface regularization. arXiv preprint arXiv:2504.14063.
Colombo, M., De Santis, A., Hanson, B.C., Fairweather, M., 2022. Prediction of horizontal gas–liquid segregated flow regimes with an all flow regime multifluid model. Processes 10, 920.
Comminal, R., Spangenberg, J., Hattel, J.H., 2015. Cellwise conservative unsplit advection for the volume of fluid method. J. Comput. Phys. 283, 582–608. http://dx.doi.org/10.1016/j.jcp.2014.12.003.
Constante-Amores, C.R., Kahouadji, L., Batchvarov, A., Shin, S., Chergui, J., Juric, D., Matar, O.K., 2021. Dynamics of a surfactant-laden bubble bursting through an interface. J. Fluid Mech. 911, A57.
Coralic, V., Colonius, T., 2014. Finite-volume WENO scheme for viscous compressible multicomponent flows. J. Comput. Phys. 274, 95–121.
Costa, P., Boersma, B.J., Westerweel, J., Breugem, W.P., 2015. Collision model for fully resolved simulations of flows laden with finite-size particles. Phys. Rev. E 92, 053012.
Costa, P., Brandt, L., Picano, F., 2020. Interface-resolved simulations of small inertial particles in turbulent channel flow. J. Fluid Mech. 883, A54.
Costa, P., Brandt, L., Picano, F., 2021. Near-wall turbulence modulation by small inertial particles. J. Fluid Mech. 922, A9.
Costa, P., Picano, F., Brandt, L., Breugem, W.P., 2016. Universal scaling laws for dense particle suspensions in turbulent wall-bounded flows. Phys. Rev. Lett. 117, 134501.
Crevacore, E., Tosco, T., Sethi, R., Boccardo, G., Marchisio, D., 2016. Recirculation zones induce non-Fickian transport in three-dimensional periodic porous media. Phys. Rev. E 94, http://dx.doi.org/10.1103/PhysRevE.94.053118.
Culick, F.E.C., 1960. Comments on a ruptured soap film. J. Appl. Phys. 31, 1128–1129.
Cundall, P., 1971. A computer model for simulating progressive, large-scale movement in blocky rock system. In: Proc. Int. Symp. Rock Mech. pp. 129–136.
Cundy, C., Mirjalili, S., Laurent, C., Ermon, S., Iaccarino, G., Mani, A., 2024. A physics-informed machine learning model for the prediction of drop breakup in two-phase flows. Int. J. Multiph. Flow 180, 104934.
Dai, Z., Xie, J., Jiang, M., 2023. A coupled peridynamics–smoothed particle hydrodynamics model for fracture analysis of fluid–structure interactions. Ocean Eng.. 279, 114582.
Dalla Barba, F., Picano, F., 2021. Direct numerical simulation of the scouring of a brittle streambed in a turbulent channel flow. Acta Mech. 232, 4705–4728.
Dalla Barba, M., Galvanetto, U., Picano, F., 2022. 3D fluid–structure interaction with fracturing: A new method with applications. Comput. Meth. Appl. Mech. Eng. 398, 115210.
Damjanac, B., Cundall, P., 2016. Application of distinct element methods to simulation of hydraulic fracturing in naturally fractured reservoirs. Comput. Geotech. 71, 283–294.
Darshan, M.B., Magnini, M., Matar, O.K., 2024. Numerical modelling of flow boiling inside microchannels: A critical review of methods and applications. Appl. Therm. Eng.. 257, 124464.
Darwish, M., Moukalled, F., 2006. Convective schemes for capturing interfaces of free-surface flows on unstructured grids. Num. Heat Trans. Part B. Fundam. 49, 19–42.
Das, A.K., Das, P.K., 2015. Modeling of liquid–vapor phase change using smoothed particle hydrodynamics. J. Comput. Phys. 303, 125–145.
De Bona, J., Buffo, A., Vanni, M., Marchisio, D., 2016. Limitations of simple mass transfer models in polydisperse liquid-liquid dispersions. Chem. Eng. J. 296, 112–121. http://dx.doi.org/10.1016/j.cej.2016.03.070.
Debrégeas, G., de Gennes, P.G., Brochard-Wyart, F., 1998. The life and death of bare viscous bubbles. Science 279, 1704–1707.
Deike, L., 2022. Mass transfer at the ocean–atmosphere interface: The role of wave breaking, droplets, and bubbles. Annu. Rev. Fluid Mech. 54, 191.
Denner, F., Evrard, F., Van Wachem, B., 2022. Breaching the capillary time-step constraint using a coupled VOF method with implicit surface tension. J. Comput. Phys. 459, 111128.
Deoclecio, L.H.P., Soares, E.J., Popinet, S., 2023. Drop rise and interfacial coalescence initiation in Bingham materials. J. Non-Newton. Fluid Mech. 319, 105075.
Desjardins, O., Moureau, V., Pitsch, H., 2008. An accurate conservative level set/ghost fluid method for simulating turbulent atomization. J. Comput. Phys. 227, 8395–8416.
Devauchelle, O., Josserand, C., Zaleski, S., 2007. Forced dewetting on porous media. J. Fluid Mech. 574, 343–364.
Diddens, C., 2017. Detailed finite element method modeling of evaporating multi-component droplets. J. Comput. Phys. 340, 670–687.
Dixit, A., Oratis, A., Zinelis, K., Lohse, D., Sanjay, V., 2025. Viscoelastic Worthington jets and droplets produced by bursting bubbles. J. Fluid Mech. 1010, A2.
Dyadechko, V., M. Shashkov, M., 2007. Reconstruction of multi-material interfaces from moment data. J. Comput. Phys. 227, 5361–5384.
Eggers, J., 1993. Universal pinching of 3D axisymmetric free-surface flow. Phys. Rev. Lett. 71, 3458–3461.
Eggleton, C.D., Stebe, K.J., 1998. An adsorption–desorption-controlled surfactant on a deforming droplet. J. Colloid Interface Sci. 208, 68–80. http://dx.doi.org/10.1006/jcis.1998.5816.
Elghobashi, S., 2019. Direct numerical simulation of turbulent flows laden with droplets or bubbles. Annu. Rev. Fluid Mech. 51, 217–244.
Elmestikawy, H., Reuter, J., Evrard, F., Mostaghim, S., Van Wachem, B., 2024. Deterministic drag modelling for spherical particles in Stokes regime using data-driven approaches. Int. J. Multiph. Flow 178, 104880.
Enright, D., Fedkiw, R., Ferziger, J., Mitchell, I., 2002. A hybrid particle level set method for improved interface capturing. J. Comput. Phys. 183, 83–116.
Estivalezes, J.L., Aniszewski, W., Auguste, F., Ling, Y., Osmar, L., Caltagirone, J.P., Chirco, L., Pedrono, A., Popinet, S., Berlemont, A., et al., 2022. A phase inversion benchmark for multiscale multiphase flows. J. Comput. Phys. 450, 110810.
Evrard, F., Chiodi, R., Han, A., van Wachem, B., Desjardins, O., 2023. First moments of a polyhedron clipped by a paraboloid. SIAM J. Sci. Comput. 45, A2250–A2274. http://dx.doi.org/10.1137/22M1524308.
Evrard, F., Denner, F., van Wachem, B., 2021. Quantifying the errors of the particle-source-in-cell Euler–Lagrange method. Int. J. Multiph. Flow 135, 103535.
Farsoiya, P.K., Popinet, S., Stone, H.A., Deike, L., 2024. Coupled volume of fluid and phase field method for direct numerical simulation of insoluble surfactant-laden interfacial flows and application to rising bubbles. Phys. Rev. Fluids 9, 094004.
Feng, Y., Li, D., Marchisio, D., Vanni, M., Buffo, A., 2023. A computational fluid dynamics—population balance equation approach for evaporating cough droplets transport. Int. J. Multiph. Flow 165, http://dx.doi.org/10.1016/j.ijmultiphaseflow.2023.104500.
Ferrari, M., Boccardo, G., Buffo, A., Vanni, M., Marchisio, D., 2023. CFD simulation of a high-shear mixer for food emulsion production. J. Food Eng.. 358, http://dx.doi.org/10.1016/j.jfoodeng.2023.111655.
Fornari, W., Ardekani, M.N., Brandt, L., 2018a. Clustering and increased settling speed of oblate particles at finite Reynolds number. J. Fluid Mech. 848, 696–721.
Fornari, W., Picano, F., Brandt, L., 2018b. The effect of polydispersity in a turbulent channel flow laden with finite-size particles. Eur. J. Mech. B Fluids 67, 54–64.
Frederix, E.M.A., Dovizio, D., Mathur, A., Komen, E.M.J., 2021. All-regime two-phase flow modeling using a novel four-field large interface simulation approach. Int. J. Multiph. Flow 145, 103822.
Fullana, T., Kulkarni, Y., Fricke, M., Popinet, S., Afkhami, S., Bothe, D., Zaleski, S., 2024. A consistent treatment of dynamic contact angles in the sharp-interface framework with the generalized Navier boundary condition. arXiv preprint arXiv:2411.10762.
Fullana, T., Zaleski, S., Amberg, G., 2025. Phase-field simulations of dynamic wetting by the Volume-Of-Fluid method. arXiv preprint arXiv:2503.14065.
Fullana, T., Zaleski, S., Popinet, S., 2020. Dynamic wetting failure in curtain coating by the Volume-of-Fluid method: Volume-of-Fluid simulations on quadtree meshes. Eur. Phys. J. Spec. Top. 229, 1923–1934.
Fuster, D., 2013. An energy preserving formulation for the simulation of multiphase turbulent flows. J. Comput. Phys. 235, 114–128.
Fuster, D., Agbaglah, G., Josserand, C., Popinet, S., Zaleski, S., 2009. Numerical simulation of droplets, bubbles and waves: state of the art. Fluid Dyn. Res. 41, 065001.
García-Villalba, M., Fuentes, B., Dušek, J., Moriche, M., Uhlmann, M., 2023. An efficient method for particle-resolved simulations of neutrally buoyant spheres. Comput. & Fluids 263, 105936.

Gemello, L., Plais, C., Augier, F., Cloupet, A., Marchisio, D., 2018. Hydrodynamics and bubble size in bubble columns: Effects of contaminants and spargers. Chem. Eng. Sci. 184, 93–102. http://dx.doi.org/10.1016/j.ces.2018.03.043.

Gerbeau, J.F., Lelievre, T., 2009. Generalized Navier boundary condition and geometric conservation law for surface tension. Comput. Meth. Appl. Mech. Eng. 198, 644–656.

Glowinski, R., Pan, T.W., Hesla, T.I., Joseph, D.D., 1999. A distributed Lagrange multiplier/fictitious domain method for particulate flows. Int. J. Multiph. Flow 25, 755–794.

Griffith, B.E., Patankar, N.A., 2020. Immersed methods for fluid–structure interaction. Annu. Rev. Fluid Mech. 52, 421. http://dx.doi.org/10.1146/annurev-fluid-010719-060228.

Gross, S., Reusken, A., 2011. Numerical methods for two-phase incompressible flows. Springer Science & Business Media.

Gsell, S., Favier, J., 2021. Direct-forcing immersed-boundary method: a simple correction preventing boundary slip error. J. Comput. Phys. 435, 110265.

Gualtieri, P., Picano, F., Sardina, G., Casciola, C.M., 2015. Exact regularized point particle method for multiphase flows in the two-way coupling regime. J. Fluid Mech. 773, 520–561.

Guildenbecher, D.R., Gao, J., Chen, J., Sojka, P.E., 2017. Characterization of drop aerodynamic fragmentation in the bag and sheet-thinning regimes by crossed-beam, two-view, digital in-line holography. Int. J. Multiph. Flow 94, 107–122. http://dx.doi.org/10.1016/j.ijmultiphaseflow.2017.04.011.

Guo, Z., Lin, P., Lowengrub, J., Wise, S.M., 2017. Mass conservative and energy stable finite difference methods for the quasi-incompressible Navier–Stokes–Cahn–Hilliard system: Primitive variable and projection-type schemes. Comput. Meth. Appl. Mech. Eng. 326, 144–174.

Han, A., Chiodi, R., Desjardins, O., 2024a. Capturing thin structures in VOF simulations with two-plane reconstruction. J. Comput. Phys. 519, 113453. http://dx.doi.org/10.1016/j.jcp.2024.113453.

Han, A., Desjardins, O., 2024. Subgrid scale modeling of droplet bag breakup in VOF simulations. Int. J. Multiph. Flow 180, 104958. http://dx.doi.org/10.1016/j.ijmultiphaseflow.2024.104958.

Han, A., Evrard, F., Desjardins, O., 2024b. Comparison of methods for curvature estimation from volume fractions. Int. J. Multiph. Flow 174, 104769. http://dx.doi.org/10.1016/j.ijmultiphaseflow.2024.104769.

Hänsch, S., Draw, M., Evdokimov, I., Khan, H., Kamble, V.V., Krull, B., Lehnigk, R., Liao, Y., Lyu, H., Meller, R., Schlegel, F., Li, S., Tekavcic, M., 2024. Multiphase cases repository by HZDR for OpenFOAM foundation software. https://rodare.hzdr.de/record/3017, RODARE.

Hänsch, S., Evdokimov, I., Schlegel, F., Lucas, D., 2021. A workflow for the sustainable development of closure models for bubbly flows. Chem. Eng. Sci. 244, 116807.

Hänsch, S., Lucas, D., Krepper, E., Höhne, T., 2012. A multi-field two-fluid concept for transitions between different scales of interfacial structures. Int. J. Multiph. Flow 47, 171–182.

Herrmann, M., 2011. On simulating primary atomization using the refined level set grid method. At. Spray 21, 283–301. http://dx.doi.org/10.1615/AtomizSpr.2011002760.

Hessenkemper, H., Wang, L., Lucas, D., Tan, S., Ni, R., Ma, T., 2024. 3D detection and tracking of deformable bubbles in swarms with the aid of deep learning models. Int. J. Multiph. Flow 179, 104932.

Hessenkemper, H., Ziegenhein, T., Rzehak, R., Lucas, D., Tomiyama, A., 2021. Lift force coefficient of ellipsoidal single bubbles in water. Int. J. Multiph. Flow 138, 103587.

Hirt, C.W., Nichols, B.D., 1981. Volume of fluid (VOF) method for the dynamics of free boundaries. J. Comput. Phys. 39, 201–225. http://dx.doi.org/10.1016/0021-9991(81)90145-5.

Hohenberg, P.C., Halperin, B.I., 1977. Theory of dynamic critical phenomena. Rev. Modern Phys. 49, 435.

Höhne, T., Porombka, P., Moya Sáez, S., 2020. Validation of AIAD sub-models for advanced numerical modelling of horizontal two-phase flows. Fluids 5, 102.

Hu, J., Zhu, K., Cheng, S., Kovalchuk, N., Soulsby, A., Simmons, M., Matar, O., 2024. Explainable AI models for predicting drop coalescence in microfluidics device. Chem. Eng. J. 481, 148465.

Huang, Z., Johnsen, E., 2024. A consistent and conservative phase-field method for compressible N-phase flows: Consistent limiter and multiphase reduction-consistent formulation. J. Comput. Phys. 501, 112801.

Huang, Z., Lin, G., Ardekani, A.M., 2020. Consistent and conservative scheme for incompressible two-phase flows using the conservative Allen-Cahn model. J. Comput. Phys. 420, 109718.

Huisman, S.G., Barois, T., Bourgoin, M., Chouippe, A., Doychev, T., Huck, P., Morales, C.E.B., Uhlmann, M., Volk, R., 2016. Columnar structure formation of a dilute suspension of settling spherical particles in a quiescent fluid. Phys. Rev. Fluids 1, 074204. http://dx.doi.org/10.1103/PhysRevFluids.1.074204.

Hunt, M.L., Zenit, R., Campbell, C.S., Brennen, C.E., 2002. Revisiting the 1954 suspension experiments of RA Bagnold. J. Fluid Mech. 452, 1–24.

Hysing, S., 2012. Mixed element FEM level set method for numerical simulation of immiscible fluids. J. Comput. Phys. 231, 2449–2465.

Icardi, M., Asinari, P., Marchisio, D., Izquierdo, S., Fox, R., 2012. Quadrature-based moment closures for non-equilibrium flows: Hard-sphere collisions and approach to equilibrium. J. Comput. Phys. 231, 7431–7449. http://dx.doi.org/10.1016/j.jcp.2012.07.012.

Icardi, M., Pasquale, N., Crevacore, E., Marchisio, D., Babler, M., 2023. Population balance models for particulate flows in porous media: Breakage and shear-induced events. Transp. Porous Media 146, 197–222. http://dx.doi.org/10.1007/s11242-022-01793-5.

Ii, S., Sugiyama, K., Takeuchi, S., Takagi, S., Matsumoto, Y., Xiao, F., 2012. An interface capturing method with a continuous function: the THINC method with multi-dimensional construction. J. Comput. Phys. 231, 2328–2358.

Ii, S., Xie, B., Xiao, F., 2014. An interface capturing method with a continuous function: the THINC method on unstructured triangular and tetrahedral meshes. J. Comput. Phys. 259, 260–269.

Jackiw, I.M., Ashgriz, N., 2022. Prediction of the droplet size distribution in aerodynamic droplet breakup. J. Fluid Mech. 940, A17. http://dx.doi.org/10.1017/jfm.2022.249.

Jacqmin, D., 1996. An energy approach to the continuum surface tension method. In: 34th Aerospace Sciences Meeting and Exhibit. p. 858.

Jacqmin, D., 1998. A variational approach to deriving smeared-interface surface tension models. In: Barriers and Challenges in Computational Fluid Dynamics. Springer, pp. 231–240.

Jacqmin, D., 2000. Contact-line dynamics of a diffuse fluid interface. J. Fluid Mech. 402, 57–88.

Jafari, A., Vahab, M., Khalili, N., 2021. Fully coupled XFEM formulation for hydraulic fracturing simulation based on a generalized fluid leak-off model. Comput. Meth. Appl. Mech. Eng. 373, 113447.

Jain, S.S., Adler, M.C., West, J.R., Mani, A., Moin, P., Lele, S.K., 2023. Assessment of diffuse-interface methods for compressible multiphase fluid flows and elastic–plastic deformation in solids. J. Comput. Phys. 475, 111866.

Jain, S.S., Mani, A., Moin, P., 2020. A conservative diffuse-interface method for compressible two-phase flows. J. Comput. Phys. 418, 109606.

Jain, R., Tschisgale, S., Fröhlich, J., 2019. A collision model for DNS with ellipsoidal particles in viscous fluid. Int. J. Multiph. Flow 120, 103087.

James, A.J., Lowengrub, J., 2004. A surfactant-conserving volume-of-fluid method for interfacial flows with insoluble surfactant. J. Comput. Phys. 201, 685.

Jiang, G.S., Shu, C.W., 1996. Efficient implementation of weighted ENO schemes. J. Comput. Phys. 126, 202–228.

Jiang, X., Xu, C., Zhao, L., 2024. Prolate spheroids settling in a quiescent fluid: clustering, microstructures and collisions. J. Fluid Mech. 1000, A49.

Jibben, Z., Carlson, N., Francois, M., 2019. A paraboloid fitting technique for calculating curvature from piecewise-linear interface reconstructions on 3D unstructured meshes. Comput. Math. Appl. 78, 643–653. http://dx.doi.org/10.1016/j.camwa.2018.09.009.

Jofre, L., Urzay, J., 2021. Transcritical diffuse-interface hydrodynamics of propellants in high-pressure combustors of chemical propulsion systems. Prog. Energy Combust. Sci. 82, 100877.

Johnsen, E., Colonius, T., 2006. Implementation of WENO schemes in compressible multicomponent flow problems. J. Comput. Phys. 219, 715–732.

Johnson, P.L., Bassenne, M., Moin, P., 2020. Turbophoresis of small inertial particles: theoretical considerations and application to wall-modelled large-eddy simulations. J. Fluid Mech. 883, A27.

Kajishima, T., Takiguchi, S., 2002. Interaction between particle clusters and particle–induced turbulence. Int. J. Heat Fluid Flow 23, 639–646. http://dx.doi.org/10.1016/S0142-727X(02)00159-5.

Kant, P., Pairetti, C., Saade, Y., Popinet, S., Zaleski, S., Lohse, D., 2023. Bag-mediated film atomization in a cough machine. Phys. Rev. Fluids 8, 074802.

Kapila, A., Menikoff, R., Bdzil, J., Son, S., Stewart, D., 2000. Two-phase modeling of DDT in granular materials: Reduced equations. Technical Report. Technical Report, LA-UR-99-3329, Los Alamos National Laboratory, USA.

Kees, C., Akkerman, M., Farthing, Y., Bazilevs, A., 2011. A conservative level set method suitable for variable-order approximations and unstructured meshes. J. Comput. Phys. 230, 4536–4558.

Kempe, T., Fröhlich, J., 2012a. Collision modelling for the interface-resolved simulation of spherical particles in viscous fluids. J. Fluid Mech. 709, 445–489.

Kempe, T., Fröhlich, J., 2012b. An improved immersed boundary method with direct forcing for the simulation of particle laden flows. J. Comput. Phys. 231, 3663–3684. http://dx.doi.org/10.1016/j.jcp.2012.01.021.

Khanwale, M.A., Lofquist, A.D., Sundar, H., Rossmanith, J.A., Ganapathysubramanian, B., 2020. Simulating two-phase flows with thermodynamically consistent energy stable Cahn-Hilliard Navier-Stokes equations on parallel adaptive octree based meshes. J. Comput. Phys. 419, 109674.

Khanwale, M., Mirjalili, S., Mani, A., Desjardin, P., Lele, S., 2023. Discussion on benchmark data for simulations of compressible multiphase flow. Cent. Turbul. Res. Annu. Res. Briefs.

Khanwale, M.A., Saurabh, K., Fernando, M., Calo, V.M., Sundar, H., Rossmanith, J.A., Ganapathysubramanian, B., 2022. A fully-coupled framework for solving Cahn-Hilliard Navier-Stokes equations: Second-order, energy-stable numerical methods on adaptive octree based meshes. Comput. Phys. Comm. 280, 108501.

Khedkar, K., Mamaghani, A.C., Ghysels, P., Patankar, N., Bhalla, A.P.S., 2025. Preventing mass loss in the standard level set method: New insights from variational analyses. J. Comput. Phys. 520, 113495.

Kidanemariam, A.G., Scherer, M., Uhlmann, M., 2022. Open-channel flow over evolving subaqueous ripples. J. Fluid Mech. 937, A26.

Kidanemariam, A.G., Uhlmann, M., 2014. Interface-resolved direct numerical simulation of the erosion of a sediment bed sheared by laminar channel flow. Int. J. Multiph. Flow 67, 174–188.

Kim, W., Choi, H., 2019. Immersed boundary methods for fluid–structure interaction: A review. Int. J. Heat Fluid Flow 75, 301–309. http://dx.doi.org/10.1016/j.ijheatfluidflow.2019.01.010.

Kim, D., Ivey, C.B., Ham, F.E., Bravo, L.G., 2021. An efficient high-resolution Volume-of-Fluid method with low numerical diffusion on unstructured grids. J. Comput. Phys. 446, 110606.

Kim, J., Lee, S., Choi, Y., 2014. A conservative Allen–Cahn equation with a space–time dependent Lagrange multiplier. Int. J. Eng. Sci. 84, 11–17.

Kim, D., Moin, P., 2020. Subgrid-scale capillary breakup model for liquid jet atomization. Combust. Sci. Tech. vol. 192, 1334–1357. http://dx.doi.org/10.1080/00102202.2020.1732950.

Kottilingal, A.B., 2023. Numerical Simulations of Cavitation in Blood Vessels using a Parallel Front Tracking Method (Ph.D. thesis). Sorbonne Universite, Appendix A.5.

Kulkarni, Y., Fullana, T., Zaleski, S., 2023. Stream function solutions for some contact line boundary conditions: Navier slip, super slip and the generalized Navier boundary condition. Proc. Roy. Soc. A 479 (2278), 20230141.

Kulkarni, Y., Pairetti, C., Villiers, R., Popinet, S., Zaleski, S., 2025. The atomising pulsed jet. J. Fluid Mech. 1009, A35.

Lācis, U., Pellegrino, M., Sundin, J., Amberg, G., Zaleski, S., Hess, B., Bagheri, S., 2022. Nanoscale sheared droplet: volume-of-fluid, phase-field and no-slip molecular dynamics. J. Fluid Mech. 940, A10.

Laurila, T., Carlson, A., Do-Quang, M., Ala-Nissila, T., Amberg, G., 2012. Thermohydrodynamics of boiling in a van der Waals fluid. Phys. Rev. E 85, 026320.

Lehnigk, R., Bruschewski, M., Huste, T., Lucas, D., Rehm, M., Schlegel, F., 2023. Sustainable development of simulation setups and addons for OpenFOAM for nuclear reactor safety research. Kerntechnik 88, 131–140.

Li, D., Marchisio, D., 2022. Implementation of CHyQMOM in OpenFOAM for the simulation of non-equilibrium gas-particle flows under one-way and two-way coupling. Powder Tech. 396, 765–784. http://dx.doi.org/10.1016/j.powtec.2021.11.004.

Li, D., Marchisio, D., Hasse, C., Lucas, D., 2019. Comparison of Eulerian QBMM and classical Eulerian–Eulerian method for the simulation of polydisperse bubbly flows. AIChE J. 65, http://dx.doi.org/10.1002/aic.16732.

Li, D., Marchisio, D., Hasse, C., Lucas, D., 2020. twoWayGPBEFoam: An open-source Eulerian QBMM solver for monokinetic bubbly flows. Comput. Phys. Comm. 250, http://dx.doi.org/10.1016/j.cpc.2019.107036.

Li, D., Wei, Y., Marchisio, D., 2021. Qeefoam: A quasi-Eulerian-Eulerian model for polydisperse turbulent gas-liquid flows. Implementation in OpenFOAM, verification and validation. Int. J. Multiph. Flow 136, http://dx.doi.org/10.1016/j.ijmultiphaseflow.2020.103544.

Liao, Y., Ma, T., Liu, L., Ziegenhein, T., Krepper, E., Lucas, D., 2018. Eulerian modelling of turbulent bubbly flow based on a baseline closure concept. Nucl. Eng. Des. 337, 450–459.

Ling, Y., Fuster, D., Zaleski, S., Tryggvason, G., 2017. Spray formation in a quasiplanar gas–liquid mixing layer at moderate density ratios: A numerical closeup. Phys. Rev. Fluids 2, 014005.

Liu, K., Luo, K., Cheng, Y., Liu, A., Li, H., Fan, J., Balachandar, S., 2024. Parameterized physics-informed neural networks (P-PINNs) solution of uniform flow over an arbitrarily spinning spherical particle. Int. J. Multiph. Flow 180, 104937.

Liu, C.Y., Vandre, E., Carvalho, M.S., Kumar, S., 2016. Dynamic wetting failure and hydrodynamic assist in curtain coating. J. Fluid Mech. 808, 290–315.

Lohse, D., 2022. Fundamental fluid dynamics challenges in inkjet printing. Annu. Rev. Fluid Mech. 54, 349.

Lohse, D., 2023. Surfactants on troubled waters. J. Fluid Mech. 976, F1.

Long, T., Pan, J., Cipriano, E., Bucci, M., Zaleski, S., 2025. Direct numerical simulation of nucleate boiling with a resolved microlayer and conjugate heat transfer. arXiv preprint arXiv:2503.12171.

Long, T., Pan, J., Zaleski, S., 2024. An edge-based interface tracking (EBIT) method for multiphase flows with phase change. J. Comput. Phys. 513, 113159.

López, J., Hernández, J., Gómez, P., Faura, F., 2004. A volume of fluid method based on multidimensional advection and spline interface reconstruction. J. Comput. Phys. 195, 718–742. http://dx.doi.org/10.1016/j.jcp.2003.10.030.

Lowengrub, J., Truskinovsky, L., 1998. Quasi–incompressible Cahn–Hilliard fluids and topological transitions. Proc. R. Soc. A: Math. Phys. Eng. Sci 454, 2617–2654.

Lu, J., Xu, X., Zhong, S., Ni, R., Tryggvason, G., 2023. The dynamics of suspensions of prolate spheroidal particles – Effects of volume fraction. Int. J. Multiph. Flow 165, 104469.

Lucas, D., Rzehak, R., Krepper, E., Ziegenhein, T., Liao, Y., Kriebitzsch, S., Apanasevich, P., 2016. A strategy for the qualification of multi-fluid approaches for nuclear reactor safety. Nucl. Eng. Des. 299, 2–11.

Maës, P.A., Amirfazli, A., Josserand, C., 2025. Birth of a bubble: drop impact onto a thin liquid film for an immiscible three-fluid system. J. Fluid Mech. 1009, A8.

Maltsev, V., Skote, M., Tsoutsanis, P., 2022. High-order methods for diffuse-interface models in compressible multi-medium flows: A review. Phys. Fluids 34.

Maluta, F., Buffo, A., Marchisio, D., Montante, G., Paglianti, A., Vanni, M., 2021. Effect of turbulent kinetic energy dissipation rate on the prediction of droplet size distribution in stirred tanks. Int. J. Multiph. Flow 136, http://dx.doi.org/10.1016/j.ijmultiphaseflow.2020.103547.

Manikantan, H., Squires, T.M., 2020. Surfactant dynamics: Hidden variables controlling fluid flows. J. Fluid Mech. 892, P1.

Maniscalco, F., Buffo, A., Marchisio, D., Vanni, M., 2021. Numerical simulation of bubble columns: LES turbulence model and interphase forces blending approach. Chem. Eng. Res. Des. 173, 1–14. http://dx.doi.org/10.1016/j.cherd.2021.06.024.

Marchioli, C., Soldati, A., 2002. Mechanisms for particle transfer and segregation in a turbulent boundary layer. J. Fluid Mech. 468, 283–315.

Marchisio, D., 2024. Reacting with the flows of similarity. Nat. Chem. Eng. 1, 440.

Marchisio, D., Fox, R., 2013. Computational models for polydisperse particulate and multiphase systems. Cambridge Univ. Press.

Marchisio, D., Fox, R., 2016. Reacting flows and the interaction between turbulence and chemistry. In: Reference Module in Chemistry, Molecular Sciences and Chemical Engineering. Elsevier, http://dx.doi.org/10.1016/B978-0-12-409547-2.11526-4.

Maric, T., Kothe, D.B., Bothe, D., 2020. Unstructured un-split geometrical Volume-of-Fluid methods – A review. J. Comput. Phys. 420, 109695.

Mathur, A., Dovizio, D., Frederix, E.M.A., Komen, E.M.J., 2019. A hybrid dispersed-large interface solver for multi-scale two-phase flow modelling. Nucl. Eng. Des. 344, 69–82.

Maxey, M., 2017. Simulation methods for particulate flows and concentrated suspensions. Annu. Rev. Fluid Mech. 49, 171–193. http://dx.doi.org/10.1146/annurev-fluid-122414-034408.

Meller, R., Schlegel, F., Lucas, D., 2021. Basic verification of a numerical framework applied to a morphology adaptive multifield two-fluid model considering bubble motions. Int. J. Numer. Meth. Fluids 93, 748–773.

Meller, R., Tekavčič, M., Krull, B., Schlegel, F., 2023. Momentum exchange modeling for coarsely resolved interfaces in a multifield two-fluid model. Int. J. Numer. Meth. Fluids 95, 1521–1545.

Mer, S., Praud, O., Neau, H., Merigoux, N., Magnaudet, J., Roig, V., 2018. The emptying of a bottle as a test case for assessing interfacial momentum exchange models for Euler–Euler simulations of multi-scale gas-liquid flows. Int. J. Multiph. Flow 106, 109–124.

Messina, F., Marchisio, D., Sethi, R., 2015. An extended and total flux normalized correlation equation for predicting single-collector efficiency. J. Colloid Interface Sci. 446, 185–193. http://dx.doi.org/10.1016/j.jcis.2015.01.024.

Mirjalili, S., Ivey, C.B., Mani, A., 2020. A conservative diffuse interface method for two-phase flows with provable boundedness properties. J. Comput. Phys. 401, 109006.

Mirjalili, S., Jain, S.S., Dodd, M., 2017. Interface-capturing methods for two-phase flows: An overview and recent developments. Cent. Turbul. Res. Annu. Res. Briefs.

Mirjalili, S., Mani, A., 2021. Consistent, energy-conserving momentum transport for simulations of two-phase flows using the phase field equations. J. Comput. Phys. 426, 109918.

Mittal, R., Bhardwaj, R., 2022. Immersed boundary methods for thermofluids problems. Annu. Rev. Heat Transf. 24, http://dx.doi.org/10.1615/AnnualRevHeatTransfer.2022041888.

Mittal, R., Iaccarino, G., 2005. Immersed boundary methods. Annu. Rev. Fluid Mech. 37, 239–261. http://dx.doi.org/10.1146/annurev.fluid.37.061903.175743.

Moës, N., Dolbow, J., Belytschko, T., 1999. A finite element method for crack growth without remeshing. Internat. J. Numer. Methods Engrg. 46, 131–150.

Morgeneyer, M., Feise, H.J., Heng, J., Lehmann, M., Marchisio, D., Rasteiro, M., Ward-Smith, S., 2022. Particle technology's contributions to the major challenges of the 21st century A predictive retrospective as a particular birthday present of IChemE. Chem. Eng. Res. Des. 188, 447–452. http://dx.doi.org/10.1016/j.cherd.2022.09.002.

Moriche, M., Hettmann, D., García-Villalba, M., Uhlmann, M., 2023. On the clustering of low-aspect-ratio oblate spheroids settling in ambient fluid. J. Fluid Mech. 963, A1.

Moriche, M., Uhlmann, M., Dušek, J., 2021. A single oblate spheroid settling in unbounded ambient fluid: a benchmark for simulations in steady and unsteady wake regimes. Int. J. Multiph. Flow 136, 103519. http://dx.doi.org/10.1016/j.ijmultiphaseflow.2020.103519.

Muradoglu, M., Tryggvason, G., 2014. Simulations of soluble surfactants in 3D multiphase flow. J. Comput. Phys. 274, 737–757. http://dx.doi.org/10.1016/j.jcp.2014.06.024.

Muzaferija, S., Peric, M., 1997. Computation of free-surface flows using the finite-volume method and moving grids. Numer. Heat Trans. Part B. Fundam. 32, 369–384.

Myers, D., 2020. Surfactant science and technology. John Wiley & Sons, New York, NY.

Nagarth, S., Jansen, K.E., Lahey, R.T., 2005. Computation of incompressible bubble dynamics with a stabilized finite element level set method. Comput. Meth. Appl. Mech. Eng. 194, 4565–4587.

Nguyen, T.T., Indraratna, B., 2020. A coupled CFD–DEM approach to examine the hydraulic critical state of soil under increasing hydraulic gradient. Int. J. Geomech 20, 04020138.

Nichols, B.D., Hirt, C.W., Hotchkiss, R.S., 1980. SOLA-VOF: A Solution Algorithm for Transient Fluid Flow with Multiple Free Boundaries. Los Alamos Scientific Laboratory, http://dx.doi.org/10.2172/5122053.

Noh, W.F., Woodward, P., 1976. SLIC (Simple Line Interface Calculation). In: van de Vooren, A.I., Zandbergen, P.J. (Eds.), Proc. Fifth Int. Conf. Numerical Methods in Fluid Dynamics June 28 – July 2 1976 Twente University, Enschede. Springer Berlin Heidelberg, pp. 330–340. http://dx.doi.org/10.1007/3-540-08004-X_336.

Nordström, J., Malan, A.G., 2025. An energy stable incompressible multi-phase flow formulation. J. Comput. Phys. 523, 113685.

Nourgaliev, R., Theofanous, T., 2007. High-fidelity interface tracking in compressible flows: unlimited anchored adaptive level set. J. Comput. Phys. 224, 836–866.

Olsson, E., Kreiss, G., 2005. A conservative level set method for two phase flow. J. Comput. Phys. 210, 225–246.

Olsson, E., Kreiss, G., Zahedi, S., 2007. A conservative level set method for two phase flow II. J. Comput. Phys. 225, 785–807.

Opfer, L., Roisman, I.V., Venzmer, J., Klostermann, M., Tropea, C., 2014. Droplet-air collision dynamics: Evolution of the film thickness. Phys. Rev. E 89, 013023. http://dx.doi.org/10.1103/PhysRevE.89.013023.

Osnes, A.N., Vartdal, M., Khalloufi, M., Capecelatro, J., Balachandar, S., 2023. Comprehensive quasi-steady force correlations for compressible flow through random particle suspensions. Int. J. Multiph. Flow 165, 104485.

Owkes, M., Desjardins, O., 2014. A computational framework for conservative, three-dimensional, unsplit, geometric transport with application to the volume-of-fluid (VOF) method. J. Comput. Phys. 270, 587–612. http://dx.doi.org/10.1016/j.jcp.2014.04.022.

Pan, S., Han, L., Hu, X., Adams, N.A., 2018. A conservative interface-interaction method for compressible multi-material flows. J. Comput. Phys. 371, 870–895.

Pan, J., Long, T., Chirco, L., Scardovelli, R., Popinet, S., Zaleski, S., 2024. An edge-based interface tracking (EBIT) method for multiphase-flow simulation with surface tension. J. Comput. Phys. 508, 113016.

Para, M., Alidoost, M., Shiea, M., Boccardo, G., Buffo, A., Barresi, A., Marchisio, D., 2022. A modelling and experimental study on the co-precipitation of Ni0.8Mn0.1Co0.1(OH)2 as precursor for battery cathodes. Chem. Eng. Sci. 254, http://dx.doi.org/10.1016/j.ces.2022.117634.

Para, M., Querio, A., Amici, J., Versaci, D., Barresi, A., Bodoardo, S., Marchisio, D., 2023. Electrochemical performance optimization of NMC811 through the structure design of its precursor. J. Electroanal. Chem. 943, http://dx.doi.org/10.1016/j.jelechem.2023.117630.

Passalacqua, A., Laurent, F., Madadi-Kandjani, E., Heylmun, J.C., Fox, R.O., 2018. An open-source quadrature-based population balance solver for OpenFOAM. Chem. Eng. Sci. 176, 306–318.

Patel, J., Natarajan, G., 2015. A generic framework for design of interface capturing schemes for multi-fluid flows. Comput. & Fluids 106, 108–118.

Paula, T., Adami, S., Adams, N.A., 2023. A robust high-resolution discrete-equations method for compressible multi-phase flow with accurate interface capturing. J. Comput. Phys. 491, 112371.

Pedregosa, F., Varoquaux, G., Gramfort, A., Michel, V., Thirion, B., Grisel, O., Blondel, M., Prettenhofer, P., Weiss, R., Dubourg, V., Vanderplas, J., Passos, A., Cournapeau, D., Brucher, M., Perrot, M., Duchesnay, E., 2011. Scikit-learn: Machine learning in Python. J. Mach. Learn. Res. 12, 2825–2830.

Pelanti, M., 2022. Arbitrary-rate relaxation techniques for the numerical modeling of compressible two-phase flows with heat and mass transfer. Int. J. Multiph. Flow 153, 104097.

Peng, C., Ayala, O.M., Wang, L.P., 2019. A direct numerical investigation of two-way interactions in a particle-laden turbulent channel flow. J. Fluid Mech. 875, 1096–1144.

Peskin, C.S., 1972. Flow patterns around heart valves: a numerical method. J. Comput. Phys. 10, 252–271. http://dx.doi.org/10.1016/0021-9991(72)90065-4.

Peskin, C.S., 2002. The immersed boundary method. Acta Numer. 11, 479–517. http://dx.doi.org/10.1017/S0962492902000077.

Peskin, C.S., McQueen, D.M., 1995. A general method for the computer simulation of biological systems interacting with fluids. Symp. Soc. Exp. Biol. 49, 265–276.

Picano, F., Breugem, W.P., Brandt, L., 2015. Turbulent channel flow of dense suspensions of neutrally buoyant spheres. J. Fluid Mech. 764, 463–487.

Pico, P., Kahouadji, L., Shin, S., Chergui, J., Juric, D., Matar, O.K., 2024. Surfactant-laden bubble bursting: Dynamics of capillary waves and Worthington jet at large Bond number. Phys. Rev. Fluids 9, 083606.

Pinelli, A., Naqavi, I.Z., Piomelli, U., Favier, J., 2010. Immersed-boundary methods for general finite-difference and finite-volume Navier–Stokes solvers. J. Comput. Phys. 229, 9073–9091. http://dx.doi.org/10.1016/j.jcp.2010.08.021.

Pollack, M., Pütz, M., Marchisio, D., Oevermann, M., Hasse, C., 2019. Zero-flux approximations for multivariate quadrature-based moment methods. J. Comput. Phys. 398, http://dx.doi.org/10.1016/j.jcp.2019.108879.

Popinet, S., 2009. An accurate adaptive solver for surface-tension-driven interfacial flows. J. Comput. Phys. 228, 5838–5866.

Popinet, S., 2018. Numerical models of surface tension. Annu. Rev. Fluid Mech. 50, 49–75.

Poulain, S., Villermaux, E., Bourouiba, L., 2018. Ageing and burst of surface bubbles. J. Fluid Mech. 851, 636–671.

Prosperetti, A., 2015. Life and death by boundary conditions. J. Fluid Mech. 768, 1–4.

Prosperetti, A., Tryggvason, G., 2009. Computational methods for multiphase flow. Cambridge Univ. Press.

Qian, T., Wang, X.P., Sheng, P., 2003. Molecular scale contact line hydrodynamics of immiscible flows. Phys. Rev. E 68, 016306.

Radhakrishnan, A., Berre, H.L., Wilfong, B., Spratt, J.S., Rodriguez, Jr., M., Colonius, T., Bryngelson, S.H., 2023. Method for portable, scalable, and performant GPU-accelerated simulation of multiphase compressible flow. arXiv preprint arXiv:2305.09163.

Radl, S., Koynov, A., Tryggvason, G., Khinast, J.G., 2008. DNS-based prediction of the selectivity of fast multiphase reactions: Hydrogenation of nitroarenes. Chem. Eng. Sci. 63, 3279–3291. http://dx.doi.org/10.1016/j.ces.2008.03.025.

Rahmani, M., Geraci, G., Iaccarino, G., Mani, A., 2018. Effects of particle polydispersity on radiative heat transfer in particle-laden turbulent flows. Int. J. Multiph. Flow 104, 42–59.

Raponi, A., Achermann, R., Romano, S., Trespi, S., Mazzotti, M., Cipollina, A., Buffo, A., Vanni, M., Marchisio, D., 2023a. Population balance modelling of magnesium hydroxide precipitation: Full validation on different reactor configurations. Chem. Eng. J. 477, http://dx.doi.org/10.1016/j.cej.2023.146540.

Raponi, A., Marchisio, D., 2024. Deep learning for kinetics parameters identification: A novel approach for multi-variate optimization. Chem. Eng. J. 489, http://dx.doi.org/10.1016/j.cej.2024.151149.

Raponi, A., Romano, S., Battaglia, G., Buffo, A., Vanni, M., Cipollina, A., Marchisio, D., 2023b. Computational modeling of magnesium hydroxide precipitation and kinetics parameters identification. Cryst. Growth Des. 23, 4748–4759. http://dx.doi.org/10.1021/acs.cgd.2c01179.

Razizadeh, M., Mortazavi, S., Shahin, H., 2018. Drop breakup and drop pair coalescence using front-tracking method in three dimensions. Acta Mech. 229, 1021–1043.

Remmerswaal, R.A., Veldman, A.E., 2022. Parabolic interface reconstruction for 2D volume of fluid methods. J. Comput. Phys. 469, 111473. http://dx.doi.org/10.1016/j.jcp.2022.111473.

Rider, W.J., Kothe, D.B., 1998. Reconstructing volume tracking. J. Comput. Phys. 141, 112–152. http://dx.doi.org/10.1006/jcph.1998.5906.

Roccon, A., Zonta, F., Soldati, A., 2023. Phase-field modeling of complex interface dynamics in drop-laden turbulence. Phys. Rev. Fluids 8, 090501.

Romano, S., Trespi, S., Achermann, R., Battaglia, G., Raponi, A., Marchisio, D., Mazzotti, M., Micale, G., Cipollina, A., 2023. The role of operating conditions in the precipitation of magnesium hydroxide hexagonal platelets using NaOH solutions. Cryst. Growth Des. 23, 6491–6505. http://dx.doi.org/10.1021/acs.cgd.3c00462.

Rosen, M.J., Kunjappu, J.T., 2012. Surfactant and interfacial phenomena. John Wiley & Sons, New York, NY.

Rossi, D., Di Giorgio, S., et al., 2024. Comparative analysis of volume of fluid and phase–field methods for numerical simulations of two-phase flows. Available on SSRN http://dx.doi.org/10.2139/ssrn.5037935.

Rzehak, R., Ziegenhein, T., Kriebitzsch, S., Krepper, E., Lucas, D., 2017. Unified modeling of bubbly flows in pipes, bubble columns, and airlift columns. Chem. Eng. Sci. 157, 147–158.

Saini, M., Sanjay, V., Saade, Y., Lohse, D., Popinet, S., 2025. Implementation of integral surface tension formulations in a volume of fluid framework and their applications to Marangoni flows. arXiv preprint arXiv:2502.02712.

Salenbauch, S., Hasse, C., Vanni, M., Marchisio, D., 2019. A numerically robust method of moments with number density function reconstruction and its application to soot formation, growth and oxidation. J. Aerosol Sci. 128, 34–49. http://dx.doi.org/10.1016/j.jaerosci.2018.11.009.

Salenbauch, S., Sirignano, M., Marchisio, D., Pollack, M., D'Anna, A., Hasse, C., 2017. Detailed particle nucleation modeling in a sooting ethylene flame using a conditional quadrature method of moments (CQMOM). Proc. Combust. Inst. 36, 771–779. http://dx.doi.org/10.1016/j.proci.2016.08.003.

Saurel, R., Abgrall, R., 1999. A multiphase Godunov method for compressible multifluid and multiphase flows. J. Comput. Phys. 150, 425–467.

Saurel, R., Pantano, C., 2018. Diffuse-interface capturing methods for compressible two-phase flows. Annu. Rev. Fluid Mech. 50, 105–130.

Saurel, R., Petitpas, F., Berry, R.A., 2009. Simple and efficient relaxation methods for interfaces separating compressible fluids, cavitating flows and shocks in multiphase mixtures. J. Comput. Phys. 228, 1678–1712.

Schenk, M., García-Villalba, M., Dušek, J., Uhlmann, M., Moriche, M., 2025. An immersed boundary method for particle-resolved simulations of arbitrary-shaped rigid particles. Int. J. Multiph. Flow 188, 105200. http://dx.doi.org/10.1016/j.ijmultiphaseflow.2025.105200.

Schlegel, F., Bilde, K., Draw, M., Evdokimov, I., Hänsch, S., Kamble, V., Khan, H., Krull, B., Lehnigk, R., Li, J., Lyu, H., Meller, R., Petelin, G., Kota, S., Tekavcic, M., 2024. Multiphase code repository by HZDR for OpenFOAM foundation software (version 11-s.1-hzdr.1). http://dx.doi.org/10.14278/rodare.3105, Rodare.

Schlegel, F., Meller, R., Krull, B., Lehnigk, R., Tekavčč, M., 2023. OpenFOAM-hybrid: A morphology adaptive multifield two-fluid model. Nucl. Sci. Eng. 197, 2620–2633.

Schmidmayer, K., Bryngelson, S.H., Colonius, T., 2020. An assessment of multicomponent flow models and interface capturing schemes for spherical bubble dynamics. J. Comput. Phys. 402, 109080.

Schwarz, S., Kempe, T., Fröhlich, J., 2015. A temporal discretization scheme to compute the motion of light particles in viscous flows by an immersed boundary method. J. Comput. Phys. 281, 591–613. http://dx.doi.org/10.1016/j.jcp.2014.10.039.

Semushin, S., 1988. Flow calculation with a contact surface on a rectangular lattice. http://dx.doi.org/10.5281/zenodo.7025161, Keldysh Institute of Applied Mathematics, USSR Academy of Sciences, Preprint Nr 134, translation available in Zenodo.

Seyed-Ahmadi, A., Wachs, A., 2021. Sedimentation of inertial monodisperse suspensions of cubes and spheres. Phys. Rev. Fluids 6, 044306. http://dx.doi.org/10.1103/PhysRevFluids.6.044306.

Shashkov, M., Kikinzon, E., 2023. Moments-based interface reconstruction, remap and advection. J. Comput. Phys. 479, 111998. http://dx.doi.org/10.1016/j.jcp.2023.111998.

Shen, J., Yang, X., 2015. Decoupled, energy stable schemes for phase-field models of two-phase incompressible flows. SIAM J. Numer. Anal. 53, 279–296.

Shi, F., Liu, J., 2021. A fully coupled hydromechanical XFEM model for the simulation of 3D non-planar fluid-driven fracture propagation. Comput. Geotech. 132, 103971.

Shi, P., Tholan, V., Sommer, A.E., Heitkam, S., Eckert, K., Galvin, K., Rzehak, R., 2023. Forces on a nearly spherical bubble rising in an inclined channel flow. Int. J. Multiph. Flow 169, 104620.

Shiea, M., Buffo, A., Vanni, M., Marchisio, D., 2020a. A novel finite-volume TVD scheme to overcome non-realizability problem in quadrature-based moment methods. J. Comput. Phys. 409, http://dx.doi.org/10.1016/j.jcp.2020.109337.

Shiea, M., Buffo, A., Vanni, M., Marchisio, D., 2020b. Numerical methods for the solution of population balance equations coupled with computational fluid dynamics. Annu. Rev. Chem. Biomol. Eng. 11, 339–366. http://dx.doi.org/10.1146/annurev-chembioeng-092319-075814.

Shin, S., Abdel-Khalik, S., Daru, V., Juric, D., 2005. Accurate representation of surface tension using the level contour reconstruction method. J. Comput. Phys. 203, 493–516. http://dx.doi.org/10.1016/j.jcp.2004.09.003.

Shin, S., Chergui, J., Juric, D., 2017. A solver for massively parallel direct numerical simulation of three-dimensional multiphase flows. J. Mech. Sci. Tech 31, 1739–1751. http://dx.doi.org/10.1007/s12206-017-0322-y.

Shin, S., Chergui, J., Juric, D., Kahouadji, L., Matar, O.K., Craster, R.V., 2018. A hybrid interface tracking – level set technique for multiphase flow with soluble surfactant. J. Comput. Phys. 359, http://dx.doi.org/10.1016/j.jcp.2018.01.010.

Shin, S., Juric, D., 2002. Modeling three-dimensional multiphase flow using a level contour reconstruction method for front tracking without connectivity. J. Comput. Phys. 180, http://dx.doi.org/10.1006/jcph.2002.7086.

Shin, S., Juric, D., 2007. High order level contour reconstruction method. J. Mech. Sci. Tech. 21, 311–326. http://dx.doi.org/10.1007/BF02916292.

Shin, S., Juric, D., 2009. A hybrid interface method for three-dimensional multiphase flows based on front tracking and level set techniques. Int. J. Numer. Meth. Fluids 60, 753–778.

Shukla, R.K., Pantano, C., Freund, J.B., 2010. An interface capturing method for the simulation of multi-phase compressible flows. J. Comput. Phys. 229, 7411–7439.

Shyue, K.M., Xiao, F., 2014. An Eulerian interface sharpening algorithm for compressible two-phase flow: The algebraic THINC approach. J. Comput. Phys. 268, 326–354.

Silling, S., 2000. Reformulation of elasticity theory for discontinuities and long-range forces. J. Mech. Phys. Solids 48, 175–209.

Soligo, G., Roccon, A., Soldati, A., 2021. Turbulent flows with drops and bubbles: What numerical simulations can tell us. J. Fluids Eng. 143, 080801.

Solomenko, Z., Spelt, P.D., Ó Náraigh, L., P, A., 2017. Mass conservation and reduction of parasitic interfacial waves in level-set methods for the numerical simulation of two-phase flows: a comparative study. Int. J. Multiph. Flow 95, 235–256.

Sommerfeld, M., 2017. Numerical methods for dispersed multiphase flows. Part. Flows 32, 7–396.

Soos, M., Marchisio, D., Sefcik, J., 2013. Assessment of gel formation in colloidal dispersions during mixing in turbulent jets. AIChE J. 59, 4567–4581. http://dx.doi.org/10.1002/aic.14268.

Sotiropoulos, F., Yang, X., 2014. Immersed boundary methods for simulating fluid–structure interaction. Prog. Aerosp. Sci. 65, 1–21. http://dx.doi.org/10.1016/j.paerosci.2013.09.003.

Sprittles, J.E., 2015. Air entrainment in dynamic wetting: Knudsen effects and the influence of ambient air pressure. J. Fluid Mech. 769, 444–481.

Stafford, D., Ward, M.J., Wetton, B., 2001. The dynamics of drops and attached interfaces for the constrained Allen–Cahn equation. Eur. J. Appl. Math. 12, 1–24.

Stickel, J.J., Powell, R.L., 2005. Fluid mechanics and rheology of dense suspensions. Annu. Rev. Fluid Mech. 37, 129–149.

Subramaniam, S., 2013. Lagrangian–Eulerian methods for multiphase flows. Prog. Energy Combust. Sci. 39, 215–245.

Subramaniam, S., Balachandar, S. (Eds.), 2023. Modeling approaches and computational methods for particle-laden turbulent flows. Academic Press.

Sun, Y., Beckermann, C., 2007. Sharp interface tracking using the phase-field equation. J. Comput. Phys. 220, 626–653.

Sussman, M., Puckett, E.G., 2000. A coupled level set and volume-of-fluid method for computing 3D and axisymmetric incompressible two-phase flows. J. Comput. Phys. 162, 301–337.

Sussman, P., Smereka, P., Osher, S., 1994. A level set approach for computing solutions to incompressible two-phase flow. J. Comput. Phys. 114, 146–159.

Tang, K., Adcock, T., Mostert, W., 2023. Bag film breakup of droplets in uniform airflows. J. Fluid Mech. 970, A9. http://dx.doi.org/10.1017/jfm.2023.605.

Taylor, G.I, 1959. The dynamics of thin sheets of fluid III. Disintegration of fluid sheets. Proc. Roy. Soc. Lond. A 253, 313–321.

Taylor, G., Michael, D., 1973. On making holes in a sheet of fluid. J. Fluid Mech. 58, 625–639.

Teigen, K.E., Song, P., Lowengrub, J., Voigt, A., 2011. A diffuse-interface method for two-phase flows with soluble surfactants. J. Comput. Phys. 230, 375.

Ten Eikelder, M., Van Der Zee, K., Akkerman, I., Schillinger, D., 2023. A unified framework for Navier–Stokes Cahn–Hilliard models with non-matching densities. Math. Models Methods Appl. Sci. 33, 175–221.

Thomas, S., Esmaeeli, A., Tryggvason, G., 2010. Multiscale computations of thin films in multiphase flows. Int. J. Multiph. Flow 36, 71–77.

Tiwari, A., Freund, J.B., Pantano, C., 2013. A diffuse interface model with immiscibility preservation. J. Comput. Phys. 252, 290–309.

Tomiyama, A., Tamai, H., Zun, I., Hosokawa, S., 2002. Transverse migration of single bubbles in simple shear flows. Chem. Eng. Sci. 57, 1849–1858.

Toro, E.F., 2013. Riemann solvers and numerical methods for fluid dynamics: A practical introduction. Springer Science & Business Media.

Torre, K.W., de Graaf, J., 2025. Hydrodynamic interactions in particle suspensions: A perspective on Stokesian dynamics. arXiv preprint arXiv:2503.16083.

Torrey, M.D., Cloutman, L.D., Mjolsness, R.C., Hirt, C.W., Torrey, M.D., Cloutman, L.D., Mjolsness, R.C., Hirt, C.W., 1985. NASA-VOF2D: A Computer Program for Incompressible Flows with Free Surfaces. NASA STI/Recon Technical Report N.

Traverso, S., Abadie, T., Matar, O.K., Magri, L., 2023. Data-driven modeling for drop size distributions. Phys. Rev. Fluids 104302.

Tronci, G., Buffo, A., Vanni, M., Marchisio, D., 2021. Validation of the diffusion mixture model for the simulation of bubbly flows and implementation in OpenFOAM. Comput. & Fluids 227, http://dx.doi.org/10.1016/j.compfluid.2021.105026.

Tryggvason, G., Bunner, B., Esmaeeli, A., Juric, D., Al-Rawahi, N., Tauber, W., Han, J., Nas, S., Jan, Y.J., 2001. A front-tracking method for the computations of multiphase flow. J. Comput. Phys. 169, 708–759. http://dx.doi.org/10.1006/jcph.2001.6726.

Tryggvason, G., Scardovelli, R., Zaleski, S., 2011. Direct numerical simulations of gas–liquid multiphase flows. Cambridge University Press.

Tschisgale, S., Kempe, T., Fröhlich, J., 2017. A non-iterative immersed boundary method for spherical particles of arbitrary density ratio. J. Comput. Phys. 339, 432–452. http://dx.doi.org/10.1016/j.jcp.2017.03.026.

Tschisgale, S., Kempe, T., Fröhlich, J., 2018. A general implicit direct forcing immersed boundary method for rigid particles. Comput. & Fluids 170, 285–298. http://dx.doi.org/10.1016/j.compfluid.2018.04.008.

Tsui, Y., Lin, S., Cheng, T., Wu, T., 2009. Flux-blending schemes for interface capture in two-fluid flows. Int. J. Heat Mass Transfer 52, 5547–5556.

Ubbink, O., Issa, R., 1999. A method for capturing sharp fluid interfaces on arbitrary meshes. J. Comput. Phys. 153, 26–50.

Uhlmann, M., 2005. An immersed boundary method with direct forcing for the simulation of particulate flows. J. Comput. Phys. 209, 448–476. http://dx.doi.org/10.1016/j.jcp.2005.03.017.

Uhlmann, M., Derksen, J., Wachs, A., Wang, L.P., Moriche, M., 2023. Efficient methods for particle-resolved direct numerical simulation. In: Subramaniam, S., Balachandar, S. (Eds.), Modelling Approaches and Computational Methods for Particle-Laden Turbulent Flows. Academic Press, pp. 147–184.

Uhlmann, M., Doychev, T., 2014. Sedimentation of a dilute suspension of rigid spheres at intermediate Galileo numbers: the effect of clustering upon the particle motion. J. Fluid Mech. 752, 310–348. http://dx.doi.org/10.1017/jfm.2014.330.

Unverdi, S.O., Tryggvason, G., 1992. A front-tracking method for viscous, incompressible, multi-fluid flows. J. Comput. Phys. 100, 25–37.

Vanella, M., Balaras, E., 2009. A moving-least-squares reconstruction for embedded-boundary formulations. J. Comput. Phys. 228, 6617–6628. http://dx.doi.org/10.1016/j.jcp.2009.06.003.

Verzicco, R., 2023. Immersed boundary methods: Historical perspective and future outlook. Annu. Rev. Fluid Mech. 55, http://dx.doi.org/10.1146/annurev-fluid-120720-022129.

Villermaux, E., 2020. Fragmentation versus cohesion. J. Fluid Mech. 898.

Vowinckel, B., Withers, J., Luzzatto-Fegiz, P., Meiburg, E., 2019. Settling of cohesive sediment: particle-resolved simulations. J. Fluid Mech. 858, 5–44.

Vowinckel, B., Zhao, K., Zhu, R., Meiburg, E., 2023. Investigating cohesive sediment dynamics in open waters via grain-resolved simulations. Flow 3, E24.

Wachs, A., 2019. Particle-scale computational approaches to model dry and saturated granular flows of non-Brownian, non-cohesive, and non-spherical rigid bodies. Acta Mech. 230, 1919–1980. http://dx.doi.org/10.1007/s00707-019-02389-9.

Wachs, A., Uhlmann, M., Derksen, J., Huet, D.P., 2023. Modeling of short-range interactions between both spherical and non-spherical rigid particles. In: Modeling Approaches and Computational Methods for Particle-Laden Turbulent Flows. Elsevier, pp. 217–264.

Wang, Y., Bourouiba, L., 2018. Unsteady sheet fragmentation: droplet sizes and speeds. J. Fluid Mech. 848, 946–967. http://dx.doi.org/10.1017/jfm.2018.359.

Wang, Y., Javadi, A., Fidelibus, C., 2023. A hydro-mechanically-coupled XFEM model for the injection-induced evolution of multiple fractures. Int. J. Numer. Anal. Methods Geomech. 47, 1539–1558.

Wang, B., Wang, J., 2021. Application of artificial intelligence in computational fluid dynamics. Ind. Eng. Chem. Res. 60, 2772–2790.

Wen, H.L., Yu, C.H., Sheu, T.H., Chau, S.W., 2023. A mass-preserving level set method for simulating 2D/3D fluid flows with deformed interface. Ocean Eng.. 283, 115063.

Weymouth, G., Yue, D.K.P., 2010. Conservative Volume-of-Fluid method for free-surface simulations on Cartesian-grids. J. Comput. Phys. 229, 2853–2865. http://dx.doi.org/10.1016/j.jcp.2009.12.018.

Xiao, F., Honma, Y., Kono, T., 2005. A simple algebraic interface capturing scheme using hyperbolic tangent function. Int. J. Numer. Meth. Fluids 48, 1023–1040.

Xiao, F., Ii, S., Chen, C., 2011. Revisit to the THINC scheme: a simple algebraic VOF algorithm. J. Comput. Phys. 230, 7086–7092.

Xie, B., Xiao, F., 2014. Two and three dimensional multi-moment finite volume solver for incompressible Navier–Stokes equations on unstructured grids with arbitrary quadrilateral and hexahedral elements. J. Comput. Phys. 104, 40–54.

Xie, B., Xiao, F., 2017. Toward efficient and accurate interface capturing on arbitrary hybrid unstructured grids: the THINC method with quadratic surface rerpresentation and Gaussian quadrature. J. Comput. Phys. 349, 415–440.

Xing, J., Zhao, C., 2023. A hydro-mechanical phase field model for hydraulically induced fractures in poroelastic media. Comput. Geotech. 159, 105418.

Yan, C., Zheng, H., Sun, G., Ge, X., 2016. Combined finite-discrete element method for simulation of hydraulic fracturing. Rock Mech. Rock Eng.. 49, 1389–1410.

Yang, C., Zhu, F., Zhao, J., 2024. Coupled total-and semi-Lagrangian peridynamics for modelling fluid-driven fracturing in solids. Comput. Meth. Appl. Mech. Eng. 419, 116580.

Yeoh, G.H., Tu, J., 2019. Computational techniques for multiphase flows. Butterworth-Heinemann.

Yokoi, K., 2007. Efficient implementation of THINC scheme: a simple and practical smoothed VOF algorithm. J. Comput. Phys. 226, 1985–2002.

Yoshioka, K., Parisio, F., Naumov, D., Lu, R., Kolditz, O., Nagel, T., 2019. Comparative verification of discrete and smeared numerical approaches for the simulation of hydraulic fracturing. GEM-Int. J. Geomath. 10, 1–35.

Youngs, D.L., 1982. Time-dependent multi-material flow with large fluid distortion. In: Morton, K., Baines, M. (Eds.), Numerical Methods for Fluid Dynamics. Academic Press, pp. 273–285.

Yousefi, A., Costa, P., Picano, F., Brandt, L., 2023. On the role of inertia in channel flows of finite-size neutrally buoyant particles. J. Fluid Mech. 955, A30.

Zhang, Q., 2013. On a family of unsplit advection algorithms for volume-of-fluid methods. SIAM J. Numer. Anal. 51, 2822–2850.

Zhang, W., Paula, T., Bußmann, A., Adami, S., Adams, N.A., 2025. Extension of the hybrid WENO5IS-THINC scheme to compressible multiphase flows with an arbitrary number of components. J. Comput. Phys. 524, 113702.

Zhang, D., Yi, L., Yang, Z., Li, X., Zhang, F., 2023. Phase field model for simulating hydraulic fracture propagation and oil–water two-phase flow in reservoir. Comput. Meth. Appl. Mech. Eng. 404, 115838.

Zhao, J., Han, D., 2021. Second-order decoupled energy-stable schemes for Cahn-Hilliard-Navier-Stokes equations. J. Comput. Phys. 443, 110536.

Zhao, C., Limare, A., Zaleski, S., 2023. General wetting energy boundary condition in a fully explicit nonideal fluids solver. Phys. Rev. E 108, 055307.

Zhao, C., Maarek, J., Taleghani, S.M., Zaleski, S., 2024. A hybrid continuum surface tension force for the three-phase VOF method. J. Comput. Phys. 504, 112872.

Zhou, K., Balachandar, S., 2021. An analysis of the spatio-temporal resolution of the immersed boundary method with direct forcing. J. Comput. Phys. 424, 109862. http://dx.doi.org/10.1016/j.jcp.2020.109862.

Zhu, L.T., Chen, X.Z., Ouyang, B., Yan, W.C., Lei, H., Chen, Z., Luo, Z.H., 2021. Review of machine learning for hydrodynamics, transport, and reactions in multiphase flows and reactors. Ind. Eng. Chem. Res. 61, 9901–9949.

Zinelis, K., Abadie, T., McKinley, G.M., Matar, O.K., 2024. Transition to elasto-capillary thinning dynamics in viscoelastic jets. J. Fluid Mech. 998, A4.